UNDERSTANDING THE RELATIONSHIP BETWEEN BISPECIFIC ANTIBODY DESIGN AND FUNCTION: HOW VALENCY AND SPATIAL CONFIGURATION CAN IMPROVE ANTI-TUMOR RESPONSES

By

Brian Horacio Santich

A dissertation

Presented to the faculty of the Louis v. Gerstner, Jr.

Graduate School of Biomedical Sciences,

Memorial Sloan Kettering Cancer Center

In partial fulfillment of the requirements for the degree of

Doctor of Philosophy

New York, NY

May 2019

Nai-Kong V. Cheung MD/PhD Dissertation Co-mentor	Date
Morgan Huse PhD Dissertation Co-mentor	Date

DEDICATION

I would like to dedicate this thesis to my family: Josip Santic, Josephine O'Donoghue, Sinead Santich and Felipe Santich. If not for their love and support over the years, surely none of this would have been possible.

ABSTRACT

T-cell bispecific antibodies (BsAb) couple cytotoxic T-lymphocytes to tumor cells, thereby inducing their destruction. Although there are over 60 classes of BsAb in development, the relative significance of parameters such as valency or spatial configuration are largely unknown. During my graduate school work, I have sought to identify design parameters that significantly enhance to BsAb potency *in vitro* and *in vivo.* The studies presented here support the roles of affinity, valency and spatial configuration in driving strong BsAb-mediated T-cell responses against antigen-expressing tumors.

To begin, we found that improving tumor binding affinity 13-fold improved *in vivo* cytotoxicity substantially and *in vitro* cytotoxicity up to 5,000-fold. Next, we compared a dual bivalent IgG-[L]-scFv design to two monovalent FDA-approved designs and found bivalency as a critical parameter in improving T-cell cytotoxicity *in vitro* and *in vivo*. Following this, we dissected the IgG-[L]-scFv platform and revealed that positioning tumor and T-cell binding domains on the same side (cis-configuration) of a BsAb elicited significantly stronger anti-tumor activity, *in vitro* and *in vivo*, compared to positioning them on opposite sides (trans-configuration) and using two such cis-modules in the same BsAb improved cytotoxicity even more (up to 2,000-fold). Finally, we showed how spacing these domains using a single Ig domain (C_L) was superior to smaller (G_4S) or larger (C_{H1}-C_{H2}-C_{H3}) domains. These findings provide critical guidelines for improving BsAb function and highlight the importance of affinity, spatial configuration and dual-bivalency as development parameters.

BIOGRAPHICAL SKETCH

Brian was born to Josip Santic and Josephine O'Donoghue on February 8th, 1989 in San Francisco, CA. At the age of four his family moved to Chico, CA, where Brian spent the rest of his childhood. Brian graduated from Pleasant Valley High School in 2007, and soon after moved to Berkeley, CA to attend the University of California, Berkeley. There he majored in Molecular and Cell Biology (BA), with a focus in immunology. While at Berkeley, Brian began his scientific training under the mentorship of Dr. Simona Zompi MD PhD, while working in the laboratory of Dr. Eva Harris PhD. During his time in the Harris lab, Brian studied the role of B- and T-cell responses in secondary infections of dengue virus. After graduating in the year 2011, Brian moved to the east coast to work at the National Institutes of Health, after being accepted into their Post-Baccalaureate training program (IRTA). At the NIH, Brian worked under the mentorship of Dr. Susan Moir PhD in the laboratory of Dr. Anthony Fauci MD. During his time there, Brian worked on multiple projects including B-cell responses to HIV infection and B-cell dysfunctions in other primary immunodeficiencies. After two years, Brian entered his doctoral training at the Louis. V. Gerstner Jr. Graduate School of Biomedical sciences at Memorial Sloan Kettering Cancer Center, where he worked under the mentorship of Drs. Nai-Kong V. Cheung and Morgan Huse.

ACKNOWLEDGEMENTS

I would first like to thank both my thesis mentors, Drs. Nai-Kong V. Cheung and Morgan Huse for all the efforts that have put into training me over the last five years. Throughout my time in graduate school, they both provided incredible mentorship and amazing support. Additionally, both gave me large amounts of independence ,which I now feel was critical to my accomplishing the work presented here.

I would like to thank Drs. Mahiuddin Ahmed, Irene Cheung, Hong Xu, and Hong-Fen Guo for providing important hands-on training and support throughout my training. Together they greatly aided in making me think more critically, carefully and creatively.

I would to thank my thesis committee members, Drs. David Scheinberg and Jedd Wolchok for their help in driving the project forward over the years. Their years of expertise in antibody development and clinical application were incredibly valuable to me, and the critiques and experimental ideas that provided me helped me gain a greater appreciation of the field of immunotherapy.

Lastly, I would like to thank the entire graduate school, past members and present. From the moment I first heard about the school, I knew it would be the perfect fit for me. The emphasis on the independent scientific, above all else, allowed me to fulfill the scientific training experience I had always hoped for. This could not have been possible without the hard work and vision from Drs. Ken Marians, Harold Varmus and Tom Kelly and our benefactor Louis V. Gerstner Jr., who together established this school and nurtured it until it became the success story it is today.

TABLE OF CONTENTS

LIST OF TABLES

LIST OF FIGURES

LIST OF ABBREVIATIONS

ATC – Activated T-cell

BsAb – Bispecific Antibody

BiTE – Bispecific T-cell Engager

CAR – Chimeric Antigen Receptor

CDC – Complement Dependent Cytotoxicity

huCD3ε-tg – human CD3ε Transgenic Mouse

CDR – Complementary Determining Region

C_{H1} – Constant Domain 1 of Heavy Chain

C_{H2} – Constant Domain 2 of Heavy Chain

C_{H3} – Constant Domain 3 of Heavy Chain

C_L – Constant Domain of Light Chain

CRS – Cytokine Release Syndrome

CTL – Cytotoxic T Lymphocyte

CZE – Capillary Zone Electrophoresis

DKO – IL-2rγ and Rag2 Double Knockout Mouse

Fab – Fragment of Antigen Binding

Fc – Fragment of Crystallization

HPLC – High Pressure Liquid Chromatography

IFN-γ – Interferon Gamma

IL-2 – Interleukin 2

ITAM - Immunoreceptor Tyrosine-based Activation Motifs

K_D – Equilibrium Dissociation Constant

LAT – Linker of Activated T-cells

Lck – Lymphocyte-specific Protein Tyrosine Kinase

mAb – Monoclonal Antibody

MHC – Major Histocompatibility Complex

NCK – Non-Catalytic Region of Tyrosine Kinase Adaptor Protein 1

PBMC – Peripheral Blood Mononuclear Cells

PDX – Patient Derived Xenograft

scFv – Single-Chain Variable Fragment

SLP76 – Lymphocyte Cytosolic Protein 2

V_L – Light Chain Variable Domain

V_H – Heavy Chain Variable Domain

ZAP70 – Zeta-Chain-Associated Protein Kinase 70

INTRODUCTION

Bispecific antibodies

Human immunoglobulins exist as complexes of light and heavy chain proteins. Each chain consists of a variable region (V_L or V_H) and a constant region (C_L and C_{H1}, C_{H2}, and C_{H3}, for IgG). The variable regions define the specificity of the antibody, primarily through three hypervariable regions called complimentary determining regions (CDR), while the constant regions determine effector or biochemical properties, such as complement dependent cytotoxicity (CDC), Fc receptor dependent activation or pharmacokinetics. In IgG monoclonal antibodies (mAb), heavy and light chains pair together, and these heavy-light chain pairs dimerize along their C_{H2} and C_{H3} domains to create a tetrameric IgG complex. Human IgG has a final molecular weight of 150 kilodaltons and remains the most abundant serum protein in humans. Antibodies first entered modern medical science with the work of Drs. von Behring, Kitasato and Ehrlich at the end of the 19th century (Kufer et al., 2004). However, by the middle of the 20th century, scientists had already begun working on improving nature's original design by expressing antibodies with two specificities (Nisonoff and Rivers, 1961), also known as bispecific antibodies (BsAb). Amazingly these early proof-of-concept experiments came before the development of hybridoma technology (Cotton and Milstein, 1973; Kohler and Milstein, 1975) and monoclonal antibodies (mAb), but the pioneering work would lead to many different approaches to create a functional BsAb. By 1985, the first T-cell engaging BsAb had been designed and characterized (Ma et al., 2012) using chemical conjugation to fuse target and T-cell specific antibodies together. Even three decades before the first FDA approval of a T-cell engaging BsAb, the utility of redirecting T-cells was clear. By linking a T-cell specific epitope together with a tumor cell epitope, one could overcome

the T-cell's natural restriction to peptides presented on major histocompatibility complex (MHC), and instead drive T-cells to recognize any antigen of interest. Many other effector cell types were also considered, but few delivered the high cytotoxicity that T-cells provided (Kufer et al., 2004). As protein and genetic engineering advanced, many scientists tried to move away from synthetic chemical conjugations, which often created heterogenous pools of conjugated and unconjugated proteins and instead attempted to create BsAb formats that folded together natively into a single protein. One of the earliest attempts simply fused two antibody producing hybridomas together (Suresh et al., 1986), however this led to many mispairings of heavy and light chains. Due to the high homology within most heavy and light chain sequences, combining two unique light chains and two unique heavy chains can lead to ten possible combinations, of which only a minor fraction would end up with the desired heterodimeric configuration. These limitations were initially overcome by the development of novel heterodimerizing protein domains (Kostelny et al., 1992) and the "Knobs-into-holes" (Ridgway et al., 1996) mutations. Both functioned by changing the C_{H2} and C_{H3} sequences of each heavy chain, either by completely replacing them with new domains, or mutating key residues that allowed for preferential heterodimerization while preventing the normal homodimerization. While these advancements did not completely fix all pairing issues, namely light chain mispairings, they provided critical advances and over the next two decades iterative improvements on these strategies led to the "CrossMab™" system that exists today (Schaefer et al., 2011). At the same time, another approach underwent development to avoid most mispairing issues through reengineering the antibody V_L and V_H domains. After removing all constant regions and fusing together the remaining variable domains with flexible peptide linkers, one could create a binding domain consisting of a single protein sequence, or single-chain

variable fragment (scFv), that contained all necessary binding motifs. Turning this into a BsAb only meant fusing two scFv domains together (tandem-scFv) or dividing the four variable domains across two peptides (diabodies) with various linkers between (Kipriyanov et al., 1999). Without the constant domains, only the inherent homology in the framework regions of V_L or V_H domains allowed pairing, and by modulating the length of the flexible linkers between these domains, one could prevent or allow pairing quite easily.

As advancements in protein engineering brought BsAb into the mainstream, designs became more complex. Intact IgG proteins could be linked to scFv domains (Coloma and Morrison, 1997b), site-specific mutations could modulate the effector functions of Fc proteins (Alegre et al., 1992; Tao and Morrison, 1989; Walker et al., 1989), and the discovery of single-domain antibodies could further reduce the protein footprints needed for antibody binding (Deschacht et al., 2010). However despite these advances, too little was known about how to make a clinical grade bispecific therapeutic. Although mAbs have existed only marginally longer than bispecific antibodies, their relative simplicity, increased stability and generally improved developability has led to over 75 FDA approvals to date, in contrast to BsAb which have only had two approvals so far (Shima et al., 2016; Topp et al., 2015), of which only one is a T-cell BsAb. Evolution has spent the last 500 million years (Pancer et al., 2004) developing antibodies without creating bispecific variants, so it is entirely expected that optimization may take some time.

T-cell biology

The human immune system can be divided into innate and adaptive classes. While continued research in immunology periodically reclassify cell populations, T-cells quite safely reside in the adaptive category, due to their defining characteristic, the T-cell

receptor (TCR). This receptor provides T-cells with their genetically determined specificities, and their primary functions of surveying host cells for infection or disruption and maintaining homeostasis (Kumar et al., 2018). The TCR complex is comprised of eight proteins: TCRα and β chains (or γ and δ for the less common γδ T-cell) CD3γ, CD3δ, two CD3ε and two CD3ζ (Davis and Bjorkman, 1988). Together these proteins form a heteromultimeric complex that allows for recognition of MHC-presented peptides (pMHC) and subsequent activation and signaling of T-cells (Krogsgaard and Davis, 2005). Very similar to antibodies, TCRα and β chains contain CDRs that allow a TCR to recognize subtle changes in charge or size from the many different small peptides that class-I or class-II MHC molecules can present (Alcover et al., 2018).

T-cells have been thoroughly studied over the years, and as a consequence, much is already known about how they recognize their cognate antigen, and the many structural and cellular changes that follow. T-cells go through an initial selection in the thymus, similar to B-cells, with non-reactive or self-reactive TCR sequences largely eliminated (Kappler et al., 1987). Upon their exit of the thymus, T-cells restrict their expression of CD8 or CD4, co-receptors that help T-cells bind to MHC molecules. Since the TCR canonically binds pMHC with very low affinity (Rosette et al., 2001; Schmid et al., 2010; Stone et al., 2009) the CD4 or CD8 co-receptors provide an important enhancement in binding, and subsequently define a T-cell's function by restricting its recognition to either MHC class I (CD8 T-cells) or MHC class II (CD4 T-cells). While MHC class I is expressed on nearly every cell type in the human body, MHC class II is much more restricted, found only on certain immune cells, such as dendritic cells or monocytes (Garrido and Algarra, 2001). As a consequence, CD8 T-cells primarily play role in directly eliminating diseased or damaged cells through cytotoxic functions, while CD4 T-

cells more often play a role, modulating other immune cells and their responses, though co-stimulation or cytokine production.

Despite their inherent differences in function, the underlying biology within CD4 and CD8 T-cells remains very similar. When TCRs bind pMHC, CD4 and CD8 proteins help recruit lymphocyte-specific protein tyrosine kinase (Lck) into the proximity of the CD3ζ chains (Artyomov et al., 2010), which contain immunoreceptor tyrosine-based activation motifs (ITAM) (Weissman et al., 1988). Once phosphorylated, the CD3ζ ITAMs recruit zeta-chain-associated protein kinase 70 (ZAP70) (Wang et al., 2010), which phosphorylates linker of activated T-cells (LAT) (Lo et al., 2018) and lymphocyte cytosolic protein 2 (SLP-76), proteins that can recruit other signaling molecules (Clements et al., 1998). Phosphorylated LAT and SLP-76 recruit downstream adapters and kinases that lead to Ca^{2+} flux, mobilization of the actin cytoskeleton and expression of several transcription factors (Billadeau et al., 2007; Lewis, 2001). In addition, the T-cell undergoes large structural changes, beginning with the formation of an immune cell synapse between itself and its target cell (Basu and Huse, 2017; Huse, 2011). The synapse allows for the differential exclusion and colocalization of many important membrane proteins, such as CD3, CD28, and CD45, (Alarcon et al., 2011; Bromley et al., 2001; Cordoba et al., 2013; Delon et al., 2001; Huse, 2011) and in the case of CD8 T-cells helps direct the release of cytotoxic granules perforin and granzyme (Huse et al., 2008). The release of these granules causes the subsequent perforation and activation of apoptotic pathways in the target cell, leading to its death. Recent studies have also shown that the binding of the TCR to pMHC leads to key structural changes in the TCR complex itself, which help facilitate downstream activation (Basu et al., 2016; Kim et al., 2012; Kim et al., 2009; Kleinewietfeld and Hafler, 2014). TCR engagement of pMHC are

thought to alter the structure of CD3ε or CD3ζ proteins, leading to exposure of domains that recruit proteins such as non-catalytic region of tyrosine kinase adaptor protein 1 (NCK) to propagate signaling (Gil et al., 2002). T-cell signaling can also be initiated by direct antibody engagement, independently of MHC. Antibodies raised against specific T-cell epitopes, usually on the CD3ε extracellular domain (Tunnacliffe et al., 1989), can induce similar physical changes to the TCR as does MHC engagement, leading to the T-cell stimulation, activation, cytokine release, proliferation, differentiation and alteration in expression of key surface proteins (Salmeron et al., 1991; Van Wauwe et al., 1980). These changes provide an important way for T-cells to adapt their response to the perturbation at hand and provide the most optimal response.

T-cell immunotherapy

Throughout cancer immunotherapy, T-cells remain one of the most actively used immune cell subsets in the clinic. To date, they are employed across three different categories: (1) checkpoint blockade, (2) adoptive T-cell therapy, and (3) T-cell bispecific antibody therapy. Part of this is due to their high abundance in peripheral blood, making up around 50% of the lymphocytes in a normal human. Additionally, they are highly potent, capable of surveying and killing targeted cells with high specificity (Stone et al., 2009). Finally, T-cells are easily maintained and modulated *in vitro* and *ex vivo*, leading to engineering feats that drastically improve their therapeutic utility. Clinically, the most available T-cell immunotherapy is checkpoint blockade (Pardoll, 2012). Here endogenous T-cells that already recognize the tumor are released from their inhibited state through the binding of inhibitory T-cell proteins by exogenous antibodies (Agata et al., 1996; Leach et al., 1996). While these methods have had enormous success across many malignancies (Hamid et al., 2013) they remain somewhat limited to patients with

pre-existing T-cell based tumor immunity. In contrast, adoptive T-cell therapies function by infusing patients with large numbers of tumor-specific T-cells that can directly engage the patient's tumor (Park et al., 2011; Restifo et al., 2012; Stevanovic et al., 2018; Zacharakis et al., 2018). These cells are usually expanded and selected *ex vivo* but may also undergo genetic perturbations such as chimeric antigen receptor (CAR) transduction, providing them with customized antigen recognition (Eshhar and Gross, 1990; Eshhar et al., 1993; Gross and Eshhar, 1992; Park et al., 2007). However, being a personalized cell therapy some major limitations remain. Unlike checkpoint blockade where a single protein can be administered to thousands of different patients, adoptive T-cell therapies require the use of a patient's own T-cells, or at least those of a closely matched donor. Additionally, this means every batch of cells will be unique, leading to greater variation in clinical responses. Although scientists are seeking methods to generate a universal T-cell donor (Torikai et al., 2012), adoptive T-cell therapy will still be somewhat limited by the need to continually propagate enough tumor specific T-cells for each patient. T-cell BsAb therapies seek to combine many of the benefits of checkpoint blockade and adoptive T-cell therapies. On the one hand, T-cell BsAb therapy depends only on the infusion of the protein itself (Shalaby et al., 1992), as is the case with check point blockade therapy. Additionally, similar to adoptive T-cell therapy, T-cell BsAb therapy functions through recognition of specific tumor antigens and does not rely on the immunogenicity of the tumor (although it can still benefit from it). While some groups are trying to combine T-cell BsAb with adoptive T-cell transfers (Yankelevich et al., 2012), T-cell BsAb do not depend on an *ex vivo* selection and expansion of patient T-cells, greatly simplifying the therapeutic process. However, many downsides still remain. T-cell BsAb do depend on expression of their target antigens, and with antigen loss most

T-cell BsAb will cease to function. The complexity of T-cell BsAb design has caused many preclinical failures, usually stemming from insufficient stability, poor pharmacokinetics or low potency. Additionally, similar to adoptive T-cell therapies, BsAb can result in overactivation of T-cells with a common side-effect of being cytokine release syndrome (CRS). Although this has largely been solved by IL-6 blockade, it remains a limiting factor in T-cell BsAb dosing and continues to play a role in preventing therapeutic dose levels from being achieved clinically.

Introduction to the thesis

To date over 60 different BsAb designs exist in the scientific literature, with many having already gone, or continuing to undergo clinical development (Brinkmann and Kontermann, 2017; Wu and Cheung, 2018). In 2014 the FDA approved its first BsAb, Blinatumomab, and to date its only T-cell engaging one (Topp et al., 2015). Blinatumomab functions by redirecting T-cells to kill CD19(+) leukemia cells using a tandem-scFv format (BiTE). In 2017, the FDA approved its only other BsAb to date, emicizumab-kxwh (Shima et al., 2016), which uses an IgG-heterodimer format to treat hemophilia patients. Today, many new T-cell BsAb continue to be developed, but few enter clinical trials, and even fewer show compelling enough anti-tumor responses to garner FDA approval. In part this stems from the high potencies of T-cells, which can elicit toxicities even when using antigens that have succeeded for monoclonal antibodies (Morgan et al., 2010). It is also a reflection of advancements in competing T-cell therapies, such as chimeric antigen receptor (CAR) T-cells (Chong et al., 2018; Neelapu et al., 2017) or checkpoint inhibitors (Hodi et al., 2010; Postow et al., 2015; Wolchok, 2015; Wolchok et al., 2013; Wolchok et al., 2010). However, the lack of major guidelines for creating the optimal T-cell BsAb continues to be one of the largest constraint of its

potential. My graduate work has largely focused on improving our understanding T-cell BsAb design and contributing to the formation of these guidelines, through iterative and systematic comparison of different T-cell BsAb. Chapter one summarizes findings regarding the influence of target cell affinity on the potency of the monomeric BiTE format. Chapter two looks at a bivalent T-cell BsAb (IgG-[L]-scFv) and compares it to the approved monomeric antibody designs. Chapter three expands our understanding of domain configuration by comparing five different IgG-[L]-scFv formats with different valencies and uncovers an important role for cis-configured binding domains. Chapter four compares the IgG-[L]-scFv design to two other dual bivalent BsAb and reveals a role for Ig domain spacing. These findings demonstrate how the potency of a BsAb results not only from its antigen binding site multiplicity but also from the specific spatial configuration of its antigen binding domains.

MATERIALS AND METHODS

Antibody engineering

Gene sequences for each BsAb were synthesized (Genscript) and cloned into a mono- or bi-cistronic vector using restriction digest. In this vector, two CMV promoters expression of either heavy or light chains. The vector contains ampicillin and hygromycin resistance to allow for bacterial and mammalian cell selection. Vectors were cloned and amplified using DH5α E. coli (New England Biosciences) and miniprep (Qiagen) or maxiprep (Invitrogen) kits, according to manufacture guidelines. DNA sequences were confirmed using Sanger sequencing. Maxiprepped DNA was transfected or nucleofected into expi293 (Invitrogen) or CHO-S (Lonza) cells. Nucleofected CHO-S cells were made into stable cell lines through single cell sorting and positive selection.

Anti-GD2 antibodies (except for GD2.2 and GD2.3) used V_H and V_L domains from hu3F8 (Cheung et al., 2014) or 5F11 (Cheng et al., 2015), as noted. Anti-CD3 antibodies used V_H and V_L domains from huOKT3 (Adair et al., 1994). Anti-CD33 antibodies used V_H and V_L domains from huM195 (Caron et al., 1992; Hoseini et al., 2018). Anti-HER2 antibodies used V_H and V_L domains from Trastuzumab (Albanell and Baselga, 1999; Lopez-Albaitero et al., 2017). Anti-GPA33 antibodies used V_H and V_L domains from huA33 (Wu et al., 2018). IgG-based proteins used a human IgG1 framework that contained both N297A and K322A mutations to eliminate Fc receptor and complement binding activities, respectively. ScFv binding domains used multiple units of G_4S polypeptides as flexible linkers. Control antibodies contained irrelevant tumor binding domains (anti-CD33, anti-HER2 or anti-GPA33) but retained identical T-cell binding domains (huCD3ε).

Antibody expression

All proteins were expressed using the Expi293 Expression System (Invitrogen) according to manufacturer's instructions. Briefly, maxiprepped expression plasmids for each antibody were diluted and incubated with expifectamine for 20 minutes before being added to cell suspensions. Cells were incubated in shaker culture for four days or until cell viability dropped <70%, whichever came first. IgG-based proteins were purified with a protein A column using a GE P920 AKTA FPLC and eluted with 50 mM citric acid. The BiTE was purified using prepacked Ni^{2+} NTA columns (GE) and eluted using 250 mM imidazole. All proteins were buffer exchanged into 25 mM sodium citrate 150 mM sodium chloride (pH 8.2) solution and run on SEC-HPLC (Shimadzu).

Heterodimerization

Heterodimerization was achieved using Fab Arm Exchange (FAE) (Labrijn et al., 2014), following standard protocols for benchtop scale. Briefly, K409R and F405L mutations were placed in the Fc regions of each reciprocal pair of IgG or IgG-[L]-scFv bispecific antibodies (Tables 4 and 7) to be heterodimerized. Each pair of homodimers were mixed at 1:1 molar ratio and incubated under reducing conditions for five hours at 31°C. Following this incubation samples were buffer exchanged overnight into a solution of 25 mM sodium citrate 150 mM sodium chloride (pH 8.2). Samples were subsequently moved to 4°C for another 18-24 hours before being analyzed by SEC-HPLC (Shimadzu) and CZE (Sciex) to assess heterodimerization yields and purity. Purity and size were confirmed by comparing sample plots and peak values to those of known standards (BioRad) or parental homodimer samples. The stability of all IgG-based antibodies was evaluated by HPLC after extended incubations (over three weeks) at 37°C or 40°C. No differences in stability were seen with any of the BsAb formats.

Primary cells and cell lines

EL.4 cell lines were obtained from ATCC. IMR32 and M14 cell lines were obtained from University of California, Los Angeles and transfected with luciferase prior to use in all assays. EL.4, IMR32 and M14 cell lines routinely tested negative for mycoplasma. IMR32 and M14 cells were periodically validated by STR. All cell lines were maintained in complete RPMI (media supplemented with 10% heat inactivated fetal calf serum , 2 mM glutamine and 1% P/S). Human peripheral blood mononuclear cells were isolated from leukopacks (New York Blood Center) by ficoll separation. Activated human T-cells (huATC) were generated by stimulating healthy donor T-cells (consented in protocol NCT02650648) with Human T-Activator CD3/CD28 Dynabeads (Invitrogen) and 30 U/ml of human IL-2 (Proleukin) according to manufacturer guidelines. T-cells were stimulated twice, at day 1 and again at day 8. Fresh IL-2 was supplemented daily. For *in vitro* assays (cytotoxicity, cell binding or conjugate assays) huATC were used between day 15 and 18 of culture (twice stimulated). For *in vivo* experiments huATC were used at day 8 of culture (once stimulated). Patient-derived xenograft (PDX) tumors were established by the antitumor core at MSKCC from surgical samples of patients (consented in protocol NCT00588068).

Cell binding measurements

Cell binding of bispecific antibodies was measured by flow cytometry. huATCs, IMR32 or M14 cells were incubated with each BsAb, followed by either an anti-human Fc secondary (Southern Biotech, Goat anti-human IgG-PE, Cat2040-09) or an anti-3F8 or anti-OKT3 idiotype antibody and the corresponding secondary, a goat anti-rat IgG-APC (Biolegend, Clone Poly4054, Cat405407) or a goat anti-mouse IgG-PE (Southern Biotech, 1010-09), respectively. Anti-idiotype antibodies were generated at Memorial

Sloan Kettering and validated by ELISA. All incubations were for 30 minutes at 4°C. Multiple independent binding experiments were combined and normalized into bar graphs that represent geometric mean fluorescence. Histogram overlays show representative examples. Samples were acquired using a BD FACSCalibur and analyzed by FlowJo 10.5.3 and GraphPad Prism 8. Error bars represent standard deviation.

Affinity measurements

Binding kinetics were evaluated using SPR (GE) as described previously (Xu et al., 2015). Briefly, SA or CM5 chips were coated with biotin-GD2 (Elicityl Oligotech) or huCD3δε (Acro Biosystems) antigens, respectively. A five step titration series of each BsAb were flowed over them, followed by two blank cycles and two regeneration cycles. Binding affinities were calculated using a two-state reaction model with the GE Biacore Evaluation software. Data was plotted using GraphPad Prism 8.

Cytotoxicity measurements

Cytotoxicity was evaluated using a ^{51}Cr release assay as described previously (Xu et al., 2015). Briefly, target cells were incubated with sodium chromate (100 μCi per one million cells) for one hour and mixed with huATC (10:1 E:T) and serially titrated bispecific, in triplicate. After four hours, released ^{51}Cr was measured using a γ-counter (Perkins-Elmer). Cell lysis was calculated using the formula [Sample Lysis – Spontaneous lysis]/[Total Lysis – Spontaneous Lysis], where spontaneous lysis measured released ^{51}Cr from target cells without antibody or T-cells, and total lysis measured released ^{51}Cr from target cells mixed with 10% SDS. Specific lysis was calculated by subtracting the measured release from a sample without antibody (T-cells and target cells only) from the calculated cell lysis. To calculate the EC_{50}, curves were fitted using a four-parameter logistic fitting with GraphPad Prism 8. Error bars represent standard deviation.

Animal models

All experiments were performed in compliance with all relevant ethical regulations and in accordance with an Institutional Animal Care and Use Committee-approved protocol (protocol 09-05-010). All mice were bred in the MSKCC animal facility. Two mouse models were used: (1) an immunodeficient xenograft model (Lopez-Albaitero et al., 2017), (2) and a transgenic huCD3ε-expressing syngeneic model (Gedeon et al., 2018).

For the xenograft model DKO mice (BALB/c IL-2rγ$^{-/-}$, Rag2$^{-/-}$) mice were implanted intravenously or subcutaneously with tumor cell lines or patient derived xenografts, M14 (two million cells) and IMR32 (four million cells) or processed patient derived xenograft (PDX) tumor (1:10). For the mixed PBMC model, tumor cells and purified human PBMCs were mixed at a 1:1 ratio before subcutaneous implantation and did not receive additional human lymphocytes. For other models, tumors were left to grow for 5-15 days, before being treated intravenously with PBMCs (10 million cells, once per week), huATC (40 or 20 million cells, once or twice per week, respectively) or armed huATC (20 million cells, twice per week). BsAb was administered intravenously for all models (25 pmol per dose, twice per week). The BiTE was dosed daily (180 pmol per dose) for two weeks to account for poorer pharmacokinetics. Mice treated with huATC received human IL-2 subcutaneously (1,000 U, twice per week) for three weeks.

For the syngeneic model, B6.Cg-Tg(CD3E)600Cpt/J (huCD3ε-tg) mice were bred with wildtype C57BL/6 mice to generate huCD3ε-tg F1 heterozygotes, which were used for all experiments. From here, 8-16 week old male mice were implanted subcutaneously with 50,000 EL.4 lymphoma cells. After seven days, mice were treated intravenously

with bispecific antibody (25 pmol, twice per week) for three weeks. The BiTE was dosed daily (7 pmol per dose) for three weeks to account for poorer pharmacokinetics.

All cell line implantations used Matrigel™ (Corning) at a ratio of 3:1 by volume (Matrigel™ to cells). PDX tumors were implanted by the anti-tumor assessment core facility at MSKCC. For all animal experiments, weights and tumor volumes were measured once per week and overall mouse health was evaluated at least three times per week. Intravenous tumors were measured by luminescence. Subcutaneous tumor volumes were calculated using a TM900 measurement device (Peira) or caliper. For caliper measurements, the following formula was used to estimate tumor volume: [(L) x (W) x (W) x 0.5], where L is the longest diameter of the tumor, and W is the diameter perpendicular to L. Mice were sacrificed once tumor volumes reached 1.5-2.0 cm^3 volumes. No treatment related toxicities (weight loss, hair loss, weakness, etc.) were observed in any mice throughout these experiments. All treatment groups contained five mice co-housed in the same cage. Data was plotted using GraphPad Prism 8. Error bars represent standard deviation or standard error, as noted.

Conjugate formation

huATC were labeled with CFSE (Invitrogen, CatC34554) and M14 melanoma cells were labeled with Cell Trace Violet (Invitrogen, CatC34557). Cells were incubated with 2.5 μM of dye (50 million cells per one ml, in PBS) for five minutes at room temperature. The reaction was quenched by the addition of 10-fold excess of complete RPMI and incubated at 37°C for 20 min. After one wash, effector and target cells were mixed (1:5 E:T) and added to serially titrated bispecific antibody, in duplicate. After 30 minutes of incubation at 37°C, cells were fixed (2% PFA) for 10 min (room temperature) and washed once in PBS. Cells were acquired using a BD Fortessa and analyzed using

FlowJo 10.5.3. Curves were fitted using a four-parameter logistic fitting with GraphPad Prism 8. Error bars represent standard deviation.

Activation assay

Human PBMCs were isolated from leukopacks (New York Blood Center) by ficoll separation. Naïve human T-cells were purified using Dynabeads™ Untouched™ Human T-cells Kit (Invitrogen). Purified T-cells were incubated with M14 melanoma cells (10:1 E:T) and serially titrated BsAb, in duplicate. After 20 hours, supernatant was collected and frozen at -80°C for subsequent analysis. Cell pellets were then stained with antibodies against CD4-APC (Biolegend, Clone OKT4, Cat317416), CD8-PerCP-Cy5.5 (Biolegend, Clone HITα, Cat300924), CD45-PE-Cy7 (Biolegend, Clone T200, Cat368532), and CD69-PE (Biolegend, Clone IV A91, Cat310906) to assess CD69 upregulation. For the 92-hour timepoint, T-cells were first labeled with 2.5 μM Cell Trace Violet, following the conjugate formation protocol. After co-culture, cells were stained with antibodies against CD4-APC (Biolegend, Clone OKT4, Cat317416), CD8-PerCP-Cy5.5 (Biolegend, Clone HITα, Cat300924), CD45-PE-Cy7 (Biolegend, Clone T200, Cat368532), and CD25-PE (Biolegend, Clone V T-072, Cat302606) to assess CD25 upregulation and Cell Trace Violet dilution. Cells were acquired using a BD Fortessa and analyzed using FlowJo 10.5.3. Curves were fitted using a four-parameter logistic fitting with GraphPad Prism 8. Error bars represent standard deviation.

Cytokine assay

Frozen supernatant from the activation assay (20 hour) was used to measure cytokine production during coculture. IL-2, IFNγ, IL-10, IL-6 and TNFα cytokines were measured with the 5-plex LEGENDplex™ Human Th1 Panel (Biolegend, Cat740723) according to manufacturer guidelines. Briefly, supernatants were diluted 5-fold and

mixed with appropriate amounts of sample buffer and prelabeled cytokine beads. After two hours of shaking incubation at room temperature, biotinylated secondary antibodies were added. Following a one hour incubation, PE-labeled streptavidin was added. After 30 minutes, samples were washed, acquired using a BD FACSCalibur and analyzed using FlowJo 10.5.3. Cytokine levels were calculated from a standard curve. Curves were fitted using a four-parameter logistic fitting with GraphPad Prism 8. Error bars represent standard deviation.

BiTE cytokine measurements were from assays using PBMCs were cultured (200,000 cells per well) with or without M14 cells (10,000 cells per well) in the presence of 6.7 nM BiTE at 37°C in a 96 well plate. Supernatants were harvested after 24 hours. The concentration of four different cytokines (IL-2, IL-10, IFN-γ and TNF-α) were assessed using an ELISA based cytokine assay (OptEIA™ human cytokine set, BD Biosciences) according to the manufacturer's instructions.

GD2 ELISA

The GD2 ELISA were performed as previously described (Cheng et al., 2015). Briefly, GD2 (1 μg/ml in 90% ethanol, 20 μl per well) was coated on vinyl 96-well plates overnight at room temperature. The plate was washed 5x with PBS in between all steps. The next day, plates were blocked for 1hr with 0.5% BSA in PBS. Subsequently, a titration of each BsAb as added and incubated at room temperature for two hours. Bound BsAb was detected with a two-step method. First a murine anti-HIS tag antibody (AbD Serotec) (1:1,000 dilutions) was added and incubated for an hour. Next, a goat anti-mouse antibody conjugated to horseradish peroxidase (1:3000 dilutions) (Jackson ImmunoResearch) was added incubated at RT for one hour. Finally, the plate was developed colorimetrically by using the o-phenylenediamine (Sigma). The optical density

of each well was measured at 490 nm using an ELISA plate reader (Dynex Technologies).

Thermal stability measurements

The thermal stabilities were measured by differential scanning fluorimetry using the Protein Thermal Shift assay (Life Technologies). 4 μM of BiTE was mixed with Protein Thermal Shift dye and fluorescence was monitored using a StepOnePlus quantitative PCR machine (Applied Biosystems) with a 1% thermal gradient from 25°C to 99°C. Data were analyzed using Protein Thermal Shift Software (Applied Biosystems) to calculate the T_m. A hu3F8-scFv construct was analyzed and used to appropriately assign the correct peaks for the hu3F8-scFv and huOKT3-scFv in the BsAb constructs.

Calcium flux assay

Glass chamber slides (Invitrogen) were coated with lipid bilayers containing biotin as described (Abeyweera et al., 2011). Briefly, lipid coated slides were incubated with streptavidin, followed by biotinylated GD2 (0.02 μg/ml) and biotinylated ICAM-1 (1 μg/ml). Biointylated-GD2 was kindly provided by the Consortium for Functional Glycomics. HuATCs were loaded with fura-2 AM (Invitrogen) and then incubated with a given concentration of BiTE (1-10 nM). Cells were directly added to a chamber on the antigen coated slide and imaged for 30 minutes at 37°C, as previously described (Xu et al., 2015). Each chamber was imaged at intervals of 30 seconds (60 images) using a 20x objective lens (Olympus). For each chamber between 6-8 imaging fields (~100 cells/field) were acquired. Calcium induced fluorescence was measured at 340 nm and 380 nm wavelengths. T-cell activation was quantified using the ratio of 340 nm to 380 nm intensities during the plateau phase of the experiment (15-30 minutes after

acquisition). Data was analyzed in Graphpad Prism 8. Error bars represent standard deviation.

Molecular modeling

Homology model of hu3F8-scFv was generated the crystal structure of murine 3F8 (pdb code 3VFG) using Discovery Studio (Dassault Systemes, San Diego CA). Images were rendered using PyMol (Schrodinger LLC, New York NY).

Statistical analyses

GraphPad Prism 8.0 was used for statistical analyses. For flow cytometry and calcium flux experiments, comparisons between pairs of groups were made by student's t test. For *in vivo* experiments, we performed two-way ANOVA with subsequent Tukey correction. We did not use statistical methods to predetermine sample size of our animal studies. A sample size of five mice per group was chosen on the basis of our previous experience.

CHAPTER 1

SUCCESSFUL ENGINEERING OF A HIGHLY POTENT SINGLE-CHAIN VARIABLE-FRAGMENT (SCFV) BISPECIFIC ANTIBODY TO TARGET DISIALOGANGLIOSIDE (GD2) POSITIVE TUMORS

1.1 Introduction

Classic antibody therapies often require Fc-mediated effector functions to achieve their anti-tumor effect (Scott et al., 2012), greatly limiting their use of cytotoxic T lymphocytes (CTL). By fusing T-cell binding domains (commonly anti-human CD3ε) to tumor binding domains, one can efficiently harness the incredible potency of polyclonal CTLs to target non-MHC restricted tumor associated antigens (Spiess et al., 2015b). One example of this is the tandem single-chain variable fragment (scFv) bispecific antibody (BsAb), also known as the Bispecific T-cell Engager (BiTE), which been exploited to target various human malignancies, such as leukemia (Bargou et al., 2008; Topp et al., 2015), pancreatic cancer (Cioffi et al., 2012), skin cancer (Torisu-Itakura et al., 2011) and brain cancer (Choi et al., 2013). In December 2014, Blinatumomab became the first FDA approved T-cell engaging BsAb, for use in the treatment of leukemia (Topp et al., 2015). In addition to the BiTE, other platforms have been developed, such as tandem diabodies (Kipriyanov et al., 1999) or IgG-[L]-scFv fusions (Xu et al., 2015), with many now testing these formats in the clinic.

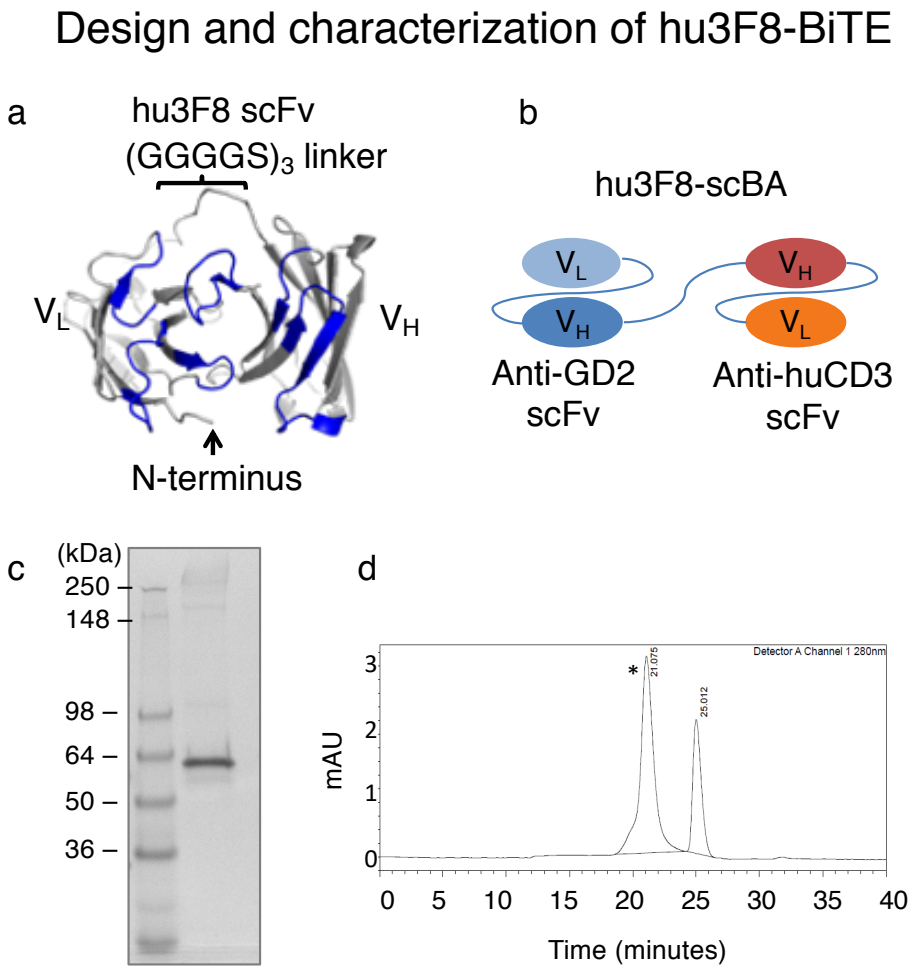

Figure 1. Design and characterization of hu3F8-BiTE

(a) Structural model showing a top down view of the antigen-biding site of hu3F8-scFv in the V_L-V_H orientation. CDR loops are colored in blue. A homology model was generated on Discovery Studio 4.1 (Dassault Systemes, San Diego, CA) using the crystal structure of murine 3F8 as a template (PDB 3VFG). The model was rendered in PyMol (Schrödinger LLC, New York, NY). (b) Diagram of hu3F8-BiTE, with anti-GD2 scFv in the V_L-V_H format, and the anti-CD3 scFv in the V_H-V_L format. (c) Reduced SDS-PAGE analysis of hu3F8-BiTE (d) HPLC profile of purified hu3F8-BiTE. The peak with a retention time of 21 minutes (*) is hu3F8-BiTE, while the following peak, with a retention time of 25 minutes, is from absorbance of salt in the buffer (sodium citrate).

Previously we have shown how affinity maturation of the anti-GD2 antibody 5F11, using a BiTE format, led to stronger potency anti-tumor responses, *in vitro* and *in vivo*, (Cheng et al., 2015). The antibody hu3F8 is a humanized variant of the murine anti-GD2 antibody 3F8 and undergoing clinical testing for GD2(+) malignancies such as neuroblastoma. Although hu3F8 bound GD2 stronger than 5F11, it had a substantially

weaker thermal stability. In the presented study, we evaluated the relative importance of tumor antigen affinity and protein thermal stability in driving T-cell dependent anti-tumor responses, *in vitro* and *in vivo*. We showed that while thermal stability influenced developability, the benefits of even small differences in binding affinity (13-fold) largely outweigh them, and lead to substantial improvements in cytotoxicity (5,000-fold) *in vitro*. Furthermore, hu3F8-BiTE suppressed tumor growth *in vivo* and prolonged mice survival much more effectively than 5F11-BiTE in both neuroblastoma and melanoma xenograft models. These findings provide important guidelines for improving BsAb function and exemplify the relative importance of developability criteria compared with functional criteria.

1.2 Design and characterization of hu3F8-BiTE

The hu3F8-scFv was designed based on the crystal structure of the original murine 3F8 antibody (pdb 3VFG), molecular docking simulations of 3F8:GD2 (Ahmed and Cheung, 2014), and the sequence of the humanized 3F8 antibody (hu3F8) (Cheung et al., 2012) (Fig. 1a). The V_L-V_H orientation was chosen to preserve the free N-terminus of the V_L domain, which was hypothesized to interact with the negatively charged head group of GD2. Utilizing identical linker and huOKT3-scFv sequences as previously reported for 5F11-BiTE (Cheng et al., 2015), hu3F8-BiTE was constructed and expressed in CHO-S cells (Fig. 1b). After selection of high expressers from stable pools, supernatants were collected and purified by affinity chromatography. Under reducing conditions, hu3F8-BiTE migrated at approximately 55 kDa (Fig. 1c). By SEC-HPLC, it migrated as the major peak (> 97%) with a retention time at 21 minutes confirming its molecular size (55 kDa) (Fig. 1d).

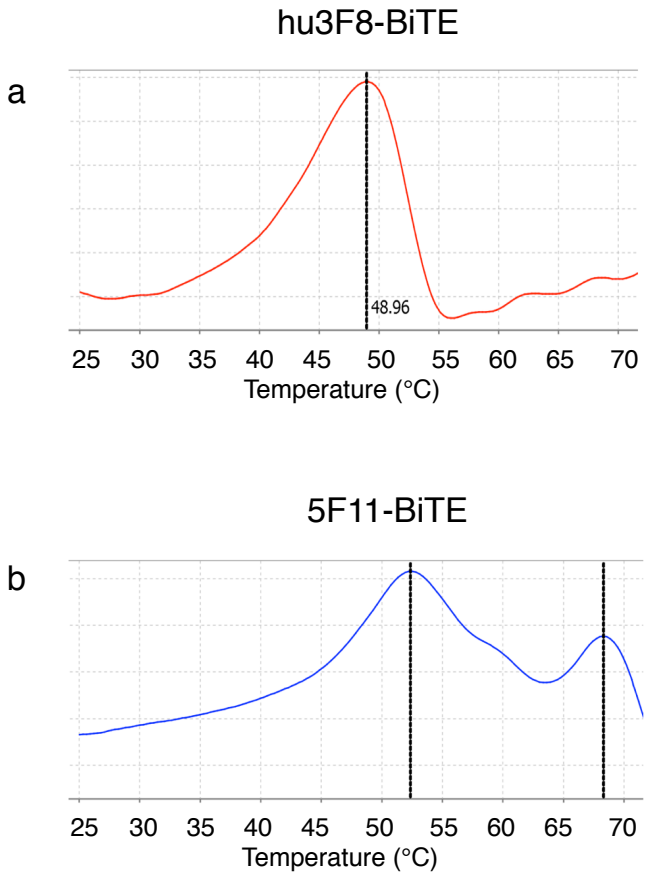

Figure 2. Thermal stability of hu3F8-BiTE and 5F11-BiTE
Melting temperature for (a) hu3F8-BiTE and (b) 5F11-BiTE was measured using differential scanning fluorimetry. Each peak corresponds to the unfolding of a domain (scFv) in the BiTE molecule. For hu3F8-BiTE both hu3F8-scFv and huOKT3-scFv peaks overlap. For 5F11-BiTE, huOKT3-scFv unfolds at 48°C while 5F11-scFv unfolds at 68°C. For reference: hu3F8-BiTE is red, and 5F11-BiTE is blue.

Table 1. Thermal stability of each scFv in 5F11-BiTE and hu3F8-BiTE

Constructs	T_m (°C) anti-GD2 scFv	T_m (°C) huOKT3 scFv
5F11-BiTE	68.2 ± 0.1	52.3 ± 0.1
hu3F8-BiTE	48.7 ± 0.2	48.7 ± 0.2

1.3 Stability and affinity of hu3F8-BiTE versus 5F11-BiTE

The best 5F11-BiTE, (Y)5VHVLDS(15)BA, which used a V_H-V_L orientation and included both a stabilizing disulfide bond and an affinity maturation mutation in the 5F11-scFv, was used as a reference for these studies (Cheng et al., 2015). Using differential scanning fluorimetry (DSF), the melting temperature (T_m) of each scFv was measured (Table 1). The T_m for hu3F8-scFv (48.7°C) was much lower than that of 5F11-scFv (68.2°C). Interestingly, the T_m of huOKT3-scFv was also influenced by the N-terminal scFv; with an N-terminal 5F11-scFv, the T_m was 52°C, but with hu3F8-scFv it became only 48.7°C (Fig. 2).

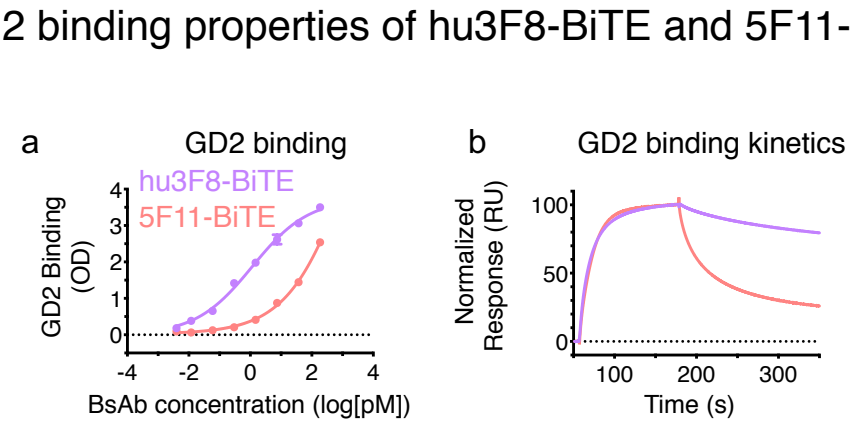

Figure 3. GD2 binding properties of hu3F8-BiTE and 5F11-BiTE
(a) Comparison of hu3F8-BiTE and 5F11-BiTE GD2 binding by ELISA (b) Comparison of hu3F8-BiTE and 5F11-BiTE GD2 binding kinetics by SPR. Sensorgram depicts 1,000 nM run from each BiTE binding to GD2, normalized to 100 RU. For reference: hu3F8-BiTE is purple, and 5F11-BiTE is red.

Additionally, hu3F8-BiTE showed much stronger binding to GD2 by ELISA (Fig. 3a). By surface plasmon resonance, the off rate (k_{off}) for hu3F8-BiTE was 25-fold slower ($8.2x10^{-4}$ 1/s) than it was for 5F11-BiTE ($2.0x10^{-2}$ 1/s), and the binding affinity (K_D), hu3F8-BiTE was 13-fold higher (19 nM) than 5F11-BiTE (250 nM) (Fig. 3b and Fig. 4).

Table 2. Cytokine release from PBMC in the presence of GD2-BiTE

	w/o GD2(+) Targets		w/ GD2(+) Targets	
Cytokines [pg/ml] (SD)	5F11-BiTE	hu3F8-BiTE	5F11-BiTE	hu3F8-BiTE
IFN-γ	2.5 (1.8)	1.94 (0.2)	94.7 (2.3)	524.9 (18)
TNF-α	12.6 (9.9)	16.4 (3.1)	1824 (16)	1743 (81)
IL-2	2.3 (1.6)	1.65 (0.1)	30.5 (2.4)	939.6 (69)
IL-10	39.4 (4.4)	39.9 (2.2)	136 (3.7)	176.9 (8.1)

1.4 Hu3F8-BiTE induces stronger Ca^{2+} flux and cytokine release than 5F11-BiTE

Despite the lower thermal stability, hu3F8-BiTE was able to stimulate human T-cells more effectively than 5F11-BiTE, as measured by both Ca^{2+} flux in T-cells and cytokine release in PBMCs (Fig. 5 and Table 2). On artificial lipid bilayers containing GD2, hu3F8-BiTE induced more Ca^{2+} flux per T-cell, over a 30min time lapse, at both 10 nM and 2 nM concentrations as compared to the 5F11-BiTE, indicative of more robust T-cell activation.

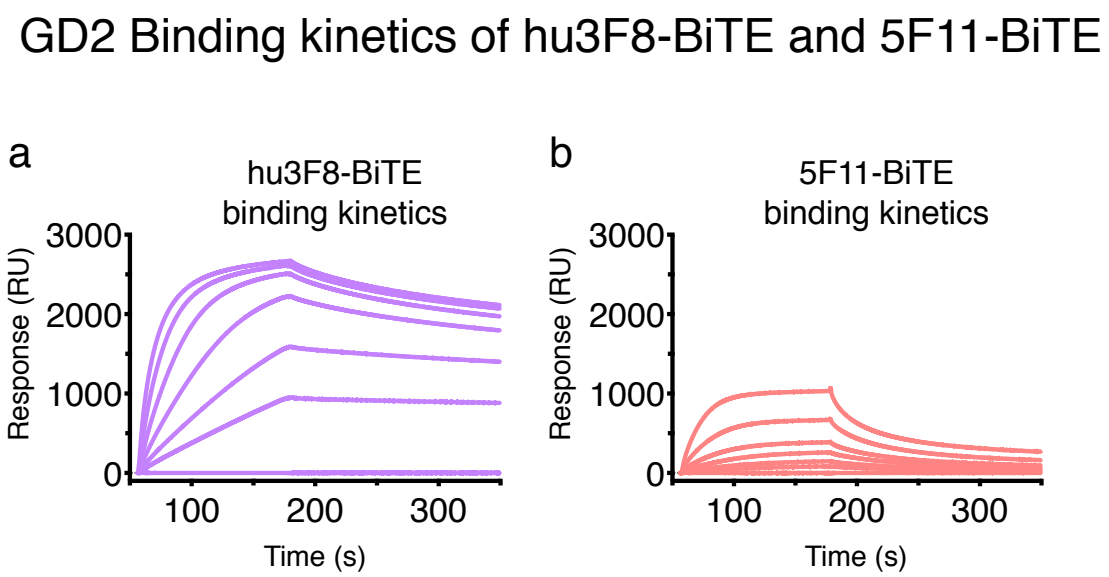

Figure 4. GD2 binding kinetics of hu3F8-BiTE and 5F11-BiTE
GD2 Binding kinetics of hu3F8-BiTE and 5F11-BiTE Surface plasmon resonance measurements of (a) hu3F8-BiTE and (b) 5F11-BiTE. Traces are shown at the following concentrations: 0, 62.5, 125, 250, 500, 1000 and 2000 nM. For reference: hu3F8-BiTE is purple, and 5F11-BiTE is red.

When incubated with GD2(+) cancer cell lines, hu3F8-BiTE induced higher cytokine release from human PBMCs than 5F11-BiTE. In the presence of M14 melanoma cells, hu3F8-BiTE induced significantly higher levels of IFN-γ, IL-2 and IL-10, production. Importantly, in the absence of target cells, levels of all four cytokines were barely detectable.

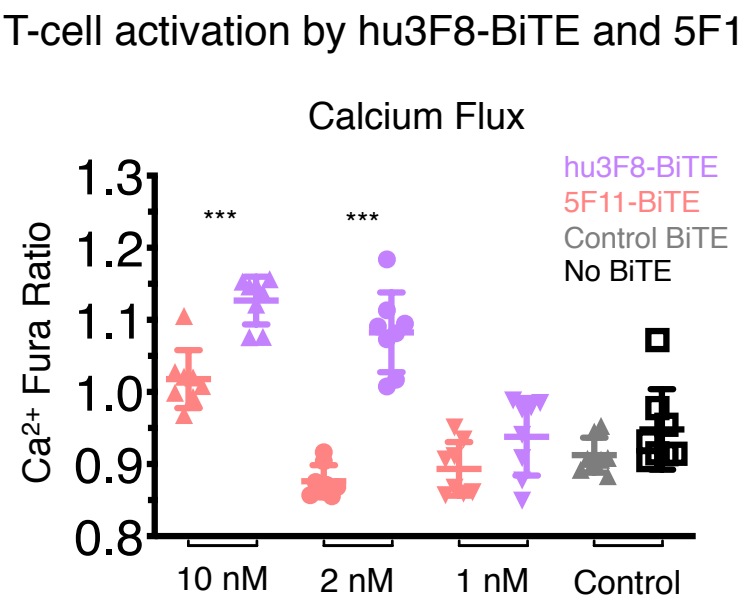

Figure 5. T-cell activation by hu3F8-BiTE and 5F11-BiTE
Human T-cells were preincubated with three different concentrations of BiTE (1-10nM) and imaged on artificial lipid bilayers containing ICAM-1 and GD2. Ca2+ responses were measured using fura-2AM. The fura ratio was calculated during the plateau phase of the calcium response (15-30 minutes), from 6-8 imaging fields per condition (~100 cells/field). Each dot represents the mean fura ratio of one field acquired over 15min. For reference: hu3F8-BiTE is purple, 5F11-BiTE is red, control BiTE is grey, and no BiTE is black. Statistical significances were obtained by unpaired students T-test ***P < 0.0001 for 5F11-BiTE compared to hu3F8-BiTE.

1.5 In vitro T-Cell dependent cytotoxicity mediated by hu3F8-BiTE versus 5F11-BiTE

The *in vitro* potency of hu3F8-BiTE in redirecting activated human T-cells (huATC) to kill cancer cell lines was assessed by chromium release assay. Hu3F8-BiTE induced highly efficient T-cell dependent killing of both neuroblastoma derived cell lines (IMR32) and melanoma derived cell lines (M14 and SKMEL-28) (Fig. 6a-c).

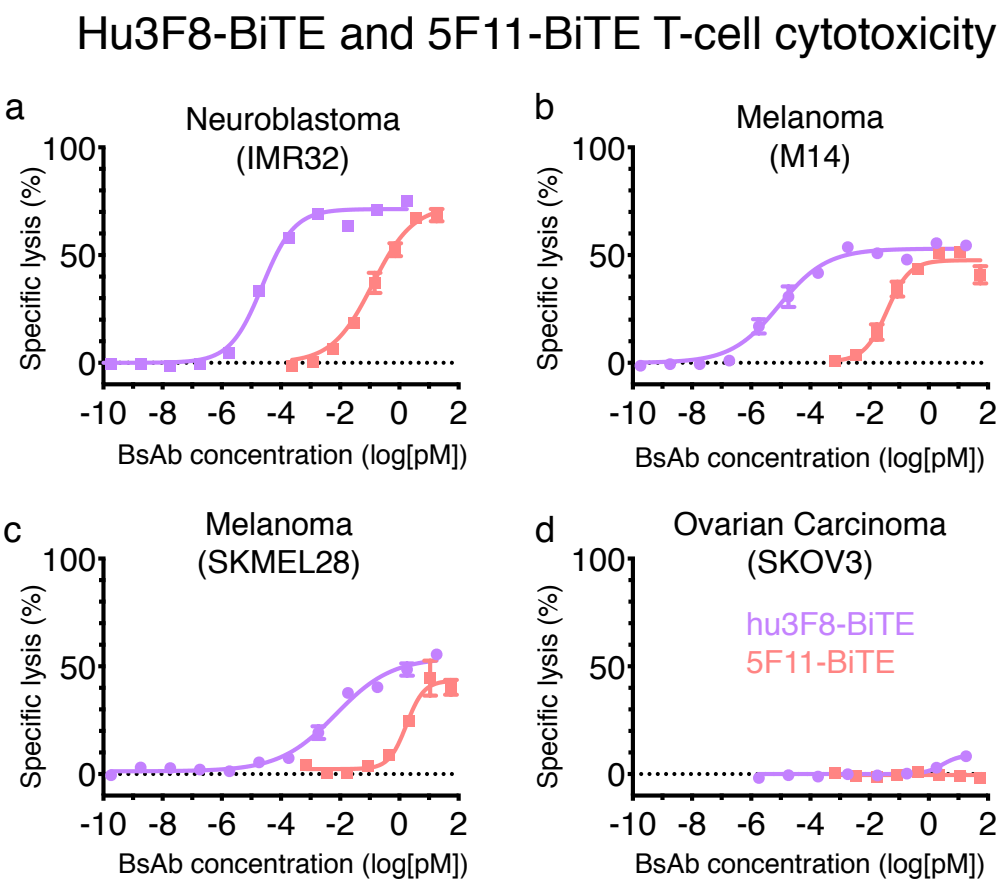

Figure 6. hu3F8-BiTE and 5F11-BiTE T-cell cytotoxicity
Cytotoxicity of each BiTE against (a) neuroblastoma, (b-c) melanoma or (d) a control cell line (GD2-negative), ovarian carcinoma. Each curve represents an antibody. For reference: hu3F8-BiTE is purple, and 5F11-BiTE is red.

The EC_{50}, as calculated from T-cell mediated killing curves, was compared between hu3F8-BiTE and 5F11-BiTE for each of the nine cancer cell lines assayed, including neuroblastoma, melanoma, osteosarcoma and ovarian carcinoma lines (Table 3). For high GD2 expressing cell lines (gMFI between 1,000 and 1,500) (Xu et al., 2015), such as IMR-32, M14, LAN-1 and NMB-7, the EC_{50} for hu3F8-BiTE (10 – 25 fM) was between 3,000- and 5,000-fold higher compared to that of 5F11-BiTE (40 – 140 pM). For low GD2 expressing cell lines (gMFI between 20 and 500) such as CRL1427, SKNBE(2)C, U2OS, SKMEL-28 (Xu et al., 2015) EC_{50} for hu3F8-BiTE (0.2 – 20 pM)

was between 100- and 1,000-fold higher compared to 5F11-BiTE (0.2 – 2.0 nM). For the GD2-negative cancer cell line SKOV3, neither hu3F8-BiTE nor 5F11-BiTE could mediate killing, confirming that both BiTE's redirection of huATCs were GD2 specific.

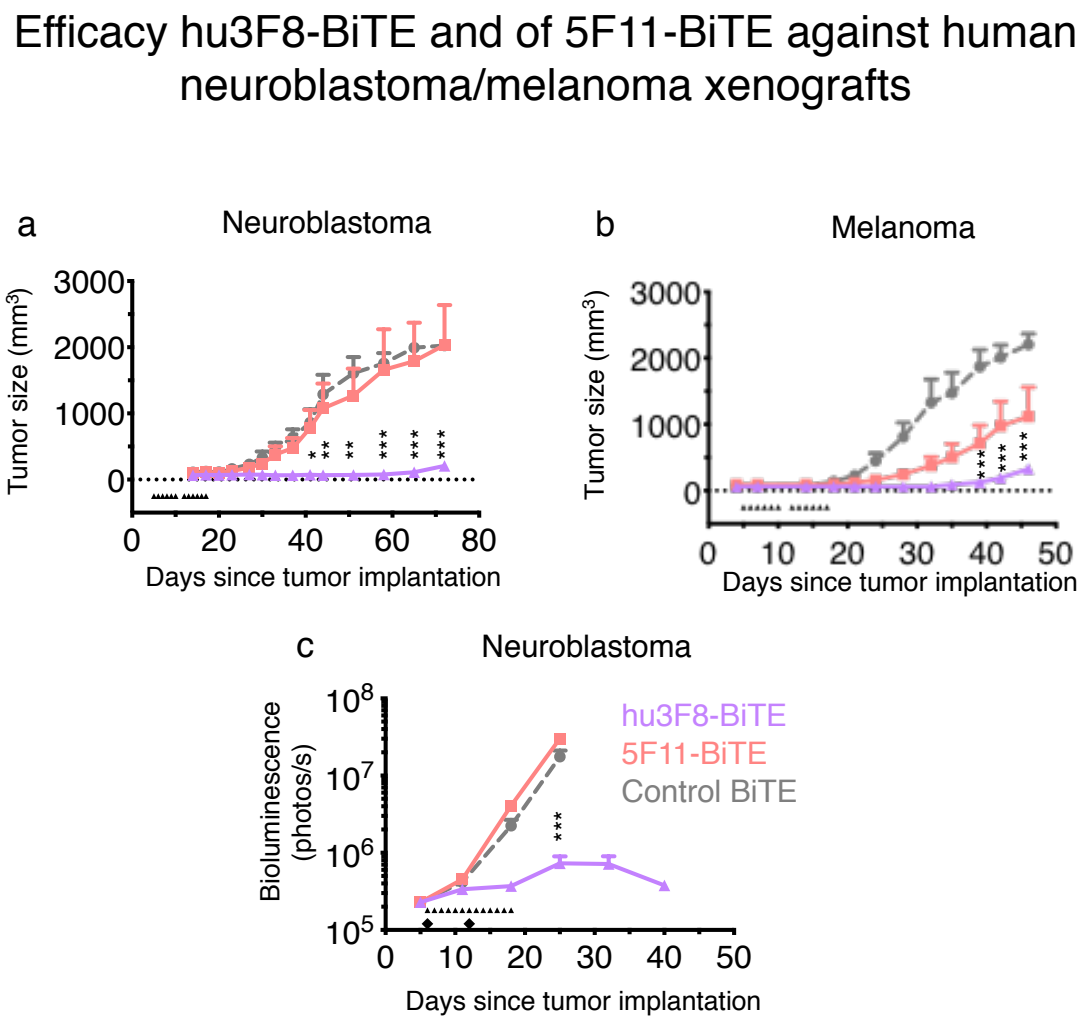

Figure 7. Efficacy of hu3F8 and 5F11-BiTE against neuroblastoma and melanoma xenografts

Tumor growth curves from xenograft models of (a) neuroblastoma or (b) melanoma. Tumors were implanted with a 1:1 mixture of PBMCs subcutaneously on day 0. (c) Systemic tumor growth of neuroblastoma cells in xenograft model. PBMCs were administered at day 6 and day 12 (black diamond). For all models, 180 pmol of BiTE was administered daily for two weeks (black triangle). Each line represents one treatment group (n=5). The dotted black line represents no measurable tumor. Day 0 represents the tumor implantation date. For reference: hu3F8-BiTE is purple, 5F11-BiTE is red and control BiTE is grey. All error bars represent standard error. Statistical significances were obtained by two-way analysis of variance (ANOVA) and Tukey correction. *P < 0.05, **P <0.001, ***P < 0.0001 for control BiTE or 5F11-BiTE compared to hu3F8-BiTE.

1.6 In vivo efficacy of hu3F8-BiTE vs. 5F11-BiTE

To compare the anti-tumor effects of hu3F8-BiTE vs. 5F11-BiTE *in vivo*, two different established (Xu et al., 2015) xenograft mouse models were used: (1) human cancer cell lines were either mixed with human PBMCs and implanted subcutaneously (PBMC model) (Fig. 7a, b) or (2) cancer cell lines were injected intravenously alone and once established, as determined by bioluminescence, human PBMCs were administered intravenously (Fig. 7c).

Table 3. EC_{50} of hu3F8- and 5F11-BiTE cytotoxicity against GD2(+) cell lines

Cancer Type	Cell Line (ATCC)	GD2 Expression (MFI)	EC_{50} (pM) (5F11-BiTE)	EC_{50} (pM) (Hu3F8-BiTE)	Fold (EC_{50})
Neuroblastoma	IMR-32 (CCL-127)	High	140	0.025	5553
Melanoma	M14	High	38	0.010	3707
Neuroblastoma	LAN-1	High	104	0.025	4121
Neuroblastoma	NMB-7	High	62	0.021	2952
Osteosarcoma	MG-63 (CRL-1427)	Low	264	0.22	1225
Neuroblastoma	SKNBE(2)C	Low	211	1.67	126
Melanoma	SKMEL-28 (HTB-72)	Low	1728	7.06	245
Osteosarcoma	U2OS (HTB-96)	Low	2038	19	105
Ovarian Carcinoma	SKOV3 (HTB-77)	Negative	N/A	N/A	NA

5F11-BiTE or hu3F8-BiTE treatments were administered daily. As shown in Fig. 7a, in the subcutaneous PMBC model (neuroblastoma), daily injection of 180 pmol of 5F11-BiTE had negligible effect on tumor growth, while the same dosing of hu3F8-BiTE suppressed tumor growth almost completely. Using another subcutaneous PBMC model (melanoma) (Fig. 7b), 5F11-BiTE treatments showed some anti-tumor effect while hu3F8-BiTE again showed significantly better tumor suppression. For the systemic tumor model (Fig. 7c), treatment was initiated on day 6, hu3F8-BiTE again suppressed tumor

growth effectively while 5F11-BiTE treatment showed no appreciable effect. Survival of mice treated with hu3F8-BiTE was substantially improved compared to those treated with 5F11-BiTE (Fig. 8).

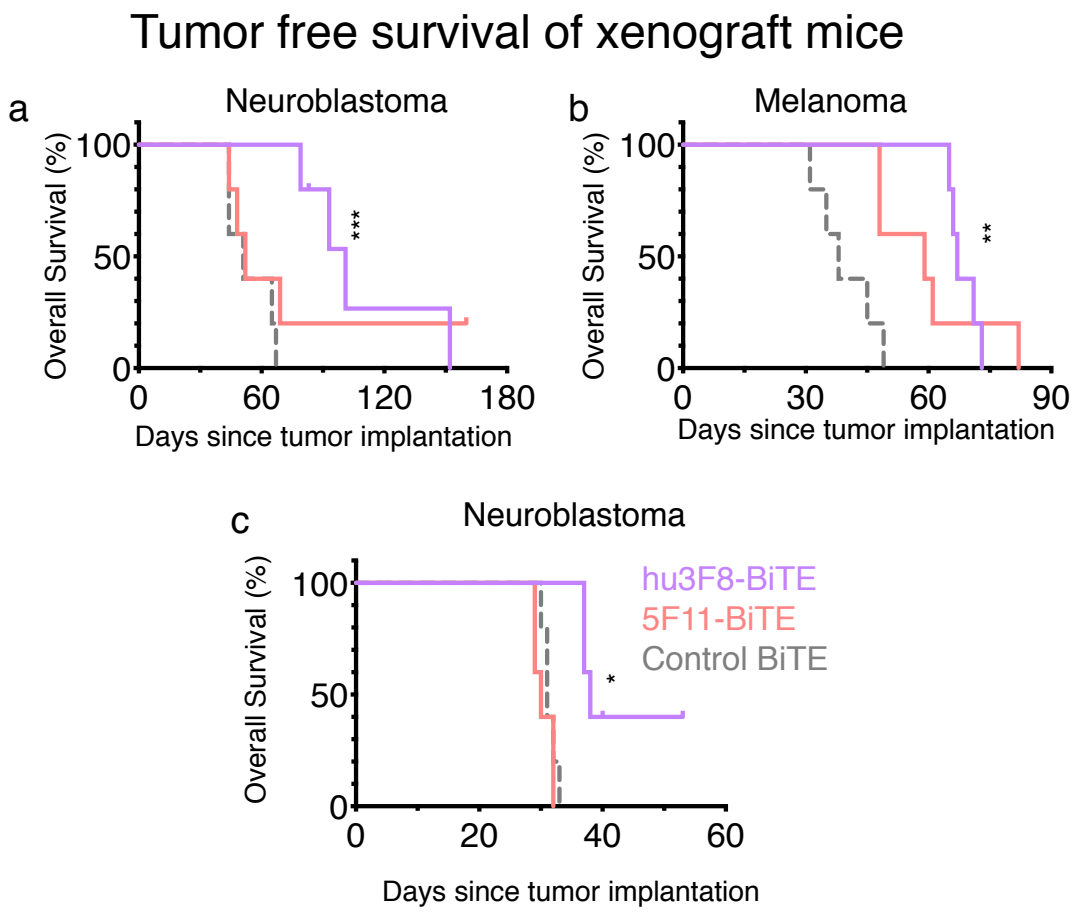

Figure 8. Tumor-free survival of xenograft mice
Tumor free survival curves correspond to tumor progression from Figure 7. For subcutaneous PBMC tumors (a, b), mice were sacrificed when tumor volume reached 2 cm^3. For the systemic tumors (c), mice either died of tumor burden or were sacrificed if they looked ill and unable to feed or ambulate. Cases were censored when mice were scarified or died without tumor. Statistical significances were obtained by Mantel-Cox test. *P < 0.05, **P <0.001, ***P < 0.0001 for control BiTE or 5F11-BiTE compared to hu3F8-BiTE.

1.7 Conclusions

In conclusion, we discovered that relatively modest increases in the affinity of an scFv can greatly increase cytotoxicity potency of BiTE molecules, despite reductions in

thermal stability. While thermal stability may play an important role in evaluating the developability and manufacturability of therapeutic proteins, our findings indicate that when seeking to improve functional activity for an scFv in BiTE therapeutics, improvements in affinity can have a significantly higher impact on tumoricidal activity.

CHAPTER 2

DUAL BIVALENCY SUBSTANTIALLY INCREASES POTENCY OF T-CELL BISPECIFIC ANTIBODIES

2.1 Introduction

To date only two bispecific antibodies (BsAb) designs have received FDA approval, the BiTE and the IgG-heterodimer (Shima et al., 2016; Topp et al., 2015). Both designs utilize monovalent interactions, and the BiTE, the only approved T-cell BsAb, continues to be a common platform for many new T-cell BsAb. Despite this, many newer but unproven designs have implemented anti-tumor bivalency, but fewer have implemented a dual bivalent strategy.

We have previously shown strong cytotoxicity using the dual-bivalent IgG-[L]-scFv and BiTE formats but have never compared them thoroughly. In the present study, we demonstrate how the IgG-[L]-scFv platform displays substantially higher potency than either of two FDA approved BsAb platforms: BiTE or IgG-Heterodimer (Fig. 9a). The IgG-[L]-scFv design proved more capable in antigen binding, *in vitro* functional assays and in two *in vivo* tumor models. As T-cell BsAb programs continue to fail clinically, more potent designs are needed. These findings provide an important framework for the development of future T-cell BsAb for cancer immunotherapy.

Table 4. *In vitro* properties and design of BsAb

BsAb	EC_{50}	Fold	GD2 Valency	CD3 Valency	K409R mAb	F405L mAb	SEC-HPLC Purity
2+2	38 fM	-	2	2	-	-	96%
1+1B	442 fM	12	1	1	-	-	86%
1+1H	79 pM	2095	1	1	IgG (hu3F8)	IgG (huOKT3)	98%
GD2.2 2+2	25 fM	-	2	2	-	-	98%
GD2.2 1+1H	21 pM	857	1	1	IgG (GD2.2)	IgG (huOKT3)	96%
GD2.3 2+2	49 fM	-	2	2	-	-	98%
GD2.3 1+1H	96 pM	1959	1	1	IgG (GD2.3)	IgG (huOKT3)	100%

2.2 Design and expression of three bispecific antibody platforms

We began our study by designing three different BsAb using a humanized anti-GD2 antibody sequence in combination with a humanized anti-huCD3ε antibody sequence, hu3F8 and huOKT3, respectively (Fig. 9a and Table 4). Variable domain gene sequences were cloned into mammalian cell expression vectors containing one or two promoters and expressed transiently in expi293 cells.

To make the BiTE (1+1B) design, hu3F8 and huOKT3 variable domains were made into scFv domains. Each scFv sequence used a 20 amino acid linker (four G_4S units) to separate V_H and V_L sequences. The two scFv domains were fused using a short five amino acid linker (G_4S), with hu3F8-scFv at the N-terminus and huOKT3-scFv at the C-terminus. A C-terminal hexahistadine tag was added for purification. BiTE designs were purified from culture supernatant by nickel purification and purity was assessed by SEC-HPLC.

Table 5. GD2 binding kinetics for BsAb using SPR

BsAb	K_D	Fold Change	k_a1 (1/Ms)	k_d1 (1/s)	k_a2 (1/s)	k_d2 (1/s)	MaxRU	Chi^2
2+2	2.5 nM	-	1.0E+06	1.1E-02	1.9E-02	5.6E-03	1514	2.6
1+1B	11 nM	5	2.2E+05	8.3E-02	2.5E-02	7.8E-04	1947	79.9
1+1H	15 nM	6	2.2E+05	5.8E-02	3.0E-02	1.8E-03	1231	2.7

The IgG-[L]-scFv format (2+2) was created by fusing a huOKT3-scFv to the C-terminus of a hu3F8-IgG light chain. Two point mutations, N297A and K322A, were also made in the hu3F8-IgG heavy chain to ablate Fc receptor (FcR) and complement activity, respectively. IgG-[L]-scFv protein was purified from culture supernatant by protein A affinity column separation.

To make the IgG-heterodimer (1+1H), hu3F8- and huOKT3-IgG proteins were first expressed as homodimers. Critically, the heavy chains of hu3F8-IgG and huOKT3-

IgG were mutated to include K409R or F405L mutations, respectively, in order facilitate heterodimerization (Table 4). Heterodimerization was achieved by using the fab-arm exchange (FAE) method (Labrijn et al., 2014). Hu3F8- and huOKT3-IgG molecules were mixed at a 1:1 molar ratio and incubated at 31°C under reducing conditions. After five hours, the reaction was dialyzed back to citrate buffer. After 18 hours of dialysis, the samples were moved to 4°C and dialyzed for another 24 hours before being analyzed by SEC-HPLC and CZE to identify yields and purity.

Table 6. huCD3ε binding Kinetics for BsAb using SPR

BsAb	K_D	Fold Change	k_a1 (1/Ms)	k_d1 (1/s)	k_a2 (1/s)	k_d2 (1/s)	MaxRU	Chi^2
2+2	5.8 nM	-	4.1E+06	2.0E-01	9.5E-03	1.3E-03	351	9.7
1+1B	13 nM	2	9.2E+07	2.5E+00	5.7E-03	5.6E-03	264	1.8
1+1H	130 nM	22	9.4E+05	1.2E+00	2.5E-02	2.7E-03	781	0.9

2.3 IgG-[L]-scFv BsAb is substantially more potent than other common BsAb designs

We began our study by comparing the IgG-[L]-scFv format to the two FDA approved BsAb designs: BiTE™ and IgG-Heterodimer (Fig. 9a and Table 4). Each BsAb was engineered to recognize ganglioside GD2 (GD2) on tumor cells and huCD3ε on T-cells using the variable domain sequences of hu3F8 (Cheung et al., 2014) and huOKT3 (Adair et al., 1994), respectively. The IgG-[L]-scFv format (hereafter called 2+2 for two anti-GD2 Fab and two anti-huCD3ε scFv) bound bivalently to both antigens, while the BiTE and IgG-heterodimer formats (hereafter called 1+1B and 1+1H, respectively, for one anti-GD2 domain and one anti-huCD3ε domain) bound each antigen monovalently.

In vitro comparison of IgG-[L]-scFv to common BsAb designs

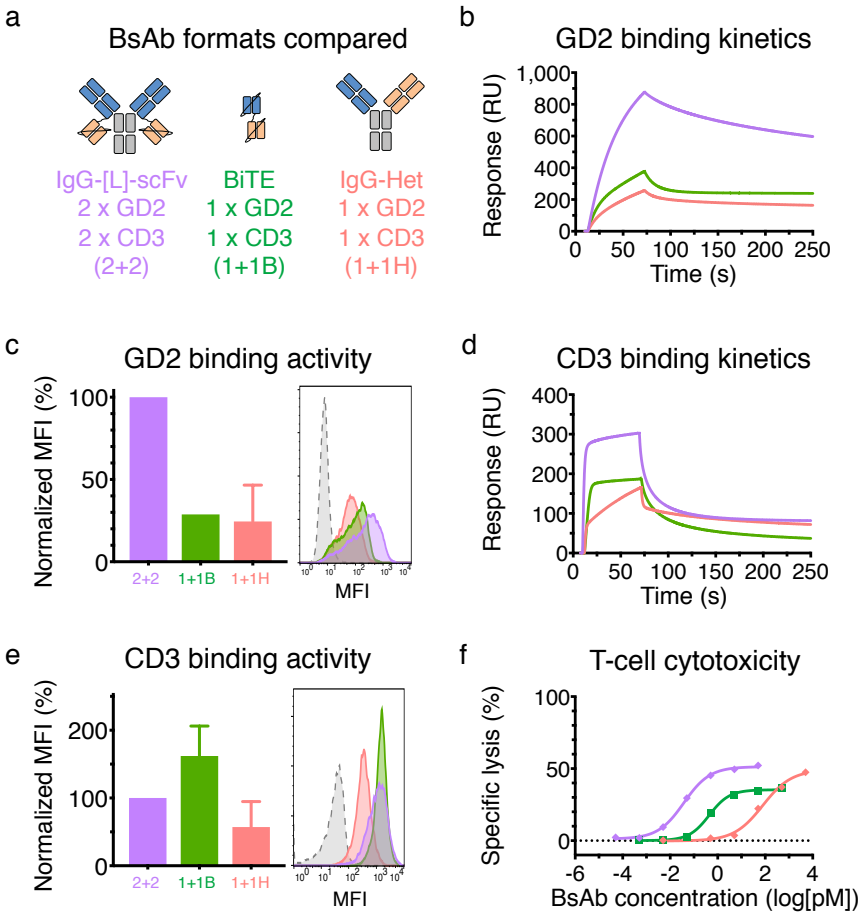

Figure 9. *In vitro* comparison of IgG-[L]-scFv to common BsAb designs
(a) Schematic of BsAb panel: IgG-[L]-scFv (2+2), BiTE™ (1+1B) and IgG-Heterodimer (1+1H). Orange represents anti-huCD3ε domains (derived from huOKT3) and blue represents anti-GD2 domains (derived from hu3F8). (b) GD2 and (d) huCD3ε binding kinetics using SPR. Each curve represents one BsAb at 50 nM. The first 60 seconds measure association (k_a) and final 180 seconds measure disassociation (k_d). Cell binding activity of each BsAb against (c) M14 (GD2) and (e) activated human T-cells (CD3), measured by flow cytometry. Bar graphs (left) represent the geometric MFI of each histogram (right) normalized to 2+2 (100%), from two independent experiments. (f) T-cell dependent cytotoxicity for each BsAb. Each curve represents one BsAb. All error bars represent standard deviation. For reference: 2+2 is purple, 1+1B is green, 1+1H is red, and the isotype control BsAb is grey.

To determine if there were any differences in antigen binding between each of these formats, we measured the binding kinetics of each BsAb against GD2 and huCD3ε using surface plasmon resonance (SPR) (Fig. 9b,d and 10, Tables 5 and 6). 2+2 displayed

substantially higher apparent affinity for both antigens (3 nM K_D for GD2 and 6 nM for huCD3ε) when compared to 1+1H (15 nM K_D for GD2 and 130 nM for huCD3ε) and 1+1B (11 K_D nM for GD2 and 13 nM for huCD3ε). Next, we evaluated binding to antigen-expressing cells by flow cytometry using anti-idiotypic antibodies that recognized the anti-huCD3ε or anti-GD2 binding domains of each BsAb (Fig. 9c,e). As expected, 2+2 bound more effectively than 1+1H to both GD2(+) human M14 melanoma cells and CD3(+) activated human T-cells (huATC). 2+2 also displayed better binding to M14 melanoma cells than did 1+1B, although both BsAb bound comparably to T-cells.

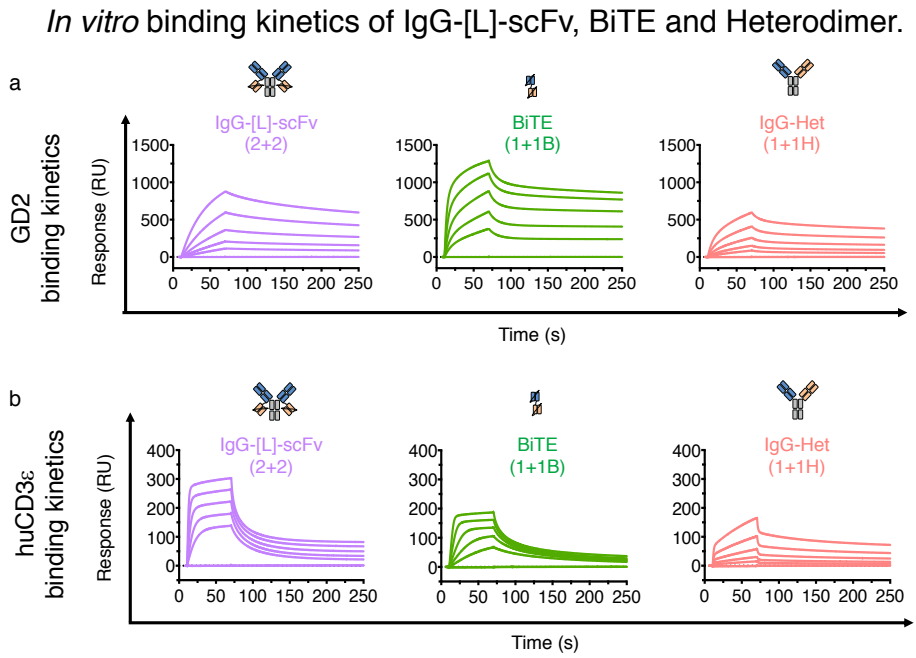

Figure 10. *In vitro* binding kinetics of IgG-[L]-scFv, BiTE and IgG-heterodimer
Binding kinetics against (a) GD2 and (b) huCD3ε, using SPR, with schematics (above) for reference. Each graph represents one BsAb and each curve represents one concentration. BsAb were titrated as follows: (GD2) IgG-[L]-scFv: 50 nM, 25 nM, 12.5 nM, 6.25 nM, 3.125 nM, 0 nM. BiTE or IgG-Heterodimer: 400 nM, 200 nM, 100 nM, 50 nM, 25 nM, 0 nM. (huCD3ε) All BsAb: 200 nM, 100 nM, 50 nM, 25 nM, 12.5 nM, 6.25 nM. For reference: 2+2 is purple, 1+1B is green, and 1+1H is red.

To compare the potency of each format, we performed *in vitro* cytotoxicity assays where the BsAb engaged huATC against M14 human melanoma cells (Fig. 9f and Table

4). Strikingly, 2+2 (38 fM EC_{50}) was over 2,000-fold more potent than 1+1H (79 pM EC_{50}) and over 10-fold more potent than 1+1B (442 fM EC_{50}). To confirm that these differences were not specific to the hu3F8 sequence, two additional anti-GD2 sequences (GD2.2, GD2.3) were used to build both 2+2 and 1+1H formats (Fig. 11 and Table 4). *In vitro*, these two constructs mirrored the cytotoxicity differences of the hu3F8-based 2+2 and 1+1H (857- and 1,959-fold respectively), suggesting that the dramatically enhanced potency of 2+2 was not specific to the hu3F8 sequence.

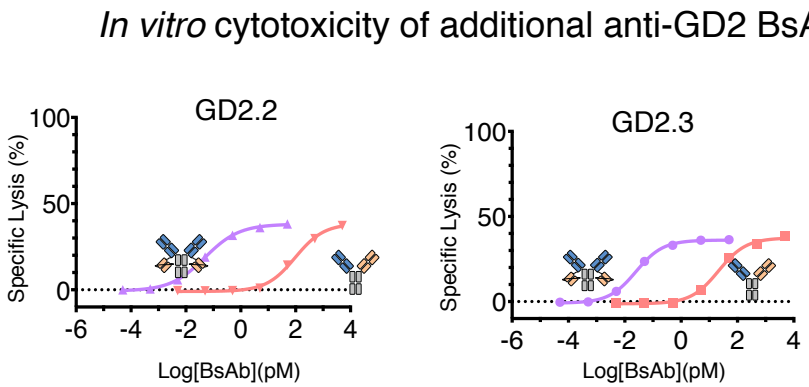

Figure 11. *In vitro* cytotoxicity of additional anti-GD2 BsAb
Each graph represents cytotoxicity from BsAb using a unique anti-GD2 sequence: GD2.2 (left) or GD2.3 (right) with schematics (above) for reference. Each curve represents one BsAb using each sequence. Error bars represent standard deviation. For reference: 2+2 is purple, 1+1H is red.

2.4 IgG-[L]-scFv bsAb is significantly more potent than other BsAb designs in vivo

We next investigated whether these substantial *in vitro* potency differences could translate into differences *in vivo* by using xenograft and syngeneic mouse tumor models (Fig. 12). First, we employed a xenograft model using immunodeficient IL-2rg$^{-/-}$ Rag2$^{-/-}$ BALB/c (DKO) (Lopez-Albaitero et al., 2017) mice (Fig. 12a). These immunodeficient mice were implanted subcutaneously with human melanoma tumors (M14) and treated intravenously with huATC and BsAb. Intravenous treatment with 2+2 elicited strong anti-tumor activity, shrinking large tumors (up to 300 mm^3) in all five treated mice (Fig.

12c and 13a). Treatment with 1+1H, by contrast, failed to confer any benefit relative to a control BsAb (IgG-[L]-scFv directed against an irrelevant tumor antigen).

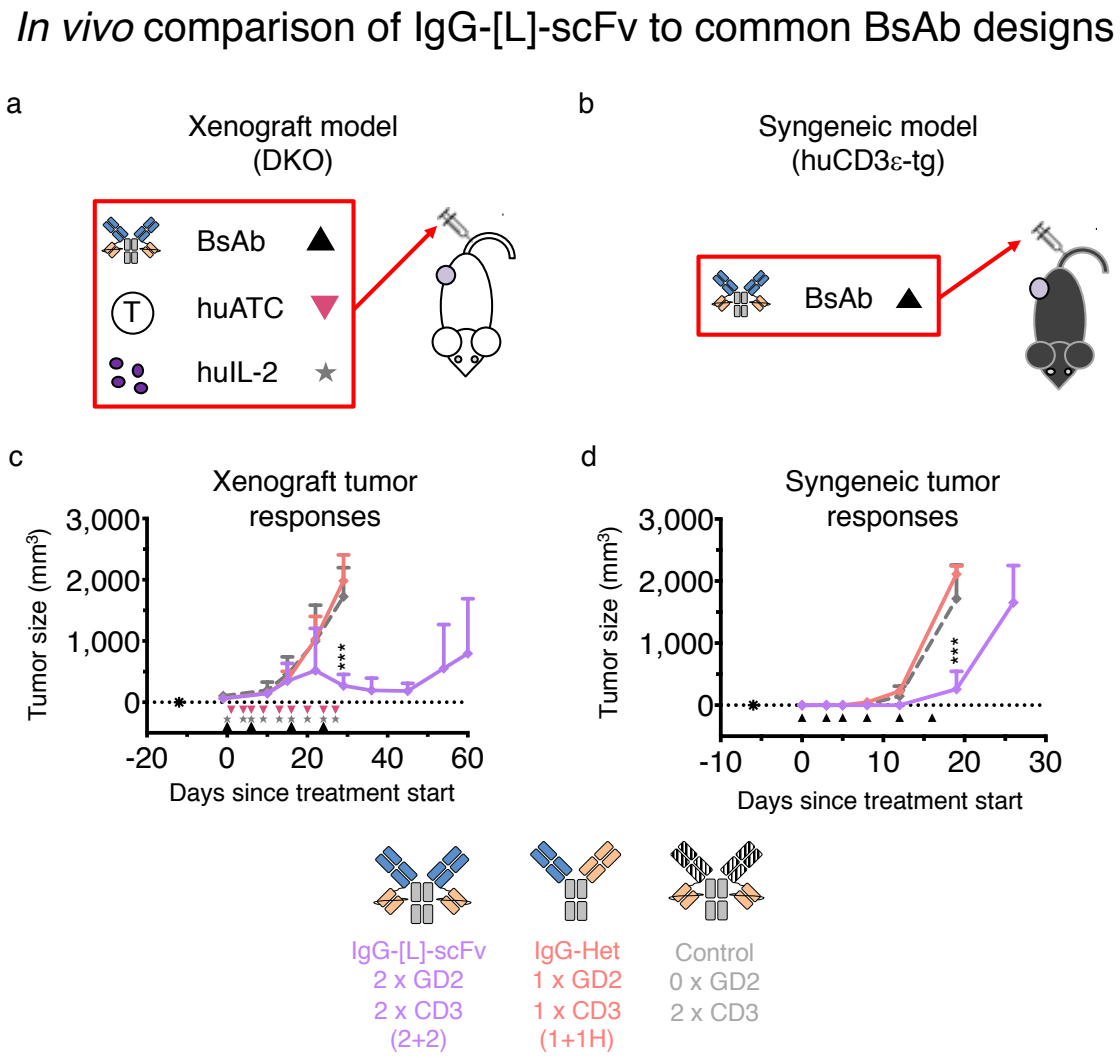

Figure 12. *In vivo* comparison of IgG-[L]-scFv to common BsAb designs
(a-b) Schematic of the treatment design for (a) xenograft tumor and (b) syngeneic models. For both models, 25 pmol of BsAb was administered intravenously twice per week (black triangle). For the xenograft model, 40 million activated human T-cells (huATC) were administered intravenously once per week (pink triangle) and human IL-2 (1,000 U) was administered subcutaneously twice per week (grey star). (c-d) Tumor growth for (c) xenograft and (d) syngeneic models. Each line represents one treatment group (n=5). (c) The xenograft model used an anti-GPA33 BsAb as a control and (d) the syngeneic model used an anti-HER2 BsAb as a control. The dotted black line represents no measurable tumor and the black asterisk represents the tumor implantation. Schematics (bottom) for reference: 2+2 is purple, 1+1H is red, and the control BsAb is grey. All error bars represent standard deviation. Statistical significances were obtained by two-way analysis of variance (ANOVA) and Tukey correction. ***P < 0.0001 for Control or 1+1H compared to 2+2.

In vitro binding kinetics of IgG-[L]-scFv, BiTE and IgG-Heterodimer

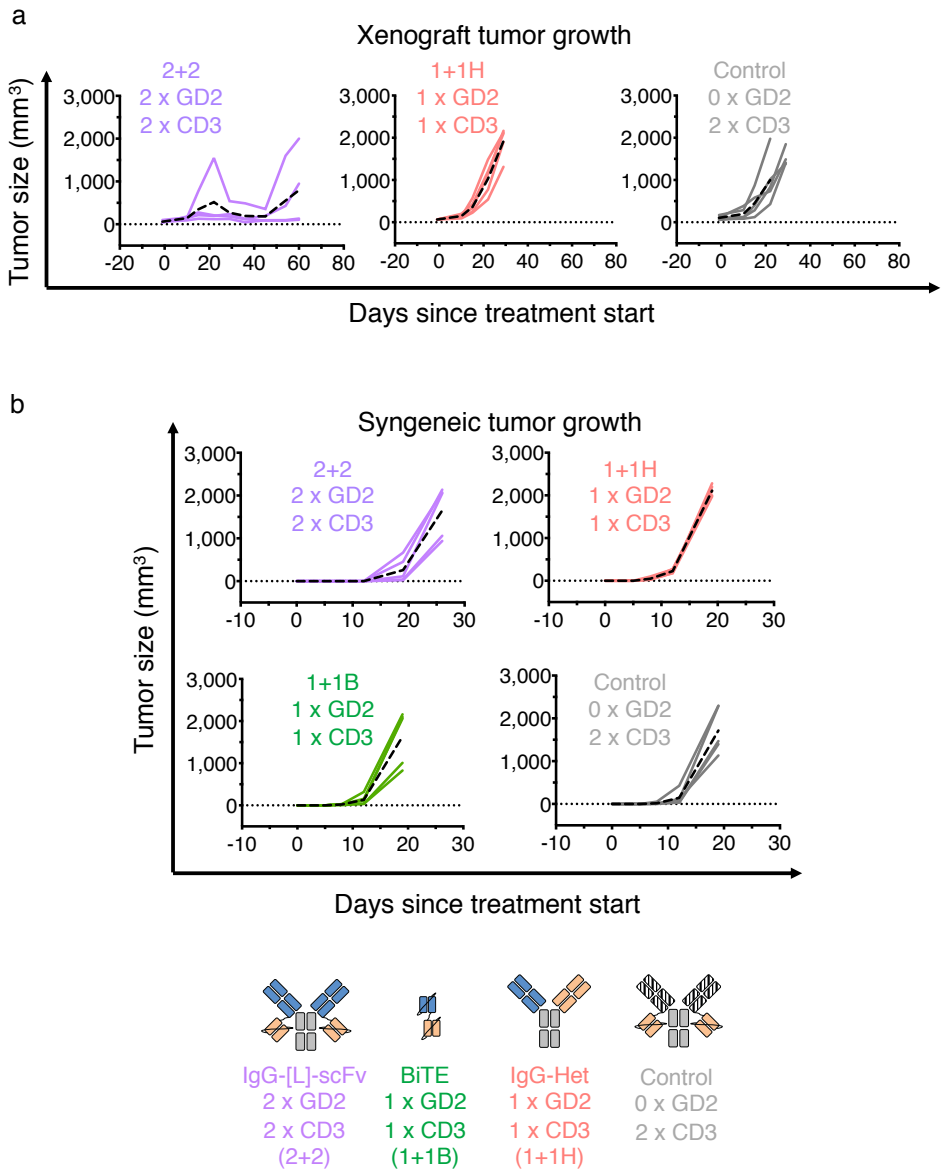

Figure 13. *In vivo* responses using xenograft and syngeneic models
Tumor growth in (a) xenograft and (b) syngeneic tumor models. Each figure represents one treatment group (n=5). Each solid line represents a single mouse, and the dotted line represents the group average. Tumor averages were calculated until one at least one mouse had to be euthanized. 1+1B received daily intravenous injections (7 pmol per dose) instead of twice per week dosing. Schematics (bottom) for reference: 2+2 is purple, 1+1B is green, 1+1H is red, and the control BsAb is grey.

Next, we compared 2+2 and 1+1H in a syngeneic mouse model (Fig. 12b) using immunocompetent C57BL/6 mice that carried a huCD3ε transgene (Gedeon et al., 2018) (huCD3ε-tg). T-cells in these mice co-expressed huCD3ε protein along with the native murine homolog, allowing us to directly test huCD3ε-specific BsAb. Similar to the xenograft model, intravenous treatment with 2+2 significantly inhibited the growth of subcutaneous GD2(+) EL.4 lymphoma tumors, while treatment with 1+1H failed to show any benefit (Fig. 12d and 13b). Additionally, attempts to treat these solid tumors with 1+1B also failed (Fig. 13b), even with daily dosing to compensate for its rapid renal clearance (Cheng et al., 2016).

Lastly, we implemented an "armed" T-cell xenograft model (Yankelevich et al., 2012) to help limit any confounding influences from the pharmacokinetic differences between each BsAb format (Fig. 14). In this model huATC were incubated with each BsAb just prior to injection into neuroblastoma PDX-bearing DKO mice, so that huATC were bound (armed) with similar amounts of anti-GD2 binding domains, as confirmed by flow cytometry. Nevertheless, only 2+2 armed huATC treated mice displayed anti-tumor activity, while 1+1H and 1+1B armed huATC failed to elicit any measurable responses. Taken together, these results demonstrated that the IgG-[L]-scFv format drove substantially more potent anti-tumor responses than either BiTE™ or IgG-Heterodimer *in vitro* and *in vivo*.

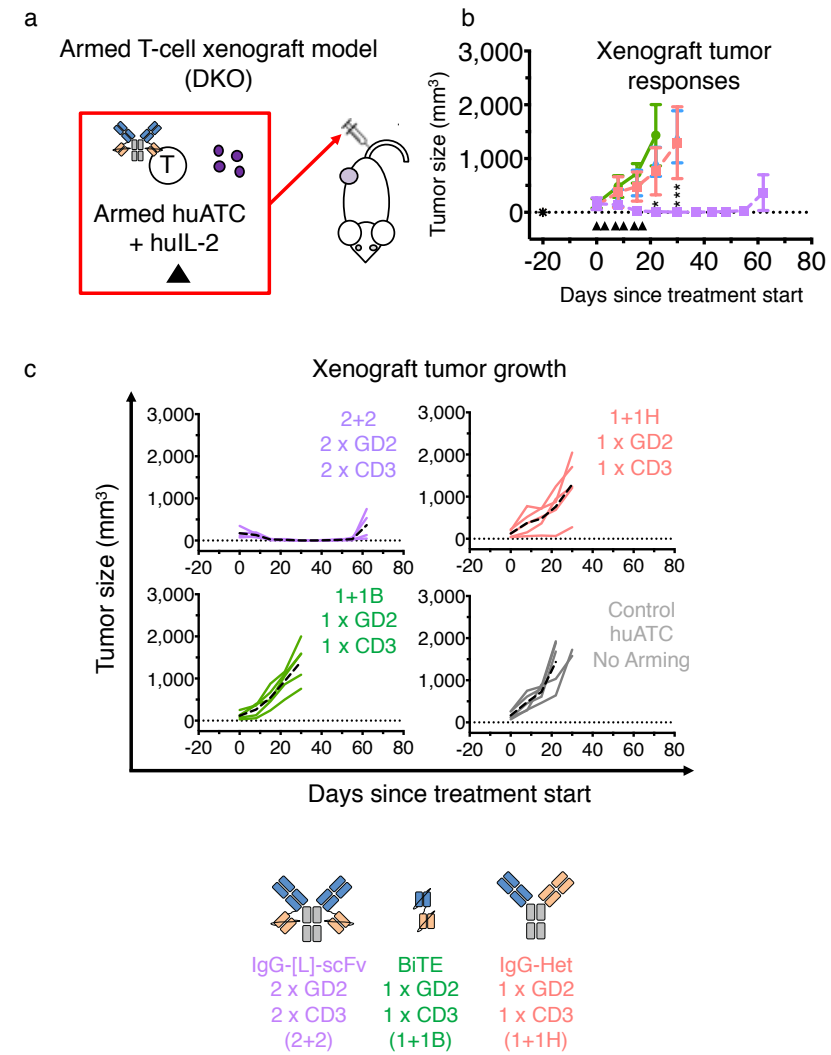

Figure 14. *In vivo* responses using "armed" T-cell xenograft model

(a) Schematic of treatment design for "armed" T-cell xenograft model. Armed human activated T-cells (huATCs) were administered intravenously along with human IL-2 (subcutaneously) twice per week. (b) Tumor growth for "armed" T-cell xenograft model. Each line represents one treatment group (n=5). Control mice received non-armed huATC as a reference (grey). Solid black triangles represent a dose of BsAb armed huATCs. The dotted black line represents no measurable tumor and the black star represents the tumor implantation. For each dose, 20 million huATC were armed with 50 pmol of IgG-[L]-scFv, 200 pmol of BiTE or 100 pmol of IgG-heterodimer. (c) Individual tumor growth for the "armed" T-cell xenograft model. Each figure represents one treatment group (n=5). Each solid line represents a single mouse, and the dotted lines represents the group average. Tumor averages were calculated until one at least one mouse had to be euthanized. All error bars represent standard deviation. Schematics (bottom) for reference: 2+2 is purple, 1+1B is green, 1+1H is red. Statistical significances were obtained by two-way analysis of variance (ANOVA) and Tukey correction. *P < 0.001, ***P < 0.0001 for Control, 1+1B or 1+1H compared to 2+2.

2.5 Conclusions

These studies confirmed that the dual bivalent IgG-[L]-scFv platform displays substantially higher potency than either BiTE of IgG-heterodimer platforms, *in vitro* and *in vivo*. Although the differences in binding did not improve dramatically with the change from monovalency to bivalency, dual bivalency demonstrated unparalleled improvements in cytotoxicity and *in vivo* anti-tumor responses. Neither monovalent construct was able to display measure able anti-tumor effects in either xenograft or syngeneic models, even with differences in pharmacokinetics were accounted for by increasing dose frequency or arming T-cells.

Our study also confirms the feasibility of developing BsAb with bivalency towards T-cells and tumor cells. While many new BsAb designs currently in clinical development use tumor bivalency to increase potency (Bacac et al., 2018; Bacac et al., 2016; Slaga et al., 2018) or to improve selectivity (Slaga et al., 2018), bivalency against T-cell epitopes has largely been avoided for fear of non-specific activation(Moore et al., 2011). However, our data suggests that this concern may be unfounded, at least for the IgG-[L]-scFv format, which failed to show any tumor-independent activation *in vitro*, and displayed no signs of cytokine release syndrome (CRS) *in vivo,* such as weight changes, piloerection, or hypotension (Amann et al., 2009; Brady et al., 2014). In fact, we have found that the IgG-[L]-scFv format induces far lower serum cytokine production *in vivo* compared to full length huOKT3 IgG (B.S. and N-K. C., manuscript in preparation). Although clinical toxicities have previously been associated with several bivalent T-cell engaging antibodies, some of these molecules retained binding affinity for Fc receptors (Gaston et al., 1991; Wing et al., 1996) and therefore could induce Fc-dependent CRS.

By contrast, all BsAb tested here contained silenced Fc domains, which eliminated both Fc and complement dependent lysis activity. It should also be noted that Blinatumomab, the FDA approved anti-CD19 BiTE, induces significant CRS despite being monovalent towards CD3 (Klinger et al., 2012). A phase I clinical trial of the GD2-specific 2+2 is currently underway (MSK IRB 18-034), and it will be interesting to compare any immune-mediated side effects with those that have been reported for monovalent BsAb.

CHAPTER 3

SPATIAL CONFIGURATION OF BINDING DOMAINS IS CRITICAL TO BISPECIFIC ANTIBODY FUNCTION

3.1 Introduction

We have previously described several highly potent T-cell engaging BsAb using the symmetric and dual bivalent IgG-[L]-scFv platform (Hoseini et al., 2018; Lopez-Albaitero et al., 2017; Wu et al., 2018; Xu et al., 2015), in which a single chain variable fragment (scFv) recognizing human CD3ε (huCD3ε) is fused to the C-termini of each antibody light chain (Fig. 15a). While this design has consistently provided exceptionally strong anti-tumor activity against multiple tumor antigens (ganglioside GD2, CD33, GPA33, HER2) *in vitro* and *in vivo*, the basis for its remarkable efficacy is poorly understood.

In the present study, we identify critical parameters behind the IgG-[L]-scFv platform's robust anti-tumor activity, many of which may be applicable to future T-cell BsAb designs. Through systematic re-engineering of the IgG-[L]-scFv design, we show that placing tumor and T-cell binding domains on the same side of a BsAb (cis-configuration), improves cytotoxic potencies 50-fold. Additionally, uniting two such cis-modules together to create a dual bivalent format increases *in vitro* cytotoxicity 30-fold, dramatically enhancing naïve T-cell responses *in vitro* and *in vivo*. Hence, the potency of a BsAb results not only from its antigen binding site multiplicity, but also from the spatial configuration of its antigen binding domains.

In vitro binding activities of IgG-[L]-scFv panel

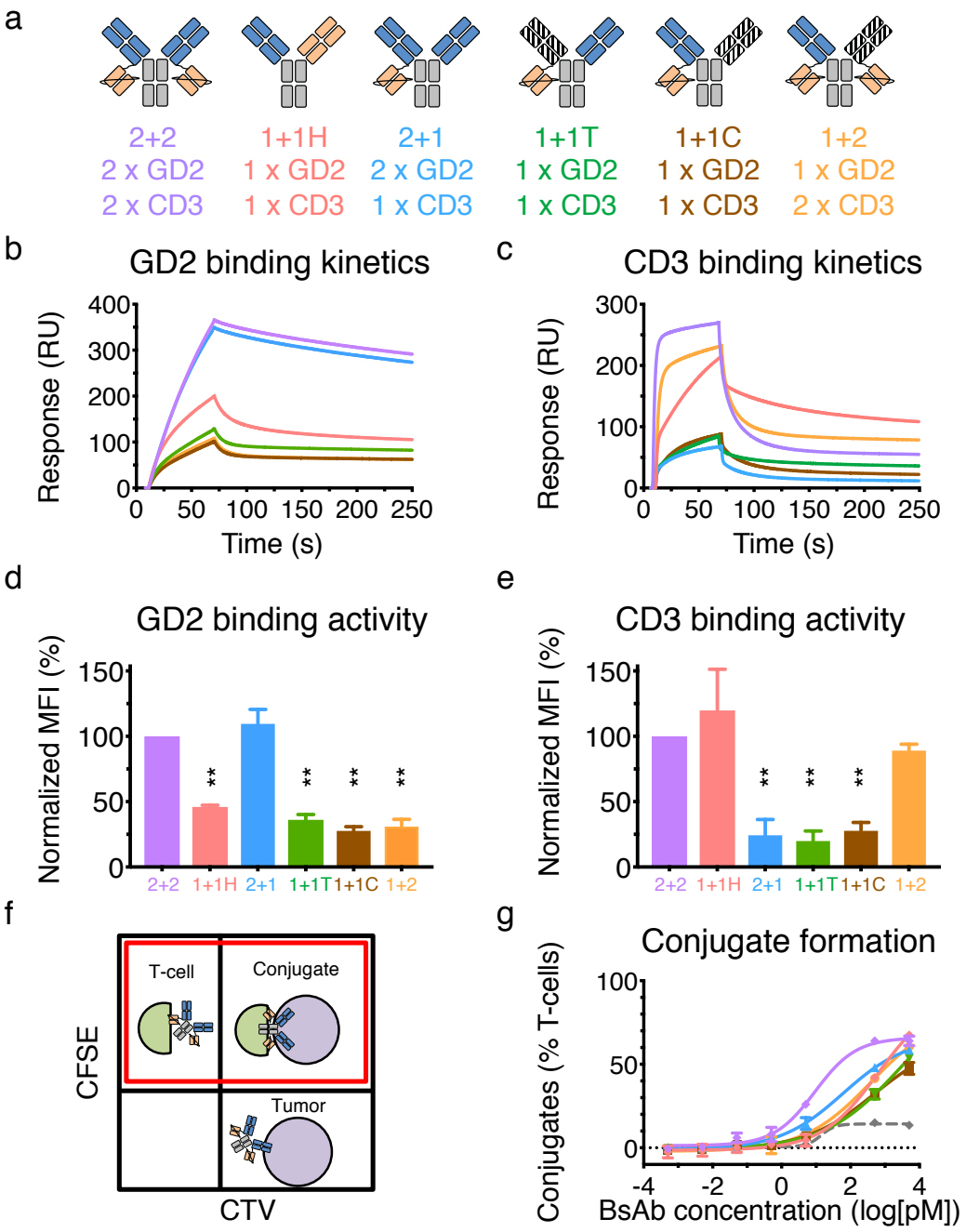

Figure 15. *In vitro* binding activities of IgG-[L]-scFv panel

(a) Schematic of IgG-[L]-scFv BsAb panel: 2+2, 1+1H, 2+1, 1+1T, 1+1C and 1+2. Orange represents anti-huCD3ε domains (derived from huOKT3), blue represents anti-GD2 domains (derived from hu3F8) and striped black represents irrelevant anti-tumor domain (derived from huM195). (b) GD2 and (c) huCD3ε binding kinetics using SPR. Each curve represents one BsAb at 50 nM. The first 60 seconds measure association (ka) and final 180 seconds measure disassociation (kd). Cell binding activity of each BsAb against (d) M14 (GD2) and (e) activated human T-cells (CD3) was measured using flow cytometry. Bar graphs represent the geometric MFI of each sample, normalized to 2+2 (100%), from three independent experiments. (f) Schematic of conjugate assay analysis. Unconjugated cells (upper left and lower right quadrants) only displayed fluorescence under one channel while conjugated cells (upper right quadrant) were double positive. For analysis, conjugate frequency was measured as the fraction of conjugated T-cells among the total T-cells (red box). (g) Graphed values represent conjugate formation per concentration of BsAb. Each curve represents one BsAb. Assays included an anti-CD33 BsAb as a control. All error bars represent standard deviation. For reference: 2+2 is purple, 1+1H is red, 2+1 is blue, 1+1T is green, 1+1C is brown, 1+2 is orange, and the control BsAb is grey. Statistical significances were obtained by two-tailed t-test. **P < 0.01 for (d) 1+1H, 1+1T, 1+1C or 1+2 compared to 2+2 or (e) 2+1, 1+1T or 1+1C compared to 2+2.

Table 7. *In vitro* properties and design of IgG-[L]-scFv panel

BsAb	EC_{50}	Fold Change	GD2 Valency	CD3 Valency	K409R mAb	F405L mAb	SEC-HPLC Purity	CZE Purity
2+2	26 fM		2	2	-	-	96%	-
1+1H	20 pM	748	1	1	IgG (hu3F8)	IgG (huOKT3)	98%	95%
2+1	240 fM	9	2	1	IgG (hu3F8)	IgG (hu3F8)-[L]-scFv (huOKT3)	95%	97%
1+2	773 fM	29	1	2	IgG (huM195)-[L]-scFv (huOKT3)	IgG (hu3F8)-[L]-scFv (huOKT3)	92%	95%
1+1C	784 fM	30	1	1	IgG (huM195)	IgG (hu3F8)-[L]-scFv (huOKT3)	94%	94%
1+1T	37 pM	1404	1	1	IgG (hu3F8)	IgG (huM195)-[L]-scFv (huOKT3)	94%	94%

3.2 Design and expression of IgG-[L]-scFv heterodimers

We began our study by designing five different BsAb. As before, variable domain gene sequences were cloned into mammalian cell expression vectors containing two promoters and expressed transiently in expi293 cells. All proteins were purified by affinity purification using Protein A. The parental IgG-[L]-scFv format (2+2) was created as discussed in chapter 2, fusing a huOKT3-scFv to the C-terminus of a hu3F8-IgG light

chain. Three additional parental molecules were generated using similar strategies (Table 7). An anti-CD33 IgG-[L]-scFv format was generated by exchanging the hu3F8-V_H and hu3F8-V_L domains with those of a humanized anti-CD33 antibody, huM195. Two IgG proteins were also expressed using either the hu3F8 or huM195 variable domain sequences. As before, all proteins contained two point mutations, N297A and K322A, to ablate Fc receptor (FcR) and complement activity, respectively. Furthermore, each heavy chain sequence included either K409R or F405L mutations to facilitate heterodimerization. All protein was purified from culture supernatant by protein A affinity column separation.

To make the various heterodimeric constructs each parental was first expressed as a homodimer. Heterodimerization was achieved by using the fab-arm exchange (FAE) method (Labrijn et al., 2014). Hu3F8 and huM195 IgG or IgG-scFv molecules were mixed at a 1:1 molar ratio and incubated at 31°C under reducing conditions. After five hours, the reaction was dialyzed back to citrate buffer. After 18 hours of dialysis, the samples were moved to 4°C and dialyzed for another 24 hours before being analyzed by SEC-HPLC and CZE to identify yields and purity.

Table 8. GD2 binding kinetics for IgG-[L]-scFv panel using SPR

BsAb	K_D	Fold Change	k_a1 (1/Ms)	k_d1 (1/s)	k_a2 (1/s)	k_d2 (1/s)	MaxRU	Chi^2
2+2	2.8 nM	-	6.2E+05	6.2E-03	2.3E-02	8.9E-03	735	0.1
2+1	2.5 nM	1	7.4E+05	7.0E-03	2.7E-02	9.9E-03	639	0.1
1+1C	30 nM	11	9.8E+04	1.1E-01	2.7E-02	7.7E-04	1336	1.1
1+2	31 nM	11	1.1E+05	9.8E-02	2.8E-02	9.7E-04	1293	4.4
1+1H	31 nM	11	1.7E+05	6.9E-02	2.2E-02	1.8E-03	1371	7.6
1+1T	27 nM	10	1.3E+05	1.0E-01	2.8E-02	9.6E-04	1286	1.8

3.3 Valency improves tumor and T-cell binding of IgG-[L]-scFv heterodimers

To better identify the properties of the IgG-[L]-scFv format responsible for the striking anti-tumor activities, we engineered four new IgG-[L]-scFv heterodimers (Fig. 15a and Table 7) to contain all possible combinations of valency and domain spatial configurations. 1+2 had one anti-GD2 domain replaced by a non-binding anti-huCD33 domain (Hoseini et al., 2018), 2+1 had one anti-huCD3ε domain removed, and each 1+1 had one anti-GD2 domain replaced and one anti-huCD3ε domain removed, either from the same side (cis) or from opposite sides (trans), named 1+1C and 1+1T, respectively.

Table 9. huCD3ε binding kinetics for IgG-[L]-scFv panel using SPR

BsAb	K_D	Fold Change	k_a1 (1/Ms)	k_d1 (1/s)	k_a2 (1/s)	k_d2 (1/s)	MaxRU	Chi^2
2+2	10 nM	-	9.7E+06	3.1E-01	4.2E-03	2.0E-03	323	8.5
2+1	310 nM	30	1.5E+05	1.4E-01	9.8E-03	5.2E-03	263	0.7
1+2	11 nM	1	3.2E+06	2.2E-01	7.5E-03	1.4E-03	308	4.9
1+1C	110nM	11	1.5E+05	6.6E-02	1.0E-02	3.5E-03	227	0.5
1+1T	94nM	9	1.0E+05	1.0E-01	2.2E-02	2.3E-03	321	0.5
1+1H	70nM	7	3.6E+05	3.6E-01	3.4E-02	2.6E-03	705	2.1

We began our comparative analyses by determining the antigen binding affinity of all constructs using SPR (Fig. 15b,c, and 16, Tables 8 and 9). As expected, BsAb containing two GD2-binding Fab (2+2 and 2+1) had higher apparent GD2 affinity (~3 nM K_D) than monovalent formats (1+2, 1+1T, 1+1C, 1+1H, ~30 nM K_D). Similarly, BsAb with two huCD3ε-binding scFv (2+2 and 1+2) had higher apparent CD3 affinity (~10 nM K_D) than formats with only one (2+1, 1+1T, 1+1C, 1+1H, 70-300 nM K_D). We also assessed the cell binding activity of each BsAb against M14 melanoma cells and huATC by flow cytometry, using an anti-Fc secondary antibody (Fig. 15d,e and 17). Consistent with the SPR data, bivalent BsAb exhibited stronger binding to cell-associated antigen than their monovalent counterparts did.

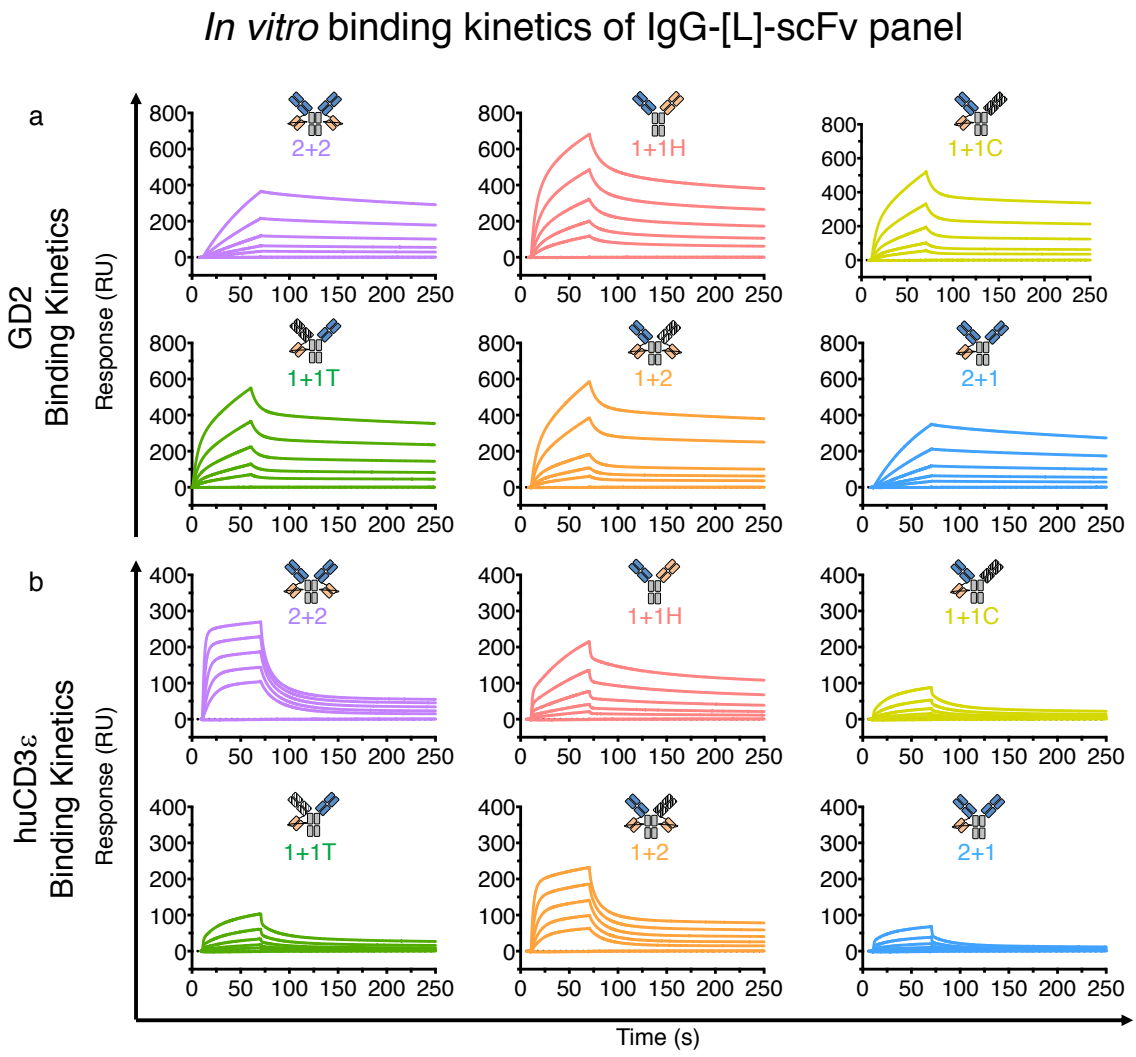

Figure 16. *In vitro* binding kinetics of IgG-[L]-scFv panel

Binding kinetics against (a) GD2 or (b) huCD3ε, using SPR, with schematics (above) for reference. Each graph represents one BsAb and each curve represents one concentration. BsAb were titrated as follows: (GD2) 2+2 or 2+1: 50 nM, 25 nM, 12.5 nM, 6.25 nM, 3.125 nM, 0 nM. 1+1T, 1+1C, 1+2, or 1+1H: 400 nM, 200 nM, 100 nM, 50 nM, 25 nM, 0 nM. (huCD3ε) All BsAb: 200 nM, 100 nM, 50 nM, 25 nM, 12.5 nM, 0 nM. For reference: 2+2 is purple, 1+1H is red, 2+1 is blue, 1+1T is green, 1+1C is yellow, 1+2 is orange, and control BsAb is grey.

To assess how differences in binding to GD2 and huCD3ε might synergize when both antigens were presented simultaneously, we performed an *in vitro* cell-to-cell conjugate assay using fluorescently labeled huATC and tumor cells (Fig. 15f). 2+2 induced T-cell:tumor cell conjugates most effectively, followed by 2+1 (Fig. 15g). The remaining formats (1+2, 1+1T, 1+1C, and 1+1H) exhibited markedly less conjugate

forming activity. These results indicated that bivalency, especially against the tumor, improved conjugate formation, an important step towards cytotoxicity. Importantly, 1+1C and 1+1T were indistinguishable in all of these experiments, indicating that the spatial configuration of tumor and T-cell binding domains did not impact either antigen binding or conjugate formation.

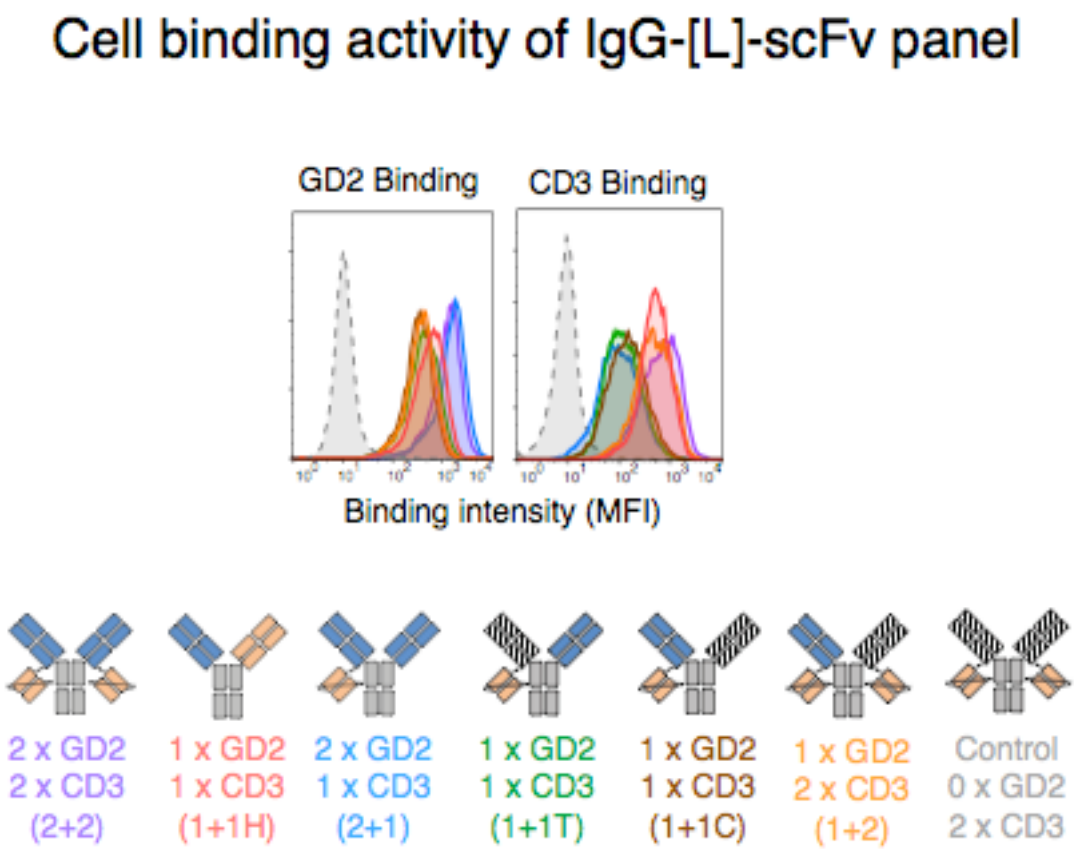

Figure 17. Cell binding activity of IgG-[L]-scFv panel
GD2 (left) and huCD3 (right) binding activity of each BsAb using flow cytometry. M14L (GD2) and human T-cells (huCD3) were stained with each 5 pmol of each BsAb. For reference: 2+2 is purple, 1+1H is red, 2+1 is blue, 1+1T is green, 1+1C is yellow, 1+2 is orange, and control BsAb is grey.

3.4 Valency and spatial configuration control IgG-[L]-scFv function in vitro

In vitro cytotoxicity assays targeting M14 melanoma cells revealed striking differences within the IgG-[L]-scFv panel (Fig. 18a and Table 7). 2+2 induced the most potent anti-tumor cytotoxicity (26 fM EC_{50}), followed by 2+1 (240 fM EC_{50}) and 1+2

(773 fM EC_{50}), which were ~9 fold and ~30 fold less potent, respectively. Surprisingly, 1+1C (780 fM EC_{50}) was essentially equipotent to 1+2, despite having markedly less huCD3ε binding activity. The potency of 1+1T (37 pM EC_{50}), by contrast, was similar to that of 1+1H (20 pM EC_{50}), which was ~50 fold worse than 1+2 and 1+1C, and nearly ~800-fold worse than 2+2. The unexpected difference in the potencies of 1+1C and 1+1T indicated that binding activity alone could not explain the exceptional efficacy of the IgG-[L]-scFv format and suggested that the spatial configuration of binding domains also played a crucial role.

To determine how differences in valency and spatial configuration impacted naïve T-cells, we performed *in vitro* co-culture assays (Fig. 19). These assays measured the capacity of each BsAb to stimulate naïve human T-cells, in the presence or absence of M14 melanoma cells, to upregulate CD25 or CD69, proliferate, and release the cytokine interleukin-2 (IL-2). In general, T-cell activation and proliferation followed the rank order observed before in cytotoxicity assays (Fig. 18b-d) and remained consistent in both CD4(+) and CD8(+) subsets (Fig. 20-22). 2+2 displayed the highest potency, both in terms of the fraction of T-cells with upregulated CD69 or CD25 and the absolute expression level of each activation marker. 1+1T was consistently the weakest variant, indistinguishable from 1+1H and about 200-fold less potent than 2+2. 2+1, 1+2, and 1+1C generally clustered together at intermediate levels of potency, with 2+1 displaying slightly more effective activation, followed by 1+2 and then 1+1C. Importantly, T-cells incubated with BsAb, but without tumor cells, did not exhibit these responses (Fig. 23), indicating that BsAb mediated T-cell activation was antigen-dependent.

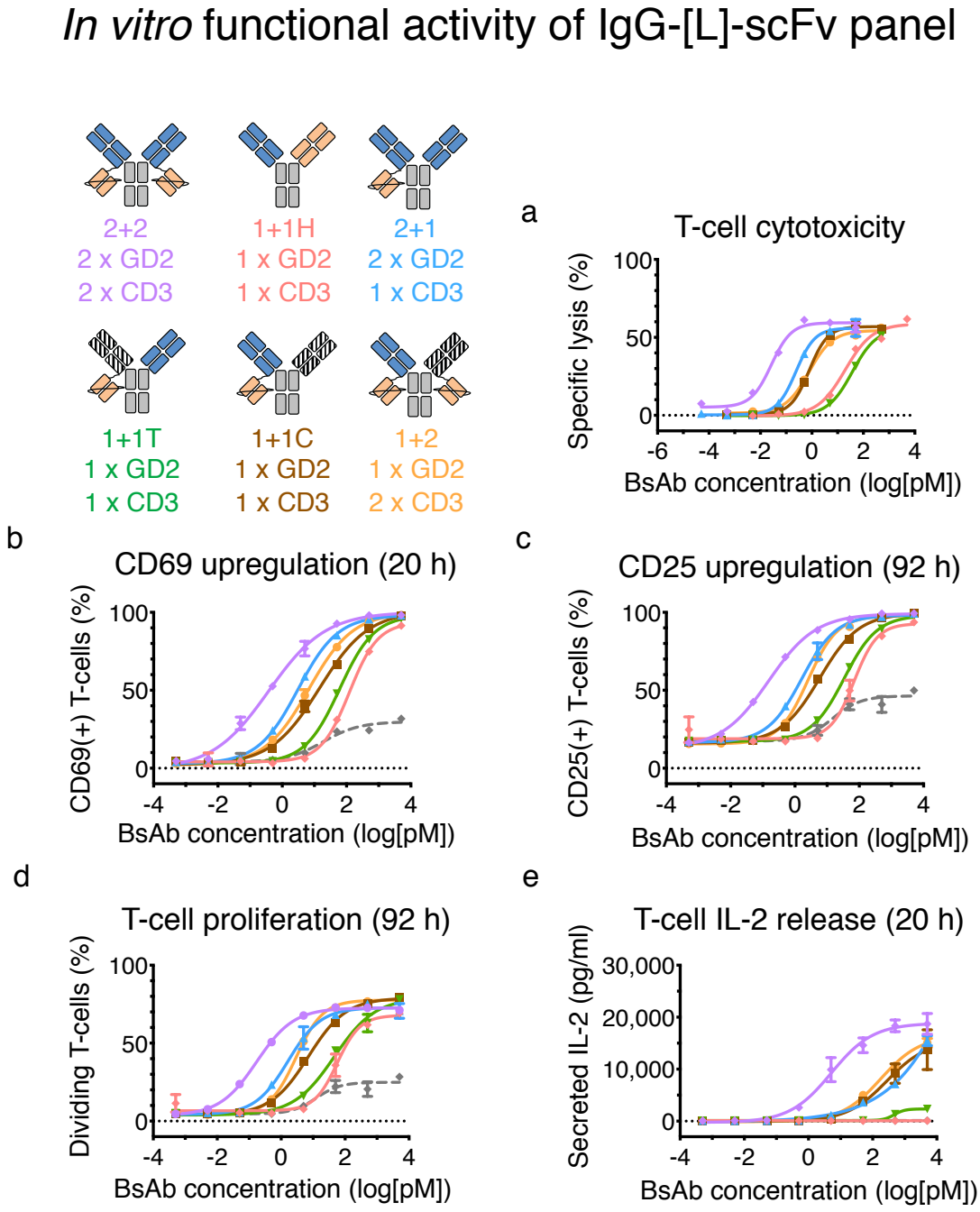

Figure 18. *In vitro* functional activity of IgG-[L]-scFv panel

(a) T-cell dependent cytotoxicity of each BsAb. Each curve represents one BsAb. (b-e) T-cell activation data from co-culture assays. Each curve represents one BsAb. (b) Frequency of T-cells upregulating CD69 after 20 hours of co-culture. (c) Frequency of T-cells upregulating CD25 after 92 hours of co-culture. (d) Fraction of dividing T-cells after 92 hours of co-culture. (e) Secreted IL-2 levels after 20 hours of co-culture. Assays included an anti-CD33 BsAb as a control. All error bars represent standard deviation. Schematics (top left) for reference: 2+2 is purple, 1+1H is red, 2+1 is blue, 1+1T is green, 1+1C is brown, 1+2 is orange, and the control BsAb is grey.

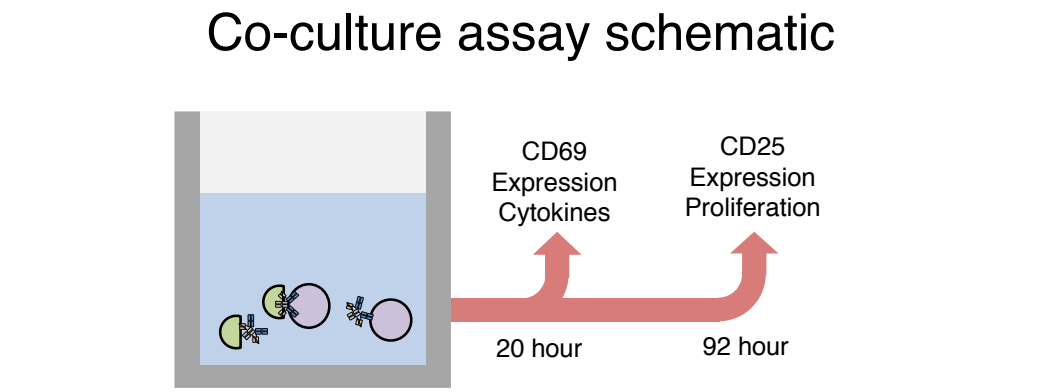

Figure 19. Co-culture assay schematic

Schematic of *in vitro* co-culture assay using naïve human T-cells (green) and M14 melanoma cells (purple). T-cells were harvested after 20- and 92-hours of coculture to analyze CD69, or CD25 upregulation, respectively. Proliferation by cell trace violet dilution was also assessed at 92 hours. Supernatants collected after 20-hours of co-culture were analyzed for cytokines.

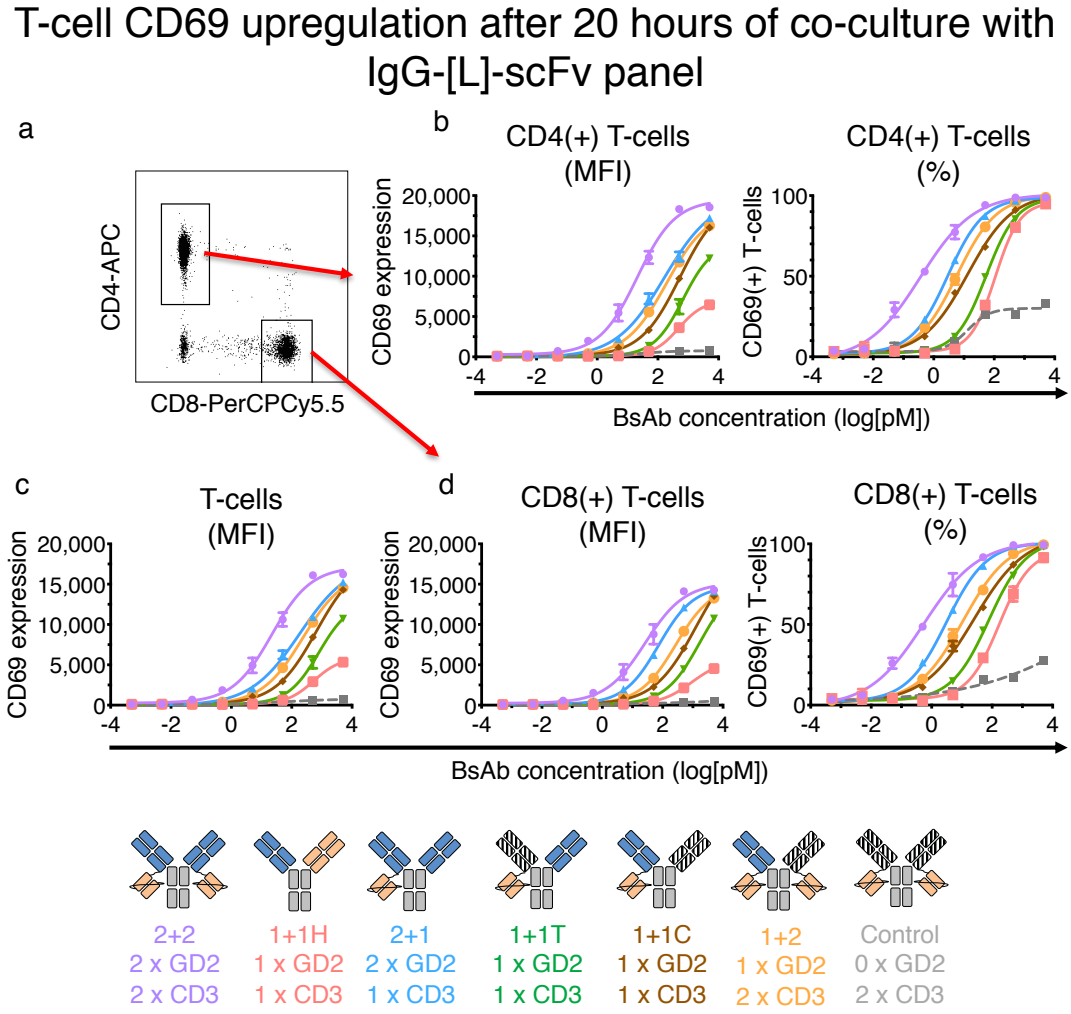

Figure 20. T-cell CD69 upregulation after 20 hours of co-culture with IgG-[L]-scFv panel

(a-d) Flow cytometry analysis from T-cells co-cultured with tumor cells and BsAb for 20-hours. (a) Representative gating strategy for reference. (b) CD4(+) T-cell CD69 expression level (left) or frequency (right). (c) Total T-cell CD69 expression level. (d) CD8(+) T-cell CD69 expression level (left) or frequency (right). Each line represents a single BsAb. All error bars represent standard deviation. Schematics (bottom) for reference: 2+2 is purple, 1+1H is red, 2+1 is blue, 1+1T is green, 1+1C is brown , 1+2 is orange, and the control BsAb is grey.

Cytokine IL-2 secretion revealed even larger differences. 2+2 was significantly more effective at inducing IL-2 secretion than all other BsAb, eliciting nearly 100-fold stronger responses than the next most potent IgG-[L]-scFv variant (Fig. 18e). 2+1, 1+2, and 1+1C exhibited intermediate levels of potency, whereas 1+1T and 1+1H induced weak IL-2 secretion just above the lower limit of detection.

The consistent and striking differences in efficacy between 1+1C and 1+1T suggested that the spatial configuration of antigen binding domains was a key determinant of BsAb activity *in vitro*. Furthermore, while 2+2 displayed clear benefits over 2+1 and 1+2, neither 2+1 nor 1+2 was substantially superior to 1+1C. Hence, the addition of antigen-binding domains improved activity most effectively when it created an additional cis-module. Taken together, these data showed that dual bivalency within the IgG-[L]-scFv framework enhanced BsAb function by improving cell binding and presenting tumor and T-cell binding domains using two cis-modules.

3.5 Valency and spatial configuration control IgG-[L]-scFv anti-tumor function in vivo

To determine how valency and spatial configuration influenced *in vivo* tumor responses, the IgG-[L]-scFv panel was examined using both xenograft and syngeneic tumor models (Fig. 24). In xenograft mice (Fig. 24c and 25), 2+2 again displayed the strongest anti-tumor activity. 2+1 initially elicited similar anti-tumor responses as 2+2 did, but ultimately displayed inferior durability. Consistent with the *in vitro* functional

studies, 1+2 and 1+1C both displayed moderate activity, while being considerably worse than 2+1 and 2+2, was still much stronger than 1+1H and 1+1T, which both failed to show any anti-tumor efficacy.

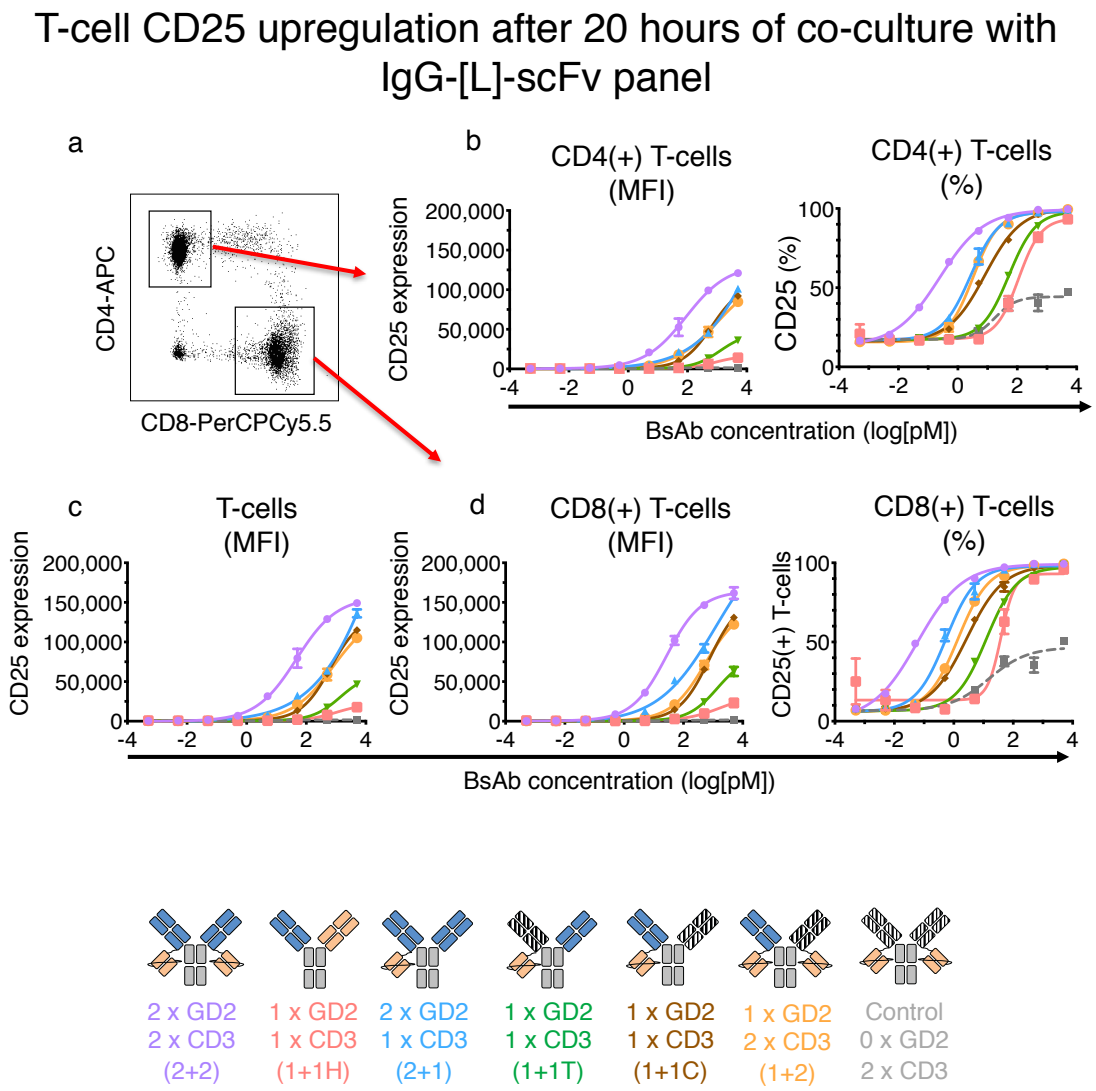

Figure 21. T-cell CD25 upregulation after 92 hours of co-culture with IgG-[L]-scFv panel

(a-d) Flow cytometry analysis from T-cells co-cultured with tumor cells and BsAb for 92-hours. (a) Representative gating strategy for reference. (a) CD4(+) T-cell CD25 expression level (left) or frequency (right). (c) Total T-cell CD25 expression level. (d) CD8(+) T-cell CD25 expression level (left) or frequency (right). Each line represents a single BsAb. All error bars represent standard deviation. Schematics (bottom) for reference: 2+2 is purple, 1+1H is red, 2+1 is blue, 1+1T is green, 1+1C is brown , 1+2 is orange, and the control the BsAb is grey.

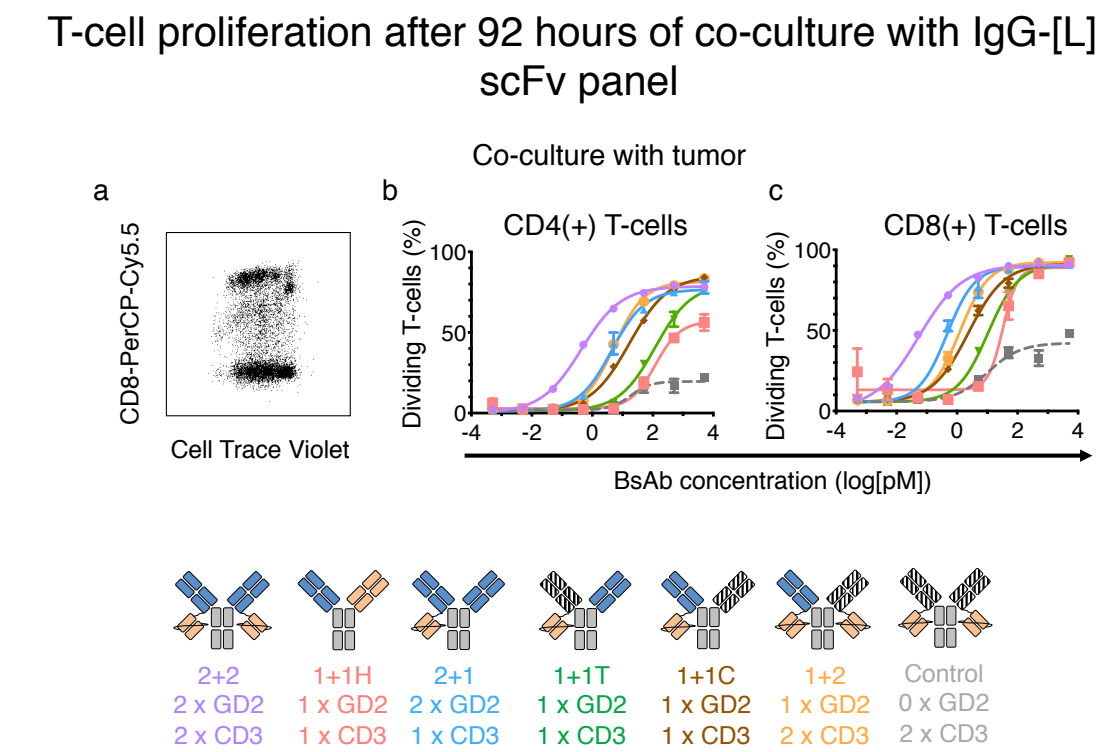

Figure 22. T-cell proliferation after 92 hours of co-culture with IgG-[L]-scFv panel (a-c) Flow cytometry analysis from T-cells co-cultured with tumor cells and BsAb for 92 hours. (a) Representative Cell Trace Violet dilution analysis. (b-c) Percentage of dividing cells for (b) CD4(+) or (c) CD8(+) T-cell subsets after 92-hours of co-culture. Each line represents a single BsAb. All error bars represent standard deviation. Schematics (bottom) for reference: 2+2 is purple, 1+1H is red, 2+1 is blue, 1+1T is green, 1+1C is brown , 1+2 is orange, and the control BsAb is grey.

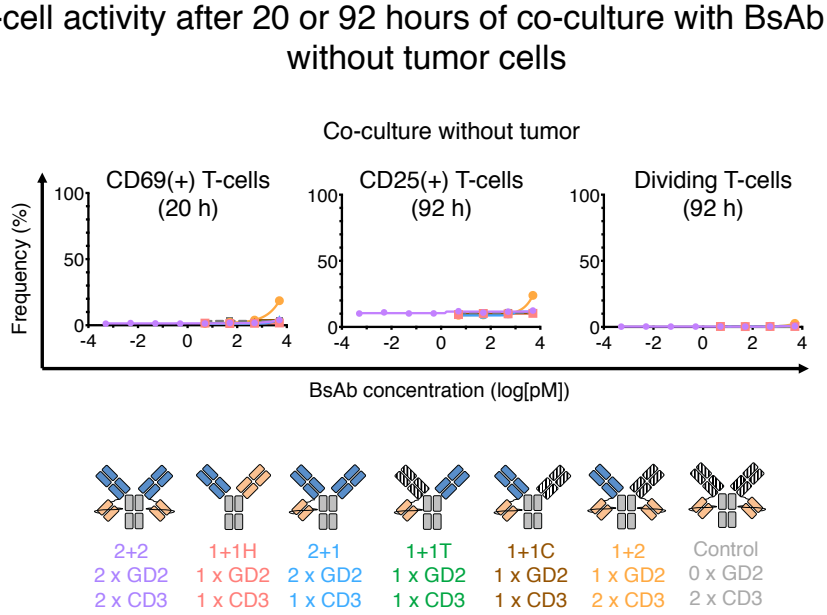

Figure 23. T-cell activity after 20 or 92 hours of co-culture with BsAb but without tumor cells

Frequency of CD69 expressing (left), CD25 expressing (center) and proliferating (right) T-cells after co-culture without tumor cells. Each line represents a single BsAb. All error bars represent standard deviation. Schematics (bottom) for reference: 2+2 is purple, 1+1H is red, 2+1 is blue, 1+1T is green, 1+1C is brown , 1+2 is orange, and the control BsAb is grey.

Results were more polarized in the syngeneic model. Here, only 2+2 displayed any measurable activity, while all other BsAb completely failed to inhibit tumor growth (Fig. 24d and 26). These results implied that the syngeneic model imposed a more stringent threshold for therapeutic efficacy than the xenograft model did, likely due to the predominance of naïve T-cells in the former compared to the activated T-cells in the latter (see Discussion). Taken together, however, these data confirmed the value of dual bivalency and the importance of cis-configured tumor and T-cell binding domains. These results imply that the huCD3ε-tg model imposed a more stringent threshold for therapeutic efficacy than the xenograft model, likely due to the predominance of naïve T-cells in the former compared to activated T-cells in the latter. Taken together, however, these data confirm the value of bivalency and cis-configured Fab and scFv domains for IgG-[L]-scFv function.

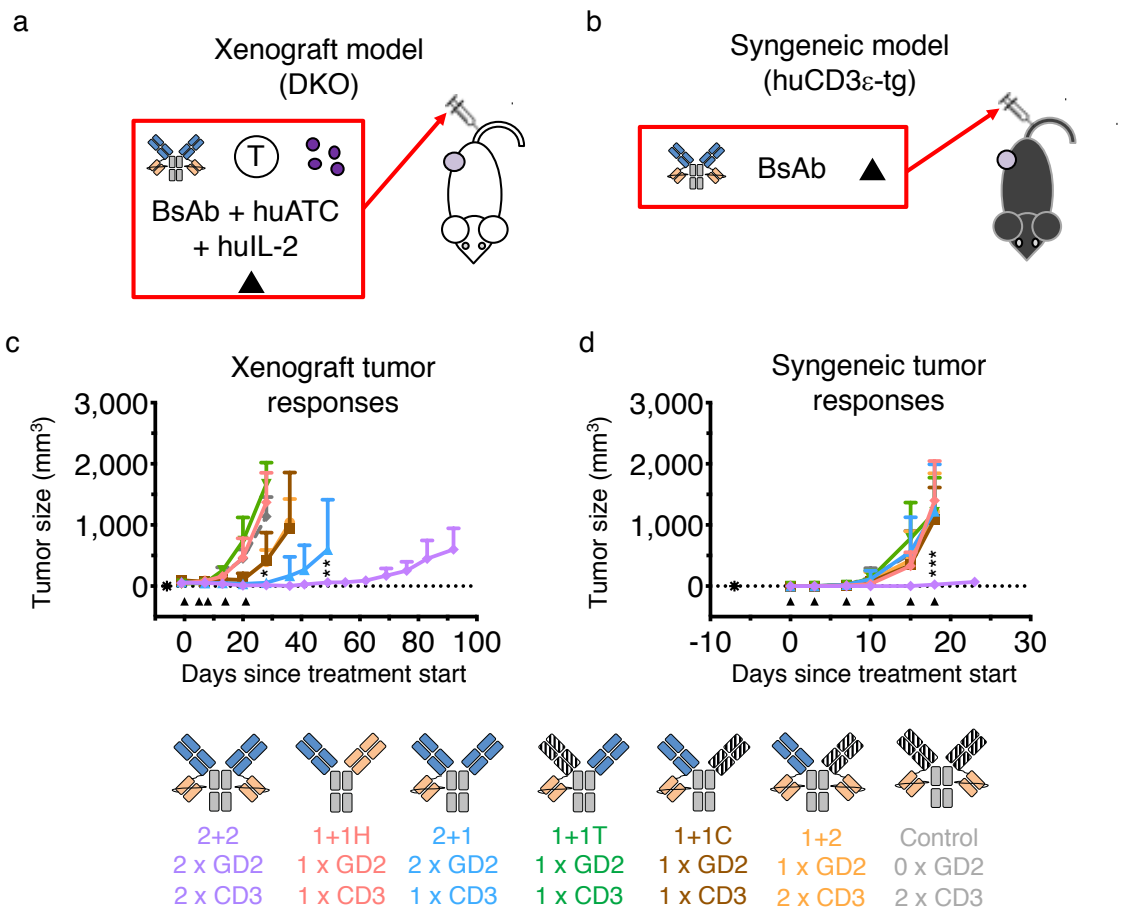

Figure 24. *In vivo* anti-tumor activity of IgG-[L]-scFv panel

Schematic of treatment design for (a) xenograft and (b) syngeneic (right) tumor models. For both models 25 pmol of BsAb was administered intravenously twice per week. For xenograft model, 20 million activated human T-cells (huATC) were administered intravenously and human IL-2 (1,000 U) was administered subcutaneously, twice per week. (c-d) Tumor growth for (c) xenograft and (d) syngeneic models. Each line represents one treatment group (n=5). Both models received anti-CD33 BsAb as a control. Solid black triangles represent a dose of BsAb (syngeneic) or a dose of BsAb, huATC and huIL-2 (xenograft). The dotted black line represents no measurable tumor and the black asterisk represents the tumor implantation. All error bars represent standard deviation. Schematics (bottom) for reference: 2+2 is purple, 1+1H is red, 2+1 is blue, 1+1T is green, 1+1C is brown, 1+2 is orange, and control BsAb is grey. Statistical significances were obtained by two-way analysis of variance (ANOVA) and Tukey correction. (c) *P < 0.05 for Control, 1+1H, 1+1T, 1+2 or 1+1C compared to 2+2 or 2+1. **P < 0.01 for 2+1 compared to 2+2. (d) ***P < 0.0001 for Control, 1+1H, 1+1T, 1+2, 1+1C or 2+1 compared to 2+2.

3.6 Conclusions

In this study, we directly examined how a GD2-specific BsAb using an IgG-[L]-scFv design displayed superior anti-tumor activity compared to multiple other formats. Our results confirmed that dual bivalency is indeed crucial for function, but surprisingly not for the reasons we had initially anticipated. While bivalency had the expected effect of improving binding to both tumor cells and T-cells, this was of secondary importance; the additional anti-huCD3ε scFv that distinguished 1+2 from 1+1C made essentially no functional difference, while the additional anti-GD2 Fab in 2+1 provided only a modest improvement over 1+1C. Rather, *in vitro* and *in vivo* anti-tumor activity was most correlated with the number of cis-configured tumor and T-cell binding domains. BsAb with zero cis-modules (1+1T) displayed low potency, BsAb with only one cis-module (2+1, 1+2, 1+1C) showed moderate potency, but only the dual bivalent IgG-[L]-scFv, which contained two cis-modules (2+2), consistently displayed high potency *in vitro* and *in vivo*. Notably, these results are consistent with the recent characterization of a high potency T-cell BsAb employing a single cis-configuration (Fab-Fab) (Bacac et al., 2018). Hence, in the case of T-cell BsAb, the total number of interactions seems to matter less than the manner in which those interactions are made.

In vivo responses for IgG-[L]-scFv panel using xenograft model

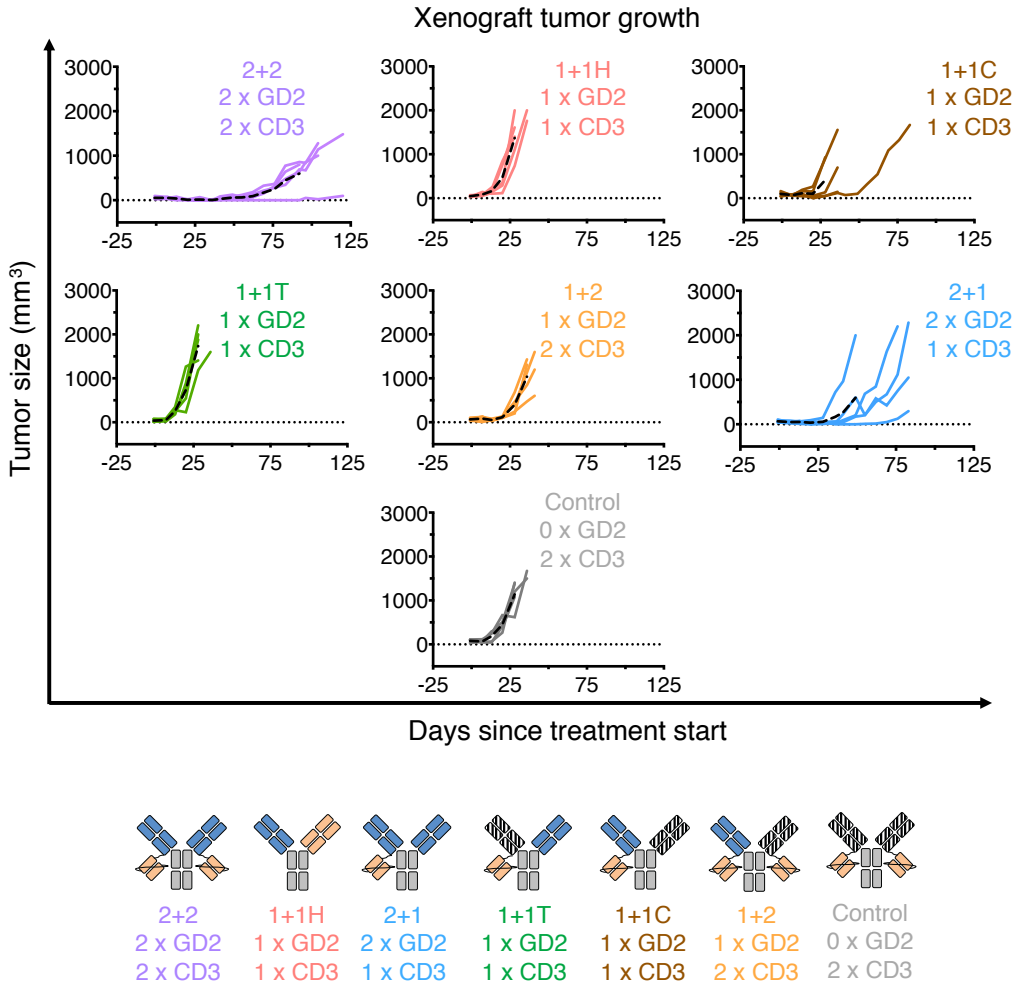

Figure 25. *In vivo* responses for IgG-[L]-scFv panel using xenograft model
Each figure represents one treatment group (n=5). Each solid line represents a single mouse, and the dotted lines represents the group average. Tumor averages were calculated until one at least one mouse had to be euthanized. Schematics (bottom) or reference: 2+2 is purple, 1+1H is red, 2+1 is blue, 1+1T is green, 1+1C is brown , 1+2 is orange, and the control BsAb is grey.

In vivo responses for IgG-[L]-scFv panel using syngeneic model

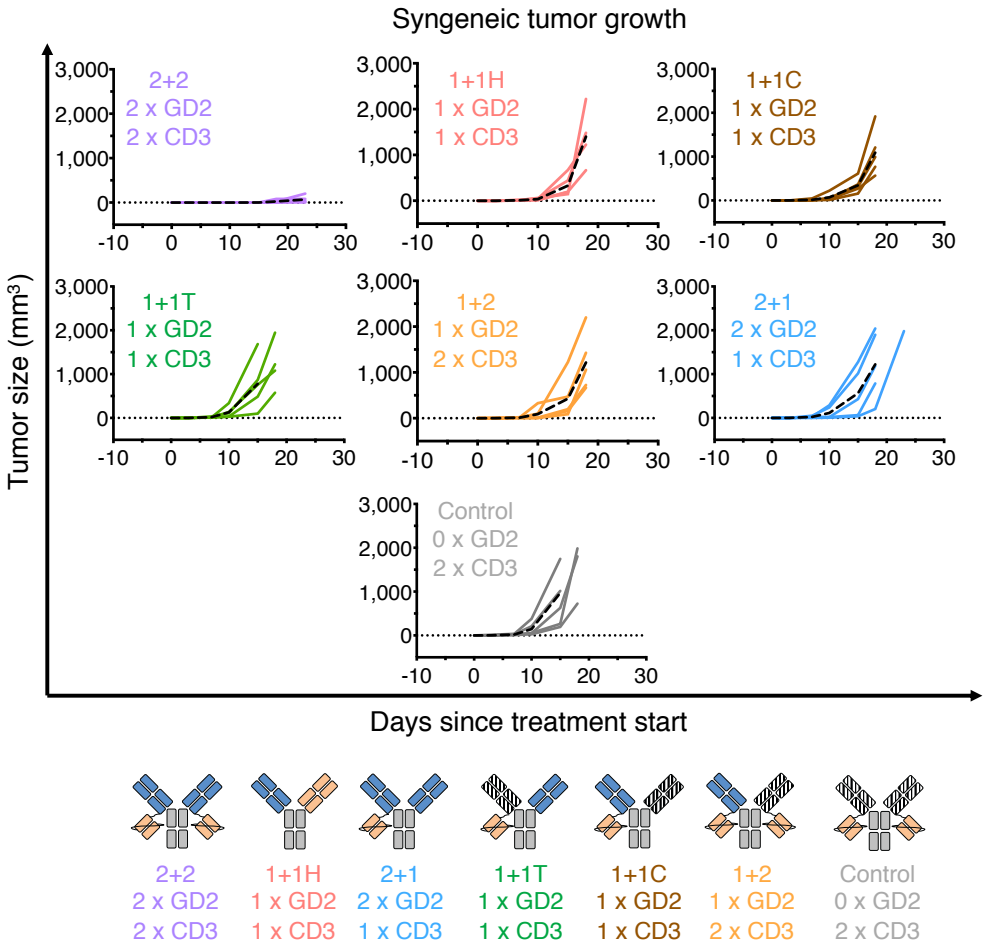

Figure 26. *In vivo* responses for IgG-[L]-scFv panel using syngeneic model (Each figure represents one treatment group (n=5). Each solid line represents a single mouse, and the dotted lines represents the group average. Tumor averages were calculated until one at least one mouse had to be euthanized. Schematics (bottom) for reference: 2+2 is purple, 1+1H is red, 2+1 is blue, 1+1T is green, 1+1C is brown , 1+2 is orange, and the control BsAb is grey.

CHAPTER 4

SPACING OF DUAL BIVALENT BINDING DOMAINS INFLUECES FUNCTIONAL ACTIVITY IN VITRO AND IN VIVO

4.1 Introduction

We have previously described several highly potent T-cell engaging BsAb using the symmetric and dual bivalent IgG-[L]-scFv platform (Hoseini et al., 2018; Lopez-Albaitero et al., 2017; Wu et al., 2018; Xu et al., 2015), in which a single chain variable fragment (scFv) recognizing human CD3ε (huCD3ε) is fused to the C-termini of each antibody light chain (Fig. 27a). While this design has consistently provided exceptionally strong anti-tumor activity against multiple tumor antigens (ganglioside GD2, CD33, GPA33, HER2) *in vitro* and *in vivo*, the basis for its remarkable efficacy is poorly understood.

Table 10. *In vitro* properties and design of dual bivalent BsAb

BsAb	EC_{50}	Fold Change	GD2 Valency	CD3 Valency	SEC-HPLC Purity
2+2	38 fM	-	2	2	96%
2+2B	133 fM	3	2	2	93%
2+2HC	80 fM	2	2	2	98%

In the present study, we demonstrate how the IgG-[L]-scFv platform displays superior *in vitro* and *in vivo* high potency compared to two additional dual bivalent BsAb designs: BiTE-Fc and IgG-[H]-scFv. These findings are unexpected and reveal a situation in which interdomain spacing appears critical to driving anti-tumor responses, but not simply due to decreased intermembrane distance. Instead the most optimal spacing is that of a single immunoglobulin domain. These findings suggest that the potency of the IgG-[L]-scFv design does not solely come from its dual bivalency, but also some yet uncharacterized feature of its interdomain spacing.

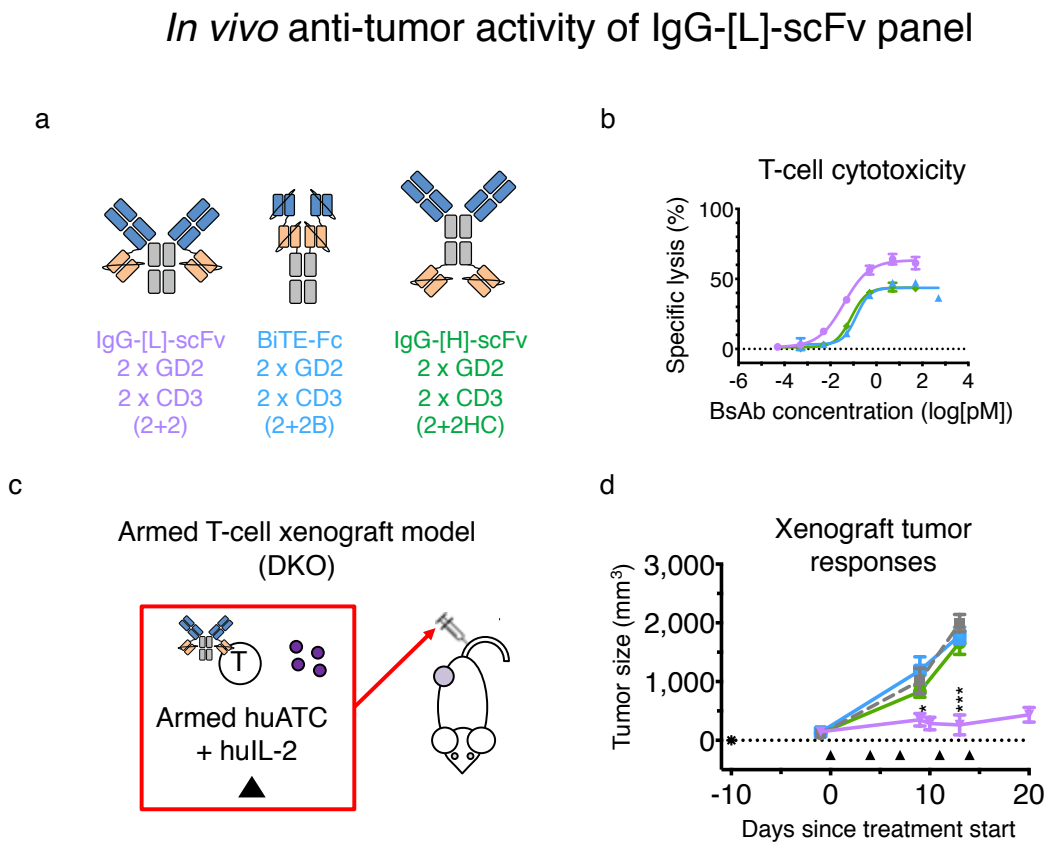

Figure 27. Comparison of dual bivalent BsAb designs

(a) Schematics of dual bivalent BsAb panel: IgG-[L]-scFv (2+2), BiTE-Fc (2+2B) and IgG-[H]-scFv (2+2HC). Orange represents anti-huCD3ε domains (derived from huOKT3) and blue represents anti-GD2 domains (derived from hu3F8). (b) T-cell dependent cytotoxicity for each BsAb. Each curve represents one BsAb. (c) Schematics of treatment design for "armed" T-cell xenograft model. Armed human activated T-cells (huATC) were administered intravenously and human IL-2 (1,000 U) was administered subcutaneously, twice per week. (d) *In vivo* tumor growth for xenograft arming model. Each line represents one treatment group (n=5). Mice received anti-GPA33 BsAb as a control. Solid black triangles represent a dose of BsAb armed huATC and huIL-2. The dotted black line represents no measurable tumor and the black star represents the tumor implantation. For each dose, 20 million huATC were armed with 10 pmol of IgG-[L]-scFv, 20 pmol of BiTE-Fc and 6.7 pmol of IgG-[H]-scFv. All error bars represent standard deviation. For reference: 2+2 is purple, 2+2B is blue, 2+2HC is green and the control BsAb is grey. Statistical significances were obtained by two-way analysis of variance (ANOVA) and Tukey correction. *P < 0.01, ***P < 0.0001 for Control, 2+2HC or 2+2B compared to 2+2.

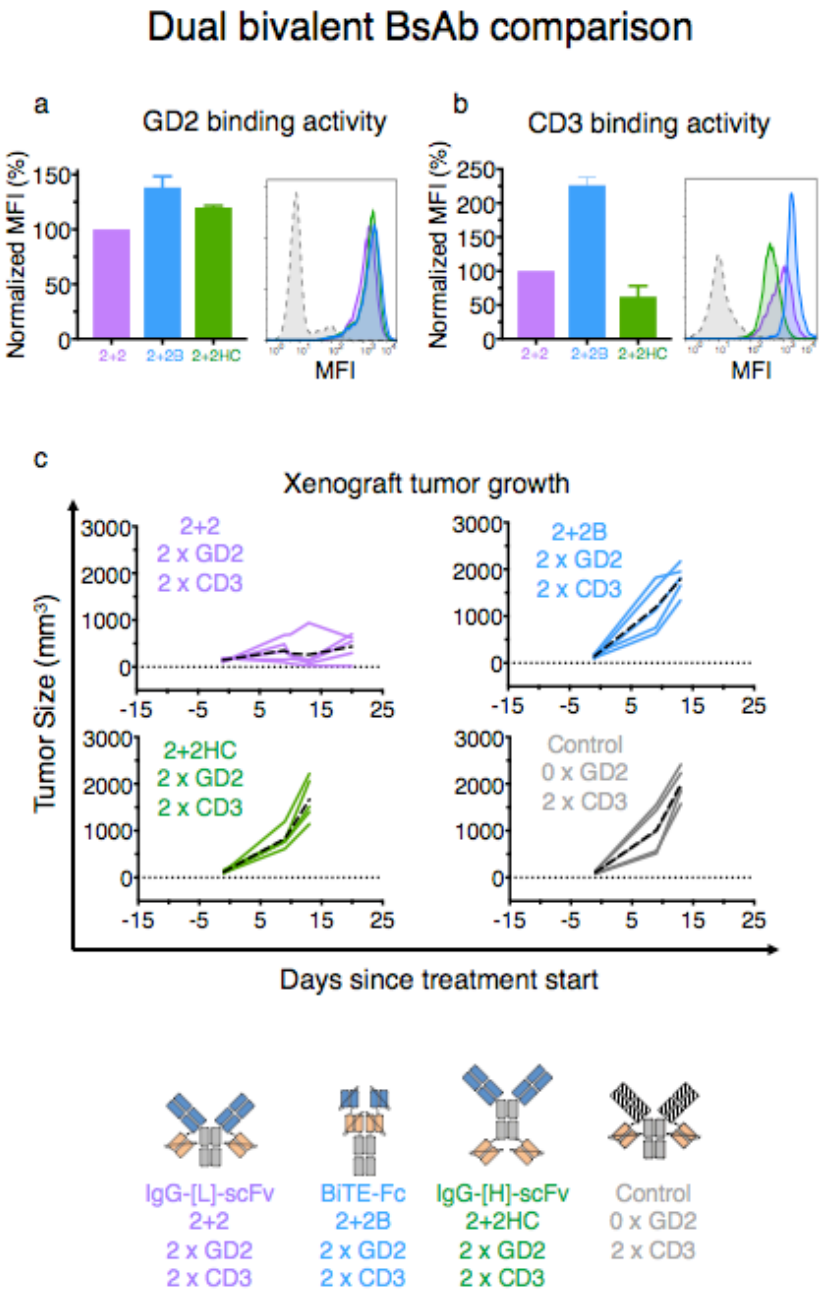

Figure 28. Dual bivalent BsAb comparison

Cell binding activity of each BsAb against (a) M14 (GD2) and (b) activated human T-cells (CD3) using flow cytometry. Bar graphs (left) represent the geometric MFI of each histogram (right), normalized to 2+2 (100%), from two independent experiments. (b) Tumor growth for "armed" T-cell xenograft model. Each figure represents one treatment group (n=5). Each solid line represents a single mouse, and the dotted lines represents the group average. Tumor averages were calculated until one at least one mouse had to be euthanized. All error bars represent standard deviation. Schematics (bottom) for reference: 2+2 is purple, 2+2B is blue, 2+2HC is green and the control BsAb is grey.

4.2 Design and expression of three dual bivalent bispecific antibodies

We began our study by designing three different dual bivalent BsAb. Variable domain gene sequences were clone into mammalian cell expression vectors containing one or two promoters and expressed transiently in expi293 cells (Table 10).

To make the BiTE-Fc design (2+2B), the hu3F8-BiTE sequence was fused to the CH2 domain of a human IgG1 Fc domain using a short 15 amino acid linker (three G_4S units) . As before, each scFv sequence used a 20 amino acid linker (four G_4S units) to separate V_H and V_L sequences, and the two scFv domains were fused together using a short five amino acid linker (G_4S). hu3F8-scFv remained at the N-terminus and huOKT3-scFv remained at the C-terminus. The C-terminal hexahistadine tag was removed and the protein was instead purified by protein A.

The IgG-[L]-scFv format (2+2) was designed and expressed as described in chapter two. To make the IgG-[H]-scFv protein (2+2H), huOKT3-scFv domains were fused the C-terminus of the heavy chains of a hu3F8-IgG molecule. IgG-[H]-scFv protein was purified from culture supernatant by protein A affinity column separation. Two point mutations, N297A and K322A, were also included in the IgG heavy chain of each molecule to ablate Fc receptor (FcR) and complement activity, respectively. Purity of each protein was determined by SEC-HPLC.

4.3 Interdomain spacing is critical to IgG-[L]-scFv in vitro activity

To explore the role of interdomain spacing in the context of dual bivalency, we sought to compare the IgG-[L]-scFv platform to two additional dual bivalent BsAb formats (Fig. 27a)—an IgG-[H]-scFv (Coloma and Morrison, 1997a) (2+2HC), and a human IgG_1 based BiTE-Fc (Spiess et al., 2015a) (2+2B)—which separated tumor and T-cell binding domains using larger or smaller spacers, respectively. In contrast to 2+2,

which spaced tumor and T-cell binding domains with a single Ig domain (C_L), 2+2HC increased the spacing to three Ig domains (C_{H1}-C_{H2}-C_{H3}) by fusing each anti-huCD3ε scFv to the C-terminus of each anti-GD2 heavy chain. Conversely, 2+2B contained a short (G_4S) linker between each pair of scFv's to reduce the spacing between tumor and T-cell binding domains. In flow cytometry assays, all three BsAb showed similar binding to GD2(+) tumor cells, while 2+2B bound T-cells more effectively than either 2+2 or 2+2HC did (Fig. 28). Hence, the altered interdomain spacing of 2+2B and 2+2HC did not negatively impact antigen binding relative to 2+2. Nevertheless, both 2+2B and 2+2HC exhibited reduced *in vitro* cytotoxicity compared to 2+2 (Fig. 27b and Table 10), lysing tumor cells with ~2- to ~3-fold lower potency (80 fM and 140 fM EC_{50}, respectively, versus 38 fM in 2+2).

4.4 Interdomain spacing is critical to IgG-[L]-scFv in vivo activity

To see how spacing influenced *in vivo* tumor responses, we chose to compare these BsAb using the more stringent "armed" T-cell xenograft model, using DKO mice that were subcutaneously implanted with another neuroblastoma PDX tumor (Fig. 27c). Under these conditions, huATC armed with 2+2B or 2+2HC completely failed to inhibit tumor growth, while huATC armed with 2+2 displayed robust anti-tumor activity (Fig. 27d and 28). These results were unexpected and suggested that reducing the interdomain spacing did not necessarily confer increases in cytotoxicity. Instead, an optimal amount of separation was needed between domains to elicit the most potent *in vitro* and *in vivo* anti-tumor responses.

4.5 Conclusions

Prior studies have demonstrated that BsAb which target epitopes close to the tumor cell membrane elicited more potent T-cell cytotoxicity than those that bound

farther away (Bluemel et al., 2010; Li et al., 2017), implying that close apposition between T-cells and tumor cells drove more effective T-cell activation and killing. This phenomenon has been linked to the exclusion of the inhibitory phosphatase CD45 (Li et al., 2017), which contains a large extracellular domain that cannot fit into tight intercellular spaces. It is tempting to speculate that this could explain why the cis-configured 1+1C performs better than the trans-configured 1+1T, both *in vitro and in vivo (see* chapter three). However, the overall superiority of the IgG-[L]-scFv format over the BiTE-Fc (2+2B) design, which has reduced spacing between the GD2 and huCD3ε binding domains, indicated the smallest distance was not always best. In that regard, it is important to note that the T-cell receptor (TCR) is a mechanosensitive protein that undergoes activating conformational changes in response to forces applied to its ligand-binding domain (Kim et al., 2009; Liu et al., 2014). Hence, the interdomain spacing imparted by a C_L domain in the IgG-[L]-scFv format may provide the most optimal physical constraint or mechanical coupling between the TCR and tumor cell, leading to stronger and/or more sustained delivery of activating signals. Comparing the capacity of different BsAb formats to induce TCR conformational change will be an interesting topic for future work.

DISCUSSION

Over the last three decades, substantial advances in our understanding of antibody structure and function have enabled the transition of BsAb from novel concepts to a clinically tested (and even approved) therapeutic agents. However, engineering the optimal BiTE's for drug development remains challenging owing to the inherent stability of these therapeutics. To improve the thermal stability of scFv's, various strategies have been applied: (1) Disulfide bond engineering at the V_H/V_L interface (Hagihara and Saerens, 2014); (2) Linker optimization (Le Gall et al., 2004)' (3) Structure-based CDR grafting into more stable frameworks (Ewert et al., 2004); (4) Stability screening of small scFv libraries encompassing rationally designed stabilizing mutations (Miller et al., 2010); or (5) Stability screening by the introduction of random mutations by yeast/phage display (Wiedermann et al., 2013). A stability-enhanced scFv usually demonstrated comparable antigen binding to the wild type scFv, although loss of antigen affinity could accompany these genetic engineering exercises. However, while affinity could be regained using phage or yeast display methods, thermodynamics-based engineering has also emerged as a promising technique for designing higher affinity scFv's (Thakkar et al., 2014).

The anti-GD2 scFv in hu3F8-BiTE was derived from the sequence of hu3F8, which is currently undergoing phase I clinical trials (clinicaltrials.gov: NCT01419834, NCT01757626, and NCT01662804). Based on the mouse 3F8 crystal structure (PDB) and molecular modeling of hu3F8, the first residue of the light chain (E1) was predicted to be involved in antigen binding and should be free of further constraints - hence the V_L-V_H orientation in hu3F8-scFv. In fact, recently we demonstrated experimentally that an E1K mutation could further enhance affinity at this position (Zhao et al., 2015). In our

first generation BiTE (5F11-BiTE) both disulfide bond stabilization and affinity maturation were included to enhance stability and affinity. Expectedly, 5F11-BiTE had superior thermal stability to hu3F8-BiTE, with a T_m difference of 20°C, given there was no disulfide bond stabilization in the hu3F8-scFv. However, in terms of antigen binding, hu3F8-BiTE showed higher GD2 binding than 5F11-BiTE, with a 13-fold increase in affinity. This difference in affinity translated to an exceptional and unexpected increase in potency against a broad spectrum of human cancer cell lines that were GD2(+) (Table 3), mediating T-cell mediated killing of high GD2 expressing cancer cell lines with a femtomolar EC_{50} (10fM). When compared to 5F11BiTE, hu3F8-BiTE demonstrated up to 5,000-fold higher potency. This affinity also led to improved T-cell activation as measured by Ca^{2+} flux and cytokine release. *In vivo* investigation using xenograft mouse models further supported that hu3F8-BiTE was much more potent than 5F11-BiTE in suppressing tumor growth. We are now working on enhancing hu3F8-BiTE further by inserting disulfide stabilizations for both hu3F8-scFv and huOKT3-scFv, optimizing the linker size, and adding affinity maturation mutations (Zhao et al., 2015)

In addition to the differences in affinity of hu3F8 and 5F11 to tumor antigen GD2, other factors may have contributed to the enhanced potency, such as subtle differences in binding geometries. The solvent accessible portion of the membrane bound GD2 molecule is a small penta-saccharide head group (approximately 1,500 daltons), which would be engulfed by the CDR loops of either antibody. Given the small size of the antigen, we expect that the epitopes of hu3F8 and 5F11 to be highly overlapping. Nevertheless, subtle differences in epitope may have contributed to the unexpectedly higher potency of the hu3F8 BiTE. While it is widely believed that epitope distance can influence potency (Bluemel et al., 2010), it is less clear how steric effects on antibody

conformation following binding to the tumor antigen may influence activity T-cell engagement. It is possible that the distribution of GD2 on the cell surface may allow for preferential binding at one angle over another, or that the remaining huOKT3-scFv can bind to T-cells more efficiently when hu3F8-scFv binds to GD2 than when 5F11-scFv binds to GD2. While our current methods cannot rule out the above from contributing to hu3F8-BiTE's large increase in potency over 5F11-BsAb, we do believe that the difference in affinity is the major contributing factor.

The comparison of BsAb in both syngeneic and xenograft animal models also revealed important differences between the various formats. Although 2+1, 1+2 and 1+1C displayed strong anti-tumor activity in the xenograft model, they were completely ineffective in syngeneic huCD3ε-tg mice, in contrast to the IgG-[L]-scFv (2+2) that displayed robust anti-tumor activity in both models. Here, it is important to note that in the xenograft model, mice were infused with *in vitro* activated T-cells, whereas the syngeneic model relied on endogenous naïve T-cells. It is therefore tempting to speculate that only the dual cis-module IgG-[L]-scFv design had the stimulatory power to elicit productive *in vivo* responses from naïve T-cells, which are more difficult to activate and take a longer time to respond. It is also notable that the capacity of each BsAb to elicit T-cell dependent IL-2 release *in vitro* was the best predictor of *in vivo* activity in the syngeneic model. This strong correlation between *in vivo* potency and *in vitro* IL-2 production in naïve T-cells, highlights the importance of T-cell cytokines as biomarkers or components of productive anti-tumor responses. In light of these results, it may be worth re-evaluating design strategies aimed at inducing less cytokine release in order to mitigate cytokine-driven side effects (Ellerman, 2018), as these same strategies might compromise clinical anti-tumor efficacy.

Additionally, the presented data highlights the importance of thorough *in vivo* validation of *in vitro* data. While the IgG-[L]-scFv format consistently elicited the strongest cytotoxicity *in vitro*, the magnitude of its superiority varied from as little as ~2-3-fold, to as high as 2,000-fold. Despite this, only the IgG-[L]-scFv format displayed strong anti-tumor responses in all three *in vivo* tumor models. By using a combination of different tumor models with different restrictions and thresholds, the margin of error in picking drug candidates for clinical development could potentially be narrowed.

Together, these studies reveal how affinity, cis-configured binding domains and dual bivalency provided log-fold improvements to T-cell BsAb potencies, *in vitro* and *in vivo.* If implemented into future BsAb design strategies, these innovations may substantially improve clinical outcomes. Additionally, the IgG-[L]-scFv platform, which combines the benefits of symmetry, spatial configuration, dual bivalency and optimal pharmacokinetics, is a vanguard in therapeutic antibody development and is poised to drive both clinical progress and academic studies in coming years.

BIBLIOGRAPHY

Abeyweera, T.P., Merino, E., and Huse, M. (2011). Inhibitory signaling blocks activating receptor clustering and induces cytoskeletal retraction in natural killer cells. J Cell Biol *192*, 675-690.

Adair, J.R., Athwal, D.S., Bodmer, M.W., Bright, S.M., Collins, A.M., Pulito, V.L., Rao, P.E., Reedman, R., Rothermel, A.L., Xu, D.*, et al.* (1994). Humanization of the murine anti-human CD3 monoclonal antibody OKT3. Hum Antibodies Hybridomas *5*, 41-47.

Agata, Y., Kawasaki, A., Nishimura, H., Ishida, Y., Tsubata, T., Yagita, H., and Honjo, T. (1996). Expression of the PD-1 antigen on the surface of stimulated mouse T and B lymphocytes. Int Immunol *8*, 765-772.

Ahmed, M., and Cheung, N.K. (2014). Engineering anti-GD2 monoclonal antibodies for cancer immunotherapy. FEBS Lett *588*, 288-297.

Alarcon, B., Mestre, D., and Martinez-Martin, N. (2011). The immunological synapse: a cause or consequence of T-cell receptor triggering? Immunology *133*, 420-425.

Albanell, J., and Baselga, J. (1999). Trastuzumab, a humanized anti-HER2 monoclonal antibody, for the treatment of breast cancer. Drugs Today *35*, 931-946.

Alcover, A., Alarcon, B., and Di Bartolo, V. (2018). Cell Biology of T Cell Receptor Expression and Regulation. Annu Rev Immunol *36*, 103-125.

Alegre, M.L., Collins, A.M., Pulito, V.L., Brosius, R.A., Olson, W.C., Zivin, R.A., Knowles, R., Thistlethwaite, J.R., Jolliffe, L.K., and Bluestone, J.A. (1992). Effect of a single amino acid mutation on the activating and immunosuppressive properties of a "humanized" OKT3 monoclonal antibody. Journal of Immunology (Baltimore, Md: 1950) *148*, 3461-3468.

Amann, M., D'Argouges, S., Lorenczewski, G., Brischwein, K., Kischel, R., Lutterbuese, R., Mangold, S., Rau, D., Volkland, J., Pflanz, S.*, et al.* (2009). Antitumor activity of an EpCAM/CD3-bispecific BiTE antibody during long-term treatment of mice in the absence of T-cell anergy and sustained cytokine release. J Immunother *32*, 452-464.

Artyomov, M.N., Lis, M., Devadas, S., Davis, M.M., and Chakraborty, A.K. (2010). CD4 and CD8 binding to MHC molecules primarily acts to enhance Lck delivery. Proc Natl Acad Sci U S A *107*, 16916-16921.

Bacac, M., Colombetti, S., Herter, S., Sam, J., Perro, M., Chen, S., Bianchi, R., Richard, M., Schoenle, A., Nicolini, V.*, et al.* (2018). CD20-TCB with Obinutuzumab Pretreatment as Next-Generation Treatment of Hematologic Malignancies. Clin Cancer Res *24*, 4785-4797.

Bacac, M., Klein, C., and Umana, P. (2016). CEA TCB: A novel head-to-tail 2:1 T cell bispecific antibody for treatment of CEA-positive solid tumors. Oncoimmunology *5*, e1203498.

Bargou, R., Leo, E., Zugmaier, G., Klinger, M., Goebeler, M., Knop, S., Noppeney, R., Viardot, A., Hess, G., Schuler, M.*, et al.* (2008). Tumor regression in cancer patients by very low doses of a T cell-engaging antibody. Science *321*, 974-977.

Basu, R., and Huse, M. (2017). Mechanical Communication at the Immunological Synapse. Trends in Cell Biology *27*, 241-254.

Basu, R., Whitlock, B.M., Husson, J., Le Floc'h, A., Jin, W., Oyler-Yaniv, A., Dotiwala, F., Giannone, G., Hivroz, C., Biais, N.*, et al.* (2016). Cytotoxic T Cells Use Mechanical Force to Potentiate Target Cell Killing. Cell *165*, 100-110.

Billadeau, D.D., Nolz, J.C., and Gomez, T.S. (2007). Regulation of T-cell activation by the cytoskeleton. Nat Rev Immunol *7*, 131-143.

Bluemel, C., Hausmann, S., Fluhr, P., Sriskandarajah, M., Stallcup, W.B., Baeuerle, P.A., and Kufer, P. (2010). Epitope distance to the target cell membrane and antigen size determine the potency of T cell-mediated lysis by BiTE antibodies specific for a large melanoma surface antigen. Cancer Immunol Immunother *59*, 1197-1209.

Brady, J.L., Harrison, L.C., Goodman, D.J., Cowan, P.J., Hawthorne, W.J., O'Connell, P.J., Sutherland, R.M., and Lew, A.M. (2014). Preclinical screening for acute toxicity of therapeutic monoclonal antibodies in a hu-SCID model. Clin Transl Immunology *3*, e29.

Brinkmann, U., and Kontermann, R.E. (2017). The making of bispecific antibodies. MAbs *9*, 182-212.

Bromley, S.K., Iaboni, A., Davis, S.J., Whitty, A., Green, J.M., Shaw, A.S., Weiss, A., and Dustin, M.L. (2001). The immunological synapse and CD28-CD80 interactions. Nat Immunol *2*, 1159-1166.

Caron, P.C., Co, M.S., Bull, M.K., Avdalovic, N.M., Queen, C., and Scheinberg, D.A. (1992). Biological and Immunological Features of Humanized M195 (Anti-CD33) Monoclonal Antibodies. Cancer Research *52*, 6761-6767.

Cheng, M., Ahmed, M., Xu, H., and Cheung, N.K. (2015). Structural design of disialoganglioside GD2 and CD3-bispecific antibodies to redirect T cells for tumor therapy. Int J Cancer *136*, 476-486.

Cheng, M., Santich, B.H., Xu, H., Ahmed, M., Huse, M., and Cheung, N.K. (2016). Successful engineering of a highly potent single-chain variable-fragment (scFv) bispecific antibody to target disialoganglioside (GD2) positive tumors. Oncoimmunology *5*, e1168557.

Cheung, N.-K.V., Guo, H., Hu, J., Tassev, D.V., and Cheung, I.Y. (2014). Humanizing murine IgG3 anti-GD2 antibody m3F8 substantially improves antibody-dependent cell-mediated cytotoxicity while retaining targeting in vivo. OncoImmunology *1*, 477-486.

Cheung, N.K., Guo, H., Hu, J., Tassev, D.V., and Cheung, I.Y. (2012). Humanizing murine IgG3 anti-GD2 antibody m3F8 substantially improves antibody-dependent cell-mediated cytotoxicity while retaining targeting in vivo. Oncoimmunology *1*, 477-486.

Choi, B.D., Kuan, C.T., Cai, M., Archer, G.E., Mitchell, D.A., Gedeon, P.C., Sanchez-Perez, L., Pastan, I., Bigner, D.D., and Sampson, J.H. (2013). Systemic administration of a bispecific antibody targeting EGFRvIII successfully treats intracerebral glioma. Proc Natl Acad Sci U S A *110*, 270-275.

Chong, E.A., Levine, B.L., Grupp, S.A., Davis, M., Siegel, D.L., Maude, S.L., Gladney, W.L., Frey, N.V., Porter, D.L., June, C.H.*, et al.* (2018). CD19-Directed CAR T-Cell (CTL019) Product Viability and Clinical Outcomes in Non-Hodgkin Lymphomas and B-Cell Acute Lymphoblastic Leukemia. Blood *132*, 197-197.

Cioffi, M., Dorado, J., Baeuerle, P.A., and Heeschen, C. (2012). EpCAM/CD3-Bispecific T-cell engaging antibody MT110 eliminates primary human pancreatic cancer stem cells. Clin Cancer Res *18*, 465-474.

Clements, J.L., Yang, B., Ross-Barta, S.E., Eliason, S.L., Hrstka, R.F., Williamson, R.A., and Koretzky, G.A. (1998). Requirement for the leukocyte-specific adapter protein SLP-76 for normal T cell development. Science *281*, 416-419.

Coloma, M.J., and Morrison, S.L. (1997a). Design and production of novel tetravalent bispecific antibodies. Nature Biotechnology *15*, 159-163.

Coloma, M.J., and Morrison, S.L. (1997b). Design and production of novel tetravalent bispecific antibodies. Nat Biotechnol *15*, 159-163.

Cordoba, S.P., Choudhuri, K., Zhang, H., Bridge, M., Basat, A.B., Dustin, M.L., and van der Merwe, P.A. (2013). The large ectodomains of CD45 and CD148 regulate their segregation from and inhibition of ligated T-cell receptor. Blood *121*, 4295-4302.

Cotton, R.G.H., and Milstein, C. (1973). Fusion of Two Immunoglobulin-producing Myeloma Cells. Nature *244*, 42.

Davis, M.M., and Bjorkman, P.J. (1988). T-cell antigen receptor genes and T-cell recognition. Nature *334*, 395-402.

Delon, J., Kaibuchi, K., and Germain, R.N. (2001). Exclusion of CD43 from the immunological synapse is mediated by phosphorylation-regulated relocation of the cytoskeletal adaptor moesin. Immunity *15*, 691-701.

Deschacht, N., De Groeve, K., Vincke, C., Raes, G., De Baetselier, P., and Muyldermans, S. (2010). A novel promiscuous class of camelid single-domain antibody contributes to the antigen-binding repertoire. J Immunol *184*, 5696-5704.

Ellerman, D. (2018). Bispecific T-cell engagers: Towards understanding variables influencing the in vitro potency and tumor selectivity and their modulation to enhance their efficacy and safety. Methods.

Eshhar, Z., and Gross, G. (1990). Chimeric T cell receptor which incorporates the anti-tumour specificity of a monoclonal antibody with the cytolytic activity of T cells: a model system for immunotherapeutical approach. Br J Cancer Suppl *10*, 27-29.

Eshhar, Z., Waks, T., Gross, G., and Schindler, D.G. (1993). Specific activation and targeting of cytotoxic lymphocytes through chimeric single chains consisting of antibody-binding domains and the gamma or zeta subunits of the immunoglobulin and T-cell receptors. Proc Natl Acad Sci U S A *90*, 720-724.

Ewert, S., Honegger, A., and Pluckthun, A. (2004). Stability improvement of antibodies for extracellular and intracellular applications: CDR grafting to stable frameworks and structure-based framework engineering. Methods *34*, 184-199.

Garrido, F., and Algarra, I. (2001). MHC antigens and tumor escape from immune surveillance. Adv Cancer Res *83*, 117-158.

Gaston, R.S., Deierhoi, M.H., Patterson, T., Prasthofer, E., Julian, B.A., Barber, W.H., Laskow, D.A., Diethelm, A.G., and Curtis, J.J. (1991). OKT3 first-dose reaction: Association with T cell subsets and cytokine release. Kidney International *39*, 141-148.

Gedeon, P.C., Schaller, T.H., Chitneni, S.K., Choi, B.D., Kuan, C.T., Suryadevara, C.M., Snyder, D.J., Schmittling, R.J., Szafranski, S.E., Cui, X.*, et al.* (2018). A Rationally Designed Fully Human EGFRvIII:CD3-Targeted Bispecific Antibody Redirects Human T Cells to Treat Patient-derived Intracerebral Malignant Glioma. Clin Cancer Res *24*, 3611-3631.

Gil, D., Schamel, W.W., Montoya, M., Sanchez-Madrid, F., and Alarcon, B. (2002). Recruitment of Nck by CD3 epsilon reveals a ligand-induced conformational change essential for T cell receptor signaling and synapse formation. Cell *109*, 901-912.

Gross, G., and Eshhar, Z. (1992). Endowing T-Cells with Antibody Specificity Using Chimeric T-Cell Receptors. Faseb Journal *6*, 3370-3378.

Hagihara, Y., and Saerens, D. (2014). Engineering disulfide bonds within an antibody. Biochim Biophys Acta *1844*, 2016-2023.

Hamid, O., Robert, C., Daud, A., Hodi, F.S., Hwu, W.J., Kefford, R., Wolchok, J.D., Hersey, P., Joseph, R.W., Weber, J.S.*, et al.* (2013). Safety and tumor responses with lambrolizumab (anti-PD-1) in melanoma. N Engl J Med *369*, 134-144.

Hodi, F.S., O'Day, S.J., McDermott, D.F., Weber, R.W., Sosman, J.A., Haanen, J.B., Gonzalez, R., Robert, C., Schadendorf, D., Hassel, J.C.*, et al.* (2010). Improved survival with ipilimumab in patients with metastatic melanoma. N Engl J Med *363*, 711-723.

Hoseini, S.S., Guo, H., Wu, Z., Hatano, M.N., and Cheung, N.V. (2018). A potent tetravalent T-cell-engaging bispecific antibody against CD33 in acute myeloid leukemia. Blood Adv *2*, 1250-1258.

Huse, M. (2011). Lymphocyte polarity, the immunological synapse and the scope of biological analogy. Bioarchitecture *1*, 180-185.

Huse, M., Quann, E.J., and Davis, M.M. (2008). Shouts, whispers and the kiss of death: directional secretion in T cells. Nat Immunol *9*, 1105-1111.

Kappler, J.W., Roehm, N., and Marrack, P. (1987). T cell tolerance by clonal elimination in the thymus. Cell *49*, 273-280.

Kim, S.T., Shin, Y., Brazin, K., Mallis, R.J., Sun, Z.Y., Wagner, G., Lang, M.J., and Reinherz, E.L. (2012). TCR Mechanobiology: Torques and Tunable Structures Linked to Early T Cell Signaling. Front Immunol *3*, 76.

Kim, S.T., Takeuchi, K., Sun, Z.Y., Touma, M., Castro, C.E., Fahmy, A., Lang, M.J., Wagner, G., and Reinherz, E.L. (2009). The alphabeta T cell receptor is an anisotropic mechanosensor. J Biol Chem *284*, 31028-31037.

Kipriyanov, S.M., Moldenhauer, G., Schuhmacher, J., Cochlovius, B., Von der Lieth, C.W., Matys, E.R., and Little, M. (1999). Bispecific tandem diabody for tumor therapy with improved antigen binding and pharmacokinetics. J Mol Biol *293*, 41-56.

Kleinewietfeld, M., and Hafler, D.A. (2014). Regulatory T cells in autoimmune neuroinflammation. Immunol Rev *259*, 231-244.

Klinger, M., Brandl, C., Zugmaier, G., Hijazi, Y., Bargou, R.C., Topp, M.S., Gokbuget, N., Neumann, S., Goebeler, M., Viardot, A.*, et al.* (2012). Immunopharmacologic response of patients with B-lineage acute lymphoblastic leukemia to continuous infusion of T cell-engaging CD19/CD3-bispecific BiTE antibody blinatumomab. Blood *119*, 6226-6233.

Kohler, G., and Milstein, C. (1975). Continuous cultures of fused cells secreting antibody of predefined specificity. Nature *256*, 495-497.

Kostelny, S.A., Cole, M.S., and Tso, J.Y. (1992). Formation of a Bispecific Antibody by the Use of Leucine Zippers. Journal of Immunology *148*, 1547-1553.

Krogsgaard, M., and Davis, M.M. (2005). How T cells 'see' antigen. Nat Immunol *6*, 239-245.

Kufer, P., Lutterbuse, R., and Baeuerle, P.A. (2004). A revival of bispecific antibodies. Trends Biotechnol *22*, 238-244.

Kumar, B.V., Connors, T.J., and Farber, D.L. (2018). Human T Cell Development, Localization, and Function throughout Life. Immunity *48*, 202-213.

Labrijn, A.F., Meesters, J.I., Priem, P., de Jong, R.N., van den Bremer, E.T., van Kampen, M.D., Gerritsen, A.F., Schuurman, J., and Parren, P.W. (2014). Controlled Fab-arm exchange for the generation of stable bispecific IgG1. Nat Protoc *9*, 2450-2463.

Le Gall, F., Reusch, U., Little, M., and Kipriyanov, S.M. (2004). Effect of linker sequences between the antibody variable domains on the formation, stability and biological activity of a bispecific tandem diabody. Protein Eng Des Sel *17*, 357-366.

Leach, D.R., Krummel, M.F., and Allison, J.P. (1996). Enhancement of antitumor immunity by CTLA-4 blockade. Science *271*, 1734-1736.

Lewis, R.S. (2001). Calcium signaling mechanisms in T lymphocytes. Annu Rev Immunol *19*, 497-521.

Li, J., Stagg, N.J., Johnston, J., Harris, M.J., Menzies, S.A., DiCara, D., Clark, V., Hristopoulos, M., Cook, R., Slaga, D.*, et al.* (2017). Membrane-Proximal Epitope Facilitates Efficient T Cell Synapse Formation by Anti-FcRH5/CD3 and Is a Requirement for Myeloma Cell Killing. Cancer Cell *31*, 383-395.

Liu, B., Chen, W., Evavold, B.D., and Zhu, C. (2014). Accumulation of dynamic catch bonds between TCR and agonist peptide-MHC triggers T cell signaling. Cell *157*, 357-368.

Lo, W.L., Shah, N.H., Ahsan, N., Horkova, V., Stepanek, O., Salomon, A.R., Kuriyan, J., and Weiss, A. (2018). Lck promotes Zap70-dependent LAT phosphorylation by bridging Zap70 to LAT. Nat Immunol *19*, 733-741.

Lopez-Albaitero, A., Xu, H., Guo, H., Wang, L., Wu, Z., Tran, H., Chandarlapaty, S., Scaltriti, M., Janjigian, Y., de Stanchina, E.*, et al.* (2017). Overcoming resistance to HER2-targeted therapy with a novel HER2/CD3 bispecific antibody. Oncoimmunology *6*, e1267891.

Ma, J., Tang, W.K., Esser, L., Pastan, I., and Xia, D. (2012). Recognition of mesothelin by the therapeutic antibody MORAb-009: structural and mechanistic insights. J Biol Chem *287*, 33123-33131.

Miller, B.R., Demarest, S.J., Lugovskoy, A., Huang, F., Wu, X., Snyder, W.B., Croner, L.J., Wang, N., Amatucci, A., Michaelson, J.S.*, et al.* (2010). Stability engineering of scFvs for the development of bispecific and multivalent antibodies. Protein Eng Des Sel *23*, 549-557.

Moore, G.L., Bautista, C., Pong, E., Nguyen, D.H., Jacinto, J., Eivazi, A., Muchhal, U.S., Karki, S., Chu, S.Y., and Lazar, G.A. (2011). A novel bispecific antibody format enables simultaneous bivalent and monovalent co-engagement of distinct target antigens. MAbs *3*, 546-557.

Morgan, R.A., Yang, J.C., Kitano, M., Dudley, M.E., Laurencot, C.M., and Rosenberg, S.A. (2010). Case report of a serious adverse event following the administration of T cells transduced with a chimeric antigen receptor recognizing ERBB2. Mol Ther *18*, 843-851.

Neelapu, S.S., Locke, F.L., Bartlett, N.L., Lekakis, L.J., Miklos, D.B., Jacobson, C.A., Braunschweig, I., Oluwole, O.O., Siddiqi, T., Lin, Y.*, et al.* (2017). Axicabtagene

Ciloleucel CAR T-Cell Therapy in Refractory Large B-Cell Lymphoma. New England Journal of Medicine *377*, 2531-2544.

Nisonoff, A., and Rivers, M.M. (1961). Recombination of a mixture of univalent antibody fragments of different specificity. Arch Biochem Biophys *93*, 460-462.

Pancer, Z., Amemiya, C.T., Ehrhardt, G.R., Ceitlin, J., Gartland, G.L., and Cooper, M.D. (2004). Somatic diversification of variable lymphocyte receptors in the agnathan sea lamprey. Nature *430*, 174-180.

Pardoll, D.M. (2012). The blockade of immune checkpoints in cancer immunotherapy. Nat Rev Cancer *12*, 252-264.

Park, J.R., Digiusto, D.L., Slovak, M., Wright, C., Naranjo, A., Wagner, J., Meechoovet, H.B., Bautista, C., Chang, W.C., Ostberg, J.R.*, et al.* (2007). Adoptive transfer of chimeric antigen receptor re-directed cytolytic T lymphocyte clones in patients with neuroblastoma. Mol Ther *15*, 825-833.

Park, T.S., Rosenberg, S.A., and Morgan, R.A. (2011). Treating cancer with genetically engineered T cells. Trends Biotechnol *29*, 550-557.

Postow, M.A., Chesney, J., Pavlick, A.C., Robert, C., Grossmann, K., McDermott, D., Linette, G.P., Meyer, N., Giguere, J.K., Agarwala, S.S.*, et al.* (2015). Nivolumab and ipilimumab versus ipilimumab in untreated melanoma. N Engl J Med *372*, 2006-2017.

Restifo, N.P., Dudley, M.E., and Rosenberg, S.A. (2012). Adoptive immunotherapy for cancer: harnessing the T cell response. Nat Rev Immunol *12*, 269-281.

Ridgway, J.B.B., Presta, L.G., and Carter, P. (1996). 'Knobs-into-holes' engineering of antibody CH3 domains for heavy chain heterodimerization. "Protein Engineering, Design and Selection" *9*, 617-621.

Rosette, C., Werlen, G., Daniels, M.A., Holman, P.O., Alam, S.M., Travers, P.J., Gascoigne, N.R., Palmer, E., and Jameson, S.C. (2001). The impact of duration versus extent of TCR occupancy on T cell activation: a revision of the kinetic proofreading model. Immunity *15*, 59-70.

Salmeron, A., Sanchez-Madrid, F., Ursa, M.A., Fresno, M., and Alarcon, B. (1991). A conformational epitope expressed upon association of CD3-epsilon with either CD3-delta or CD3-gamma is the main target for recognition by anti-CD3 monoclonal antibodies. J Immunol *147*, 3047-3052.

Schaefer, W., Regula, J.T., Bahner, M., Schanzer, J., Croasdale, R., Durr, H., Gassner, C., Georges, G., Kettenberger, H., Imhof-Jung, S.*, et al.* (2011). Immunoglobulin domain crossover as a generic approach for the production of bispecific IgG antibodies. Proc Natl Acad Sci U S A *108*, 11187-11192.

Schmid, D.A., Irving, M.B., Posevitz, V., Hebeisen, M., Posevitz-Fejfar, A., Sarria, J.C., Gomez-Eerland, R., Thome, M., Schumacher, T.N., Romero, P.*, et al.* (2010). Evidence

for a TCR affinity threshold delimiting maximal CD8 T cell function. J Immunol *184*, 4936-4946.

Scott, A.M., Wolchok, J.D., and Old, L.J. (2012). Antibody therapy of cancer. Nat Rev Cancer *12*, 278-287.

Shalaby, M.R., Shepard, H.M., Presta, L., Rodrigues, M.L., Beverley, P.C., Feldmann, M., and Carter, P. (1992). Development of humanized bispecific antibodies reactive with cytotoxic lymphocytes and tumor cells overexpressing the HER2 protooncogene. J Exp Med *175*, 217-225.

Shima, M., Hanabusa, H., Taki, M., Matsushita, T., Sato, T., Fukutake, K., Fukazawa, N., Yoneyama, K., Yoshida, H., and Nogami, K. (2016). Factor VIII-Mimetic Function of Humanized Bispecific Antibody in Hemophilia A. N Engl J Med *374*, 2044-2053.

Slaga, D., Ellerman, D., Lombana, T.N., Vij, R., Li, J., Hristopoulos, M., Clark, R., Johnston, J., Shelton, A., Mai, E*., et al.* (2018). Avidity-based binding to HER2 results in selective killing of HER2-overexpressing cells by anti-HER2/CD3. Sci Transl Med *10*.

Spiess, C., Zhai, Q., and Carter, P.J. (2015a). Alternative molecular formats and therapeutic applications for bispecific antibodies. Mol Immunol *67*, 95-106.

Spiess, C., Zhai, Q., and Carter, P.J. (2015b). Alternative molecular formats and therapeutic applications for bispecific antibodies. Mol Immunol.

Stevanovic, S., Helman, S.R., Wunderlich, J.R., Doran, S.L., Langhan, M.M., Kwong, M.L.M., Somerville, R.P.T., Klebanoff, C.A., Kammula, U., Sherry, R.M*., et al.* (2018). A phase II study of tumor-infiltrating lymphocyte therapy for human papillomavirus-associated epithelial cancers. Clin Cancer Res, clincanres.2722.2018.

Stone, J.D., Chervin, A.S., and Kranz, D.M. (2009). T-cell receptor binding affinities and kinetics: impact on T-cell activity and specificity. Immunology *126*, 165-176.

Suresh, M.R., Cuello, A.C., and Milstein, C. (1986). Bispecific monoclonal antibodies from hybrid hybridomas. Methods Enzymol *121*, 210-228.

Tao, M.H., and Morrison, S.L. (1989). Studies of aglycosylated chimeric mouse-human IgG. Role of carbohydrate in the structure and effector functions mediated by the human IgG constant region. Journal of Immunology (Baltimore, Md: 1950) *143*, 2595-2601.

Thakkar, S., Nanaware-Kharade, N., Celikel, R., Peterson, E.C., and Varughese, K.I. (2014). Affinity improvement of a therapeutic antibody to methamphetamine and amphetamine through structure-based antibody engineering. Scientific reports *4*, 3673.

Topp, M.S., Gokbuget, N., Stein, A.S., Zugmaier, G., O'Brien, S., Bargou, R.C., Dombret, H., Fielding, A.K., Heffner, L., Larson, R.A*., et al.* (2015). Safety and activity of blinatumomab for adult patients with relapsed or refractory B-precursor acute lymphoblastic leukaemia: a multicentre, single-arm, phase 2 study. Lancet Oncol *16*, 57-66.

Torikai, H., Reik, A., Liu, P.-Q., Zhou, Y., Zhang, L., Maiti, S., Huls, H., Miller, J.C., Kebriaei, P., Rabinovitch, B.*, et al.* (2012). A foundation for universal T-cell based immunotherapy: T cells engineered to express a CD19-specific chimeric-antigen-receptor and eliminate expression of endogenous TCR. Blood *119*, 5697-5705.

Torisu-Itakura, H., Schoellhammer, H.F., Sim, M.S., Irie, R.F., Hausmann, S., Raum, T., Baeuerle, P.A., and Morton, D.L. (2011). Redirected lysis of human melanoma cells by a MCSP/CD3-bispecific BiTE antibody that engages patient-derived T cells. J Immunother *34*, 597-605.

Tunnacliffe, A., Olsson, C., and de la Hera, A. (1989). The majority of human CD3 epitopes are conferred by the epsilon chain. Int Immunol *1*, 546-550.

Van Wauwe, J.P., De Mey, J.R., and Goossens, J.G. (1980). OKT3: a monoclonal anti-human T lymphocyte antibody with potent mitogenic properties. J Immunol *124*, 2708-2713.

Walker, M.R., Lund, J., Thompson, K.M., and Jefferis, R. (1989). Aglycosylation of human IgG1 and IgG3 monoclonal antibodies can eliminate recognition by human cells expressing Fc gamma RI and/or Fc gamma RII receptors. The Biochemical Journal *259*, 347-353.

Wang, H., Kadlecek, T.A., Au-Yeung, B.B., Goodfellow, H.E., Hsu, L.Y., Freedman, T.S., and Weiss, A. (2010). ZAP-70: an essential kinase in T-cell signaling. Cold Spring Harb Perspect Biol *2*, a002279.

Weissman, A.M., Hou, D., Orloff, D.G., Modi, W.S., Seuanez, H., O'Brien, S.J., and Klausner, R.D. (1988). Molecular cloning and chromosomal localization of the human T-cell receptor zeta chain: distinction from the molecular CD3 complex. Proc Natl Acad Sci U S A *85*, 9709-9713.

Wiedermann, U., Davis, A.B., and Zielinski, C.C. (2013). Vaccination for the prevention and treatment of breast cancer with special focus on Her-2/neu peptide vaccines. Breast Cancer Res Treat *138*, 1-12.

Wing, M.G., Moreau, T., Greenwood, J., Smith, R.M., Hale, G., Isaacs, J., Waldmann, H., Lachmann, P.J., and Compston, A. (1996). Mechanism of first-dose cytokine-release syndrome by CAMPATH 1-H: involvement of CD16 (FcgammaRIII) and CD11a/CD18 (LFA-1) on NK cells. J Clin Invest *98*, 2819-2826.

Wolchok, J.D. (2015). PD-1 Blockers. Cell *162*, 937.

Wolchok, J.D., Kluger, H., Callahan, M.K., Postow, M.A., Rizvi, N.A., Lesokhin, A.M., Segal, N.H., Ariyan, C.E., Gordon, R.A., Reed, K.*, et al.* (2013). Nivolumab plus ipilimumab in advanced melanoma. N Engl J Med *369*, 122-133.

Wolchok, J.D., Neyns, B., Linette, G., Negrier, S., Lutzky, J., Thomas, L., Waterfield, W., Schadendorf, D., Smylie, M., Guthrie, T., Jr.*, et al.* (2010). Ipilimumab monotherapy

in patients with pretreated advanced melanoma: a randomised, double-blind, multicentre, phase 2, dose-ranging study. Lancet Oncol *11*, 155-164.

Wu, Z., and Cheung, N.V. (2018). T cell engaging bispecific antibody (T-BsAb): From technology to therapeutics. Pharmacol Ther *182*, 161-175.

Wu, Z., Guo, H.F., Xu, H., and Cheung, N.V. (2018). Development of a Tetravalent Anti-GPA33/Anti-CD3 Bispecific Antibody for Colorectal Cancers. Mol Cancer Ther *17*, 2164-2175.

Xu, H., Cheng, M., Guo, H., Chen, Y., Huse, M., and Cheung, N.K. (2015). Retargeting T cells to GD2 pentasaccharide on human tumors using Bispecific humanized antibody. Cancer Immunol Res *3*, 266-277.

Yankelevich, M., Kondadasula, S.V., Thakur, A., Buck, S., Cheung, N.K., and Lum, L.G. (2012). Anti-CD3 x anti-GD2 bispecific antibody redirects T-cell cytolytic activity to neuroblastoma targets. Pediatr Blood Cancer *59*, 1198-1205.

Zacharakis, N., Chinnasamy, H., Black, M., Xu, H., Lu, Y.C., Zheng, Z., Pasetto, A., Langhan, M., Shelton, T., Prickett, T.*, et al.* (2018). Immune recognition of somatic mutations leading to complete durable regression in metastatic breast cancer. Nat Med *24*, 724-730.

Zhao, Q., Ahmed, M., Guo, H.F., Cheung, I.Y., and Cheung, N.K. (2015). Alteration of Electrostatic Surface Potential Enhances Affinity and Tumor Killing Properties of Anti-ganglioside GD2 Monoclonal Antibody hu3F8. J Biol Chem *290*, 13017-13027.